UNIVERSITY OF TWENTE.

GREEN

Optimal Energy Management for Semi Off-Grid Systems with Health-Aware Hydrogen Asset Operation: A Case Study of Fuel Cell Power Banks

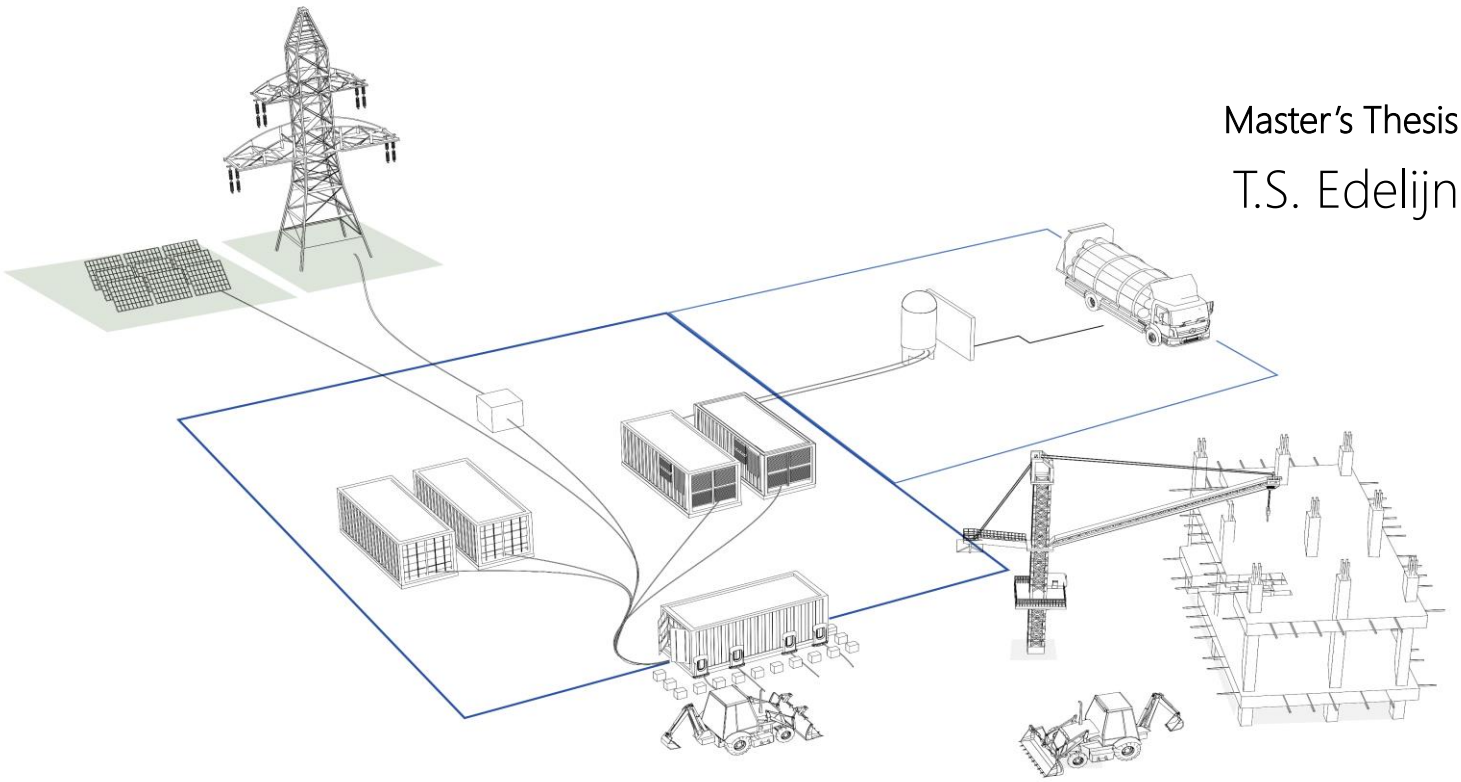

Master's Thesis

T.S. Edelijn

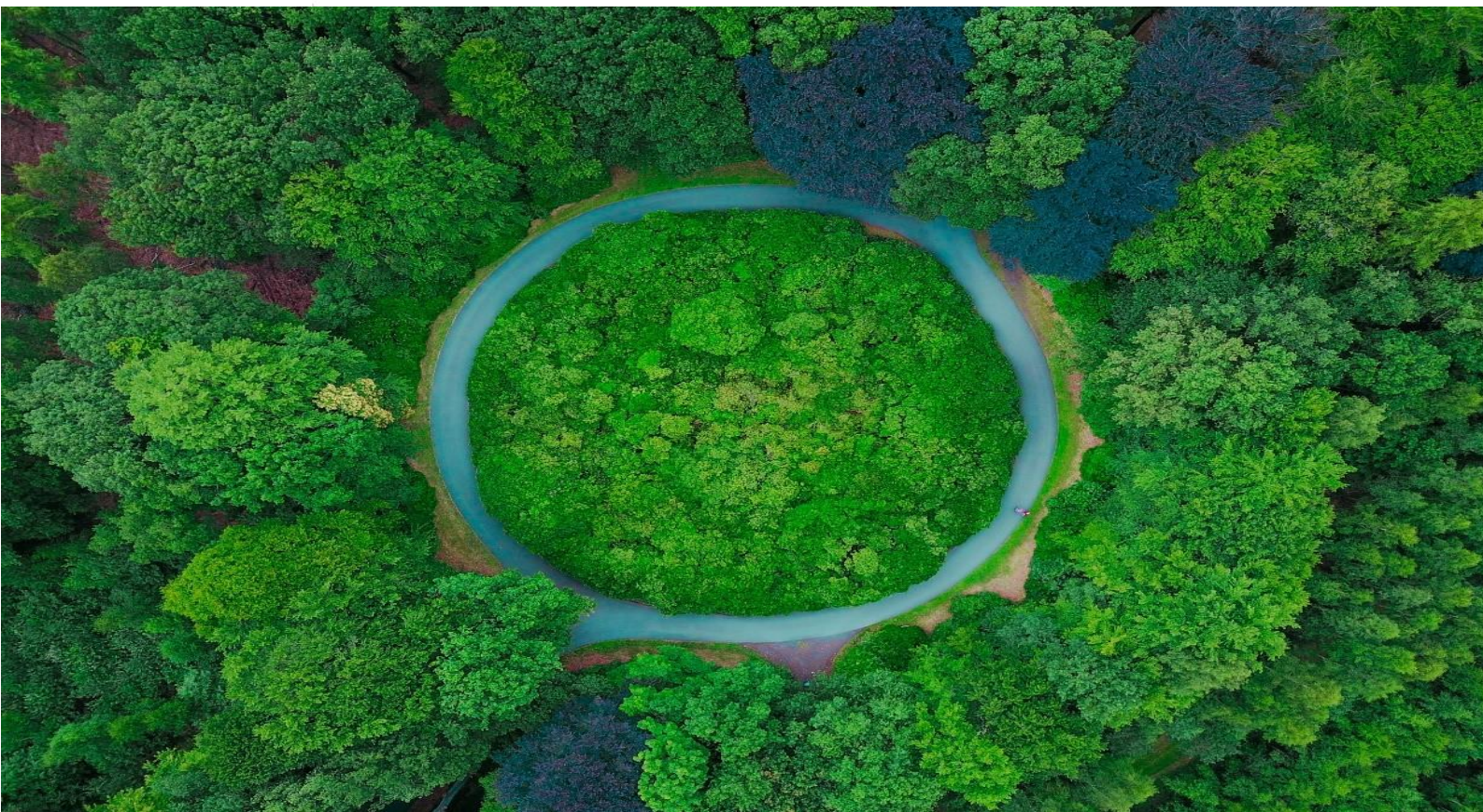

Optimal Energy Management for Semi Off-Grid Systems with Health-Aware Hydrogen Asset Operation: A Case Study of Fuel Cell Power Banks

by

Tom Sebastian Edelijn

Master Graduation Assignment for the master's program
Mechanical Engineering
Energy and Flow

CONFIDENTIAL

Until made available on November 7th , 2025

To be publicly defended on November 7th, 2024
Enschede

Student Number:	s2166461
Time period:	15/01/24 - 15/09/24 (8 months)
Graduation Committee	
UT	dr. C. Acar
UT	dr. ir. E. Shirazi
UT	prof. dr. ir. W. Rohlfs
Emmett Green	ir. drs. M. Wildschut
Company Supervisor	
Emmett Green	Ir. J. Stoter

Faculty of Engineering Technology
Department of Thermal and Fluid Engineering

UNIVERSITY OF TWENTE.

EMMETT GREEN

ABSTRACT

This thesis addresses the urgent need for emission-free construction sites in the Netherlands, driven by a tight housing market and stringent NOx emissions restrictions. It explores the potential of a semi off-grid Fuel Cell Power Bank (FCPB) combination as a viable solution. The design and management of a hydrogen-supported and congested DC-microgrid (DCMG) that connects the FCPB elements is associated with multiple challenges. This thesis investigates safe DCMG design, fuel cell (degradation) characteristics and Energy Management Systems (EMS), consequently developing an integrated EMS solution for the rapid implementation of emission-free construction sites.

The research proposes a Mixed Logical Dynamical (MLD) framework within a hierarchical Optimal Power Flow (OPF) scheduling algorithm. This approach ensures health-aware fuel cell operation and load fulfillment without compromising computational efficiency. A year-long simulation of the semi off-grid construction site underscores the robustness of the proposed model, achieving a 13 % improvement in system economy over the benchmark. Additionally, the proposed algorithm demonstrates a 96 % reduction in computational effort compared to conventional Model Predictive Control (MPC) and extends the fuel cell lifetime by 32 % through the incorporation of degradation characteristics. Furthermore, the analysis emphasises the importance of adequate load forecasting in future research.

NOMENCLATURE

AC-OPF	Alternating Current Optimal Power Flow
AFC	Alkaline Fuel Cell
BESS	Battery Energy Storage System
BP	Bipolar Plate
C-rate	Charge-rate
CAPEX	Capital Expenditure
DCMG	Direct Current MicroGrid
DoD	Depth-of-Discharge
DP	Dynamic Programming
ECSA	Electro-Chemical Surface Area
ED	Economic Dispatch
EMPC	Economic Model Predictive Control
EMS	Energy Management System
EoL	End of Life
FCPB	Fuel Cell Power Bank
KPI	Key Performance Indicator
LFP	Lithium Iron Phosphate
LHV/HHV	Lower/Higher Heating Value
LiB	Lithium-ion Battery
LP/MP/HP	Low, Medium or High Power
MILP/MIQP	Mixed-Integer Linear/Quadratic Programming
MLD	Mixed Logical Dynamical
NOx	Nitrogen Oxides
PEMFC	Proton Exchange Membrane Fuel Cell
PV	Photo-Voltaic
RBS	Rule-Based Strategy
SHE	Standard Hydrogen Electrode
SoC	State of Charge
SOFC	Solid-Oxide Fuel Cell
SoH	State of Health
STB	Standby

List of Figures

List of Tables

Contents

1 INTRODUCTION

With the rapidly increasing housing demand and decreasing building permits due to NOx emissions, the need for emission-free building sites arises. A semi off-grid battery and fuel cell combination or in short the FCPB (Fuel Cell Power Bank) is targeted as a promising solution for this purpose. With restricted access to grid energy on these locations the FCPB is able to provide a continuous supply of renewable energy for charging electric equipment. The main assets of the system are currently known and a first technical design of the DC-microgrid (DCMG) has been made. As a next step, an optimisation of several designs aspects should be carried out and a robust control strategy should be applied. The optimisation at hand will be addressed in this thesis where the major focus is on guaranteeing autonomous operation.

Although the first working fuel cell was demonstrated in 1839 by Sir William Grove the commercialisation of the technology has only been accelerated in recent years [1]. High costs related to the production of hydrogen and low oil prices are the main contributors to this slow introduction. However, with the renewed interest in emission free electricity generation the attention has shifted away from combustion engines, paving the way for hydrogen technology. Another obstacle to widespread implementation are the non-competitive prices of green hydrogen, although the future promises a reduction from 7 €/kg to 1.5 €/kg by 2050 [2]. Lastly, concerns are raised about the decreasing lifetime of Proton Exchange Membrane Fuel Cell (PEMFC) devices under harmful operating conditions, primarily driven by the lack of maturity [3].

The flexible FCPB platform asks for a sturdy EMS that is able to cope with the different renewable energy profiles, asset combinations, user demands and fuel cell degradation. Other than in most economical optimisations, the semi off-grid property necessitates an approach that goes beyond financial gains only. Future uncertainties should be promptly addressed to serve the load within the site that has both an energy and power deficit. From an electrical perspective the grid isolation impacts the stability within the DCMG. Therefore, the need for a reliable fundamental layer of safe operation arises. The goal of this thesis is to gain insights into the aforementioned fundamentally safe operation layer, develop a robust optimisation algorithm and integrate it with the (adapted) EMS system of Emmett Green. The outcomes of the thesis should aid a rapid implementation of the FCPB for emission-free construction sites, relieving the Dutch housing and nitrogen crises on top of reducing the greenhouse gas emissions.

1.1 Problem statement

For the implementation of the FCPB, dedicated research into several topics related to the design is required. Furthermore, the implications of fuel cell characteristics to its operation should be identified and robust optimisation algorithms are to be investigated. When a suitable solution to these topics has been found, a thorough analyses of the FCPB site aimed at identifying influential parameters and system sizing has to be performed. Hence the formulation of the following research questions:

1. For the following involved assets PEMFC, LFP battery, grid connection and PV panels, what are the risks of operation and how can they be mitigated?
2. What are the challenges related to intrinsically safe DCMG in terms of electrical safety as well as component protection?
3. What constraints do the dynamic behaviour and the degradation characteristics of the PEMFC pose on the control strategy?
4. What control strategies can be applied to the DCMG that provide a robust optimisation framework?
5. How to combine the robust optimisation and health-aware operation into a single integrated optimisation algorithm?
6. What are the decisive parameters within the optimisation framework?

7. Given the proposed EMS algorithm what is the impact of asset sizing within the FCPB system?

By answering these research questions the research topic: **Optimal Energy Management for Semi Off-Grid Systems with Health-Aware Hydrogen Asset Operation** should be covered. Consequently, the FCPB project provides a case study to confirm the adequacy of the findings.

A traditional thesis structure is applied. The first two questions are answered in the conclusions of the corresponding chapters in the literature review in Appendix D. The parts of the literature that are relevant for the understanding of the proposed methodology are summarised in the literature overview in Chapter 2, thereby answering questions 3 and 4. Question 5, standing as the primary contribution of this thesis, will be discussed in the methodology in Chapter 3. Finally, questions 6 and 7 are covered in Chapter 4.

2 LITERATURE OVERVIEW

The complete literature review performed before the start of this thesis can be retrieved from the Appendix D. The overview presented in this section is meant to provide background to the reader as well as highlight the identified research gap.

2.1 PEM fuel cell characteristics

Over time many concepts of fuel cells have evolved among which Alkaline (AFC), Solid-Oxide (SOFC) and Proton Exchange Membrane (PEMFC) are most noticeable. All technologies differ in operating conditions due to the used electrolyte rendering them useful for specific applications. PEMFCs are particularly of interest for transport or auxiliary power purposes due to their low temperature, high efficiency and compact size [4], hence best suited for the FCPB application.

A PEM fuel cell, being a electrochemical cell, has a lot of similarities to a LiB when it comes to the working principle. It consist out of a positive and negative electrode separated by an ionically conductive membrane that is an electric insulator, pushing the electrons to the external load (see Figure 1). At the anode hydrogen is supplied which travels through the diffusion layer and reacts with the catalyst (usually platinum) in the catalyst layer. The oxidation reaction that occurs, $H_2 \rightarrow 2H^+ + 2e^-$, splits the hydrogen molecules into protons and electrons. The distribution plates collects the electrons while the protons diffuse through the membrane. At the cathode side oxygen is supplied to react with the protons and electrons, $\frac{1}{2}O_2 + 2H^+ + 2e^- \rightarrow H_2O$, forming water and completing the electrical circuit.

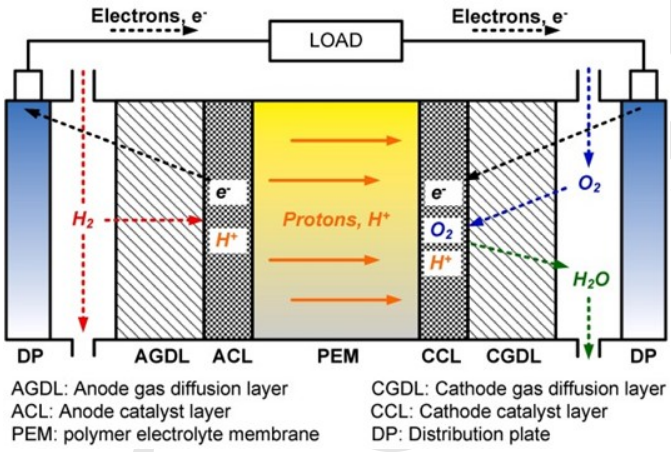

Fig. 1: Schematic overview of the PEMFC working principle with its components [3] (reproduced with permission of Elsevier).

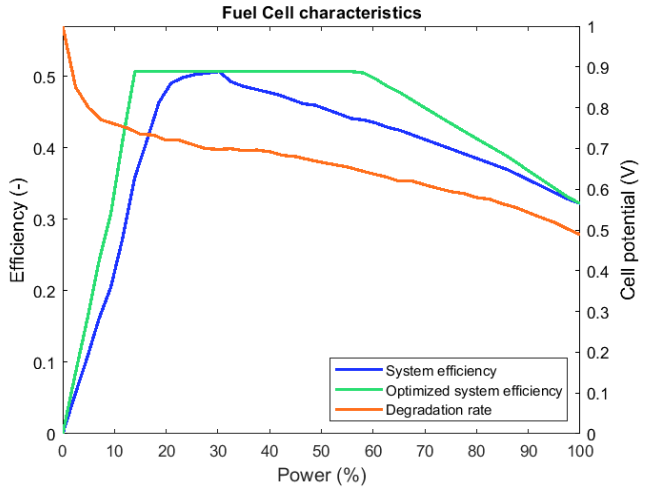

Fig. 2: Voltage [5], system efficiency [5] and optimised system efficiency [6] as a function of power for a certain PEMFC (own work).

2.1.a Operational conditions

For the purpose of modeling the PEMFC it is detrimental to understand the characteristics that dictate the allowed operating regime. This section will briefly cover the characteristics of PEMFCs that set it aside from other electrochemical cells like batteries. Many of these conditions follow from the fact that a PEMFC is a complex system encompassing not only the electrochemical cell but also several auxiliary systems as compressors, pumps and humidifiers that regulate the fluid flows and temperature.

Start-stop procedure A primary obstacle to the widespread implementation of fuel cells is the prolonged start-up and shutdown procedures. Before the chemical reaction in the cell can commence, the catalyst must be heated to its working temperature, the electrolyte must be hydrated, and the reactant gases must be available at

the correct pressure. These factors are highly system-dependent. For reference, the commercial CellKraft [7] PEMFC has a start-up time of less than 30 seconds, which has been validated by [8]. Additionally, it should be noted that a cold start during freezing temperatures significantly increases the staring time due to the need to thaw the moisture within the system. The shutdown procedure follows the same steps as the startup procedure, but in reverse order. As discussed in greater detail in Section 2.1.b, the degradation associated with the shutdown process is crucial. Various strategies are examined by Oyarce et al. [9], concluding that, from a protection perspective, purging the cathode side with hydrogen is most effective. However, this solution is less practical in most applications and raises concerns about mixing hydrogen and air. Therefore, the study concludes that rapidly consuming the oxygen with an auxiliary load is the best alternative. Using this method, the authors in [10] investigated how to optimally implement it, achieving a shutdown time of 13.5 seconds from full power. In conclusion, the timelines during the startup and shutdown of a PEMFC do not represent a considerable limiting factor to the operations of the FCPB case study.

Ramp rate A second concern that is often associated with fuel cells is the inability of load tracking and fast power ramping. The limiting factor in this case are the ancillaries that provide the air and hydrogen flows and thermal management [11]. Rapidly increasing the current demand to the cell will result in an undershoot of voltage due to gas starvation. On the cathode side this effect is magnified by the lower diffusivity of oxygen compared to hydrogen [12]. Conversely, the issues of gas starvation are not present for rapidly decreasing the load and therefore voltage overshoot is less severe. In an attempt to reduce the oxygen starvation, [11] found that increasing the air stoichiometry is an effective approach, although incurring higher ancillary power. With this approach the ramp rate was increased from 20% per second to 20% per 0.1 second. In conclusion, while the observed ramp rates in PEMFCs do not pose an extensive limitation for the FCPB application, it is important to consider potential degradation (see Section 2.1.b) when applying rapid load transients.

Efficiency In theory, assuming an ideal world, reversibility and a high air stoichiometry, a hydrogen-air fuel cell can reach 100% maximum efficiency [13]. However, in practice, the theoretical value is not reached due to several losses such as reaction activation loss, ohmic resistance loss, other electrical losses and purging losses [7]. In the context of fuel cell systems, the efficiency is defined as the hydrogen input divided by the net electricity output. To calculate the hydrogen input in kWh, the distinction between Higher Heating Value (HHV) and Lower Heating Value (LHV) should be clear. The former applies when liquid water is the reaction product, which is the case for low temperature PEMFCs. For high temperature PEMFC systems (operating above 120 °C), the LHV can be used if the steam is used effectively. In combined heat and power plants the output heat can be integrated in the efficiency as well, which proves useful in extremely high-temperature SOFC systems.

In a PEMFC the voltage efficiency intrinsically depends on the potential of the half reactions and is proportional to the current density. At low current densities this does not hold due to gas permeation of the membrane and current losses in the cell [14], as shown in the voltage vs current density plot in Figure 2. As power increases, concentration losses play a more important role, leading to a faster decrease in voltage at high current densities [14]. Combined with all other component efficiencies an indicative system efficiency as a function of current density is shown in Figure 2. Larger PEMFC installations compromising several parallel stacks can widen their high-efficiency window by individually turning on the stacks as to let them operate at their maximum efficiency point. This effect is shown in Figure 2 and is a factor to take into account for the FCPB application as well.

2.1.b Operational impact on degradation

Practical applications demand a focus on operational conditions rather than abstract internal behaviours, as operational parameters are controllable. Accordingly, this section will delineate literature findings pertaining to the correlation between operational conditions and internal degradation mechanisms.

In the context of mitigating degradation, it is preferable for the PEMFC to operate at a constant nominal current. The authors in [14, 15] have identified various operational conditions, such as idling, high load, load fluctuation, and start-stop cycles, as primary contributors to degradation. These conditions lead to elevated potentials, water

flooding, dynamic states, and even higher potentials respectively. According to their research in demanding automotive applications, dynamic loads account for 56 %, followed by 33 % for start/stop cycles, and 5 % each for idling and high power operation.

Idling state The idling state of the PEMFC can be regarded as a standby mode, in which the FC primarily provides power to its internal subsystems, such as the water pump, recirculation pump and control systems, typically necessitating only 1 % of the rated power. Conversely, the air compressor may consume up to 15 % of the power and is deactivated during stand-by mode [15]. During idling, the current demand is minimal, resulting in a high potential and increased gas permeation through the membrane. This elevated potential induces various chemical reactions, including the migration of metal ions and Pt dissolution at the cathode, as elucidated in Equation (1) [14]. The cell potential during idling can reach up to 0.95 V, approaching the cathode potential since the anode overpotential is negligible [16]. Consequently, Pt dissolution typically occurs with the intermediate step of Pt oxide formation.

$$\begin{cases} \text{Pt dissolution:} & Pt - 2e^- \rightarrow Pt^{2+}, & E_0 = 1.188 \text{ V vs SHE} \\ \text{Pt oxide formation:} & Pt + H_2O - 2e^- \rightarrow PtO + 2H^+, & E_0 = 0.980 \text{ V vs SHE} \\ \text{Pt oxide dissolution:} & PtO + 2H^+ \rightarrow Pt^{2+} + H_2O, & E_0 = 0.837 \text{ V vs SHE} \end{cases} \quad (1)$$

The increased gas permeation is directly influenced by the lower reaction rate, pressure build-up, and subsequent diffusion according to Fick's law. The presence of oxygen at the anode and a favorable potential accelerates the formation of H_2O_2, which reacts with metal ions such as Fe^{2+} and Cu^{2+}. These ions, originating from the bipolar plates (BPs) or the production process, participate in Fenton reactions, producing several radicals [14], along with their associated consequences. At the same time, crossover H_2 might react directly with O_2 on the cathode in a reaction that results in local hot spots. Where the increased temperature accelerates Pt dissolution and chemical degradation of the membrane [17]. In conclusion, prioritizing the avoidance of prolonged idling periods is imperative.

High power In contrast to idling conditions, high-power operation is associated with decreased cell potentials, thus mitigating many related issues. However, this heightened operational state also leads to increased reaction rates and current density, resulting in elevated temperatures and the occurrence of flooding. Notably, temperature has been empirically demonstrated to accelerate phenomena such as Pt particle growth, oxidation, deposition, and radical formation within the membrane [17]. Moreover, water flooding impedes mass transport resulting in reactant starvation and the accompanied cathode corrosion. Fortunately, the occurrence of water flooding can be detected by monitoring pressure drop within the cell, enabling timely intervention through temporary reduction of current demand [18]. Consequently, the extent of permanent degradation is diminished.

Dynamic loads During dynamic operation, the rise rate of current exhibits significantly faster dynamics compared to that of reactant supply to the FC, leading to hydrogen, oxygen, or both being subjected to starvation. The starvation behaviour results in a characteristic transient voltage response which over/undershoots and consequently recovers in time depending on the load step [12]. Although starvation is transient, it can inflict substantial irreversible damage to the cell. Oxygen deprivation at the cathode induces protons generating hydrogen instead of water, which is experimentally observed at the exhaust under air starvation conditions [14]. Consequently, adjacent to local areas experiencing air starvation, the generated hydrogen may directly react with oxygen, creating hot spots that must be avoided. On the other hand, hydrogen deprivation manifests as either local starvation or global starvation. The former stems from an uneven distribution of hydrogen, generating local low-pressure zones that drive air permeation through the membrane at these sites. Thereby, reversing the current within the cell locally, elevating cathode potential and promoting carbon corrosion at the cathode [16]. Under more severe circumstances, complete anode-side hydrogen deprivation can occur, elevating the anode

potential from near 0 V to 2.5 V vs SHE [19]. This results in the anode potential exceeding that of the cathode, causing the entire fuel cell to reverse polarity, resembling an electrolyzer. This inherently disrupts flows and operations, with extreme potentials posing the greatest threat due to carbon corrosion on the anode side [16].

Secondly, dynamic operations induce fluctuations in temperature and water content. The degradation resulting from these processes is better understandable, as both temperature and water content cycles lead to shrinking and swelling, accompanied by associated mechanical degradation [20]. Potential cycling represents another detrimental effect associated with dynamic loads. Pt oxide formation and dissolution (as seen in Equation (1)) are the primary contributors, with their consecutive occurrence leading to intensified dissolution, a phenomenon known as the place-exchange mechanism [21]. Since both reactions are influenced by different potentials, this phenomenon is not triggered under constant power conditions, but occurs during load changes, even at low powers. Overall, the dynamic states and fluid starvation induced by load changes pose a considerable challenge to the integrity of the PEMFC.

Start/Stop cycles Lastly, phenomena related to start-stop operation are addressed. During both start-up and shut-down procedures, the transient presence of air at the anode is unavoidable, leading to carbon corrosion similar to the hydrogen starvation process. Electrochemical corrosion of the carbon supports is governed by the reactions presented in Equation (2). Although relatively low equilibrium potentials accompany this reaction, research indicates that corrosion begins at potentials exceeding 1 V [16]. Additionally, [22] found that the lack of current density uniformity in the cell during start-up results in areas more susceptible to degradation. Moreover, in subzero temperatures, the freezing of water induces increased mechanical stresses on the cell, which should be mitigated [14].

$$\begin{cases} \text{Carbon corrosion:} & C + 2H_2O - 4e^- \rightarrow CO_2 + 4H^+, \quad E_0 = 0.21 \text{ V vs SHE} \\ & C + H_2O - 2e^- \rightarrow CO + 2H^+, \quad E_0 = 0.52 \text{ V vs SHE} \end{cases} \tag{2}$$

A comprehensive summary of all mechanisms discussed in this section is presented in Figure 3. The avoidance of all conditions outlined undeniably constrains the practical application of the PEMFC to a vast extent, a goal not pursued within this section. Nonetheless, these acceleration effects require consideration in formulating a successful implementation strategy for the PEMFC. Idling, high-power, and start-stop cycles present concrete conditions that can be avoided. In dynamic operational scenarios however, complexities arise, as the decision-making process incorporates the ramp rate, or speed of upscaling. Slowing the ramp rate mitigates issues related to starvation and dynamic water management, while temperature fluctuations are minimised through effective cooling strategies. Alternatively, preemptively increasing reactant supply to anticipate load changes can enhance ramp rate capability, without inducing gas starvation, from 2 % per 0.1 s to 50 % per 0.1 s [11]. Nevertheless, potential cycling (and the place-exchange mechanism) remains an inherent challenge irrespective of ramp rate and cycling frequency [14].

2.1.c Quantification of degradation

Numerous studies have experimentally demonstrated that degradation within PEMFC can be quantified in terms of voltage loss, per unit time or per specific event. For example, [23] compiled a comprehensive list of the degradation mechanisms, along with their corresponding voltage loss rates per hour. Notably, flooding, excess heat, and ice formation were identified as particularly detrimental factors. In a more practical approach, [24] assigned empirical voltage decay rates to each operational condition. By establishing this direct correlation, the study linked operational conditions to operational costs, thereby offering on average reasonably accurate lifetime predictions. Expanding upon this earlier model, [25] incorporated additional factors such as the acceleration effects of temperature and relative humidity, along with a form of natural degradation, in an effort to capture a more physical behaviour. Especially, the inclusion of load change degradation dependent on the ramp rate appears advantageous, considering the starvation phenomena discussed in Section 2.1.b. Additionally, the extension to power-dependent degradation as shown in Figure 4 overcomes the problem of not triggering one of the discrete degradation states. An alternative approach was proposed by [26], wherein a model was constructed

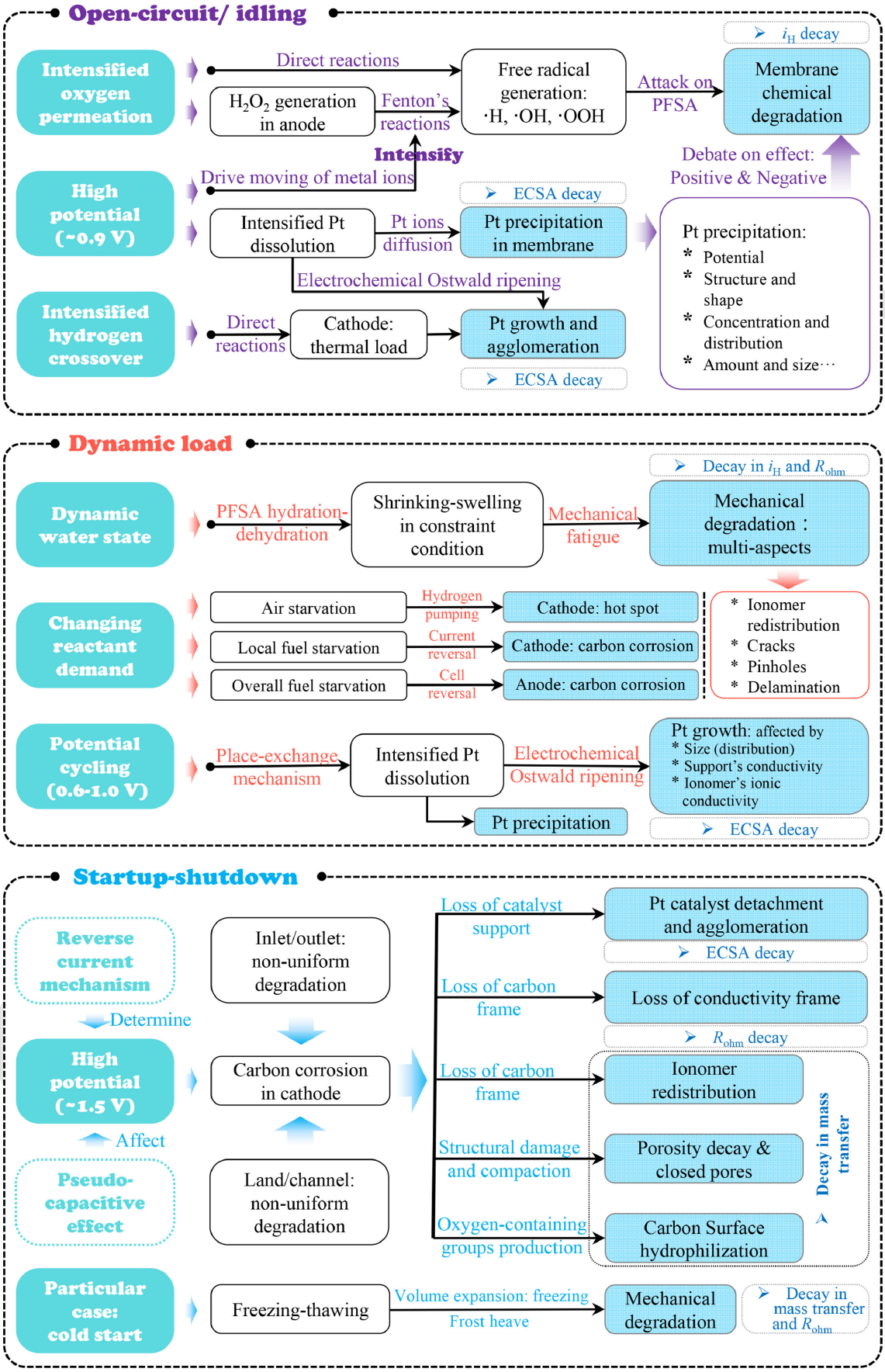

Fig. 3: Summary of degradation mechanisms grouped by the underlying operational conditions [14] (reproduced with permission of Elsevier).

Table 1: An overview of experimental degradation quantification.

State	**Low power** ($\mu V/hr$)	**High power** ($\mu V/hr$)	**Start-stop** ($\mu V/cycle$)	**Load change** ($\mu V/cycle$)
[24]	8.662	10.00	13.79	0.4185
[27]	8.820	10.29	13.72	0.4151

to account for steady ECSA loss based on electrochemical dissolution, as well as transient ECSA loss based on empirical data. Both steady-state and transient contributions from the operational profile influence ECSA loss, with findings indicating that a 75 % reduction in ECSA correlates with a 35 % decline in power output at end of life.

These studies present similar numbers for degradation rates as summarised in Table 1; a single start/stop cycle causes about 14 μV/cycle or 0.002 % of degradation equalling approximately 35 load change cycles. Idling and high power operation contributions are in a similar order of magnitude between 8 and 10 μV/hr [24, 25, 27]. The costs of degradation can be extrapolated out of the voltage loss when a certain end of life (EoL) criterion, usually 10 % or 0.07 V [25], has been set and the CAPEX is known.

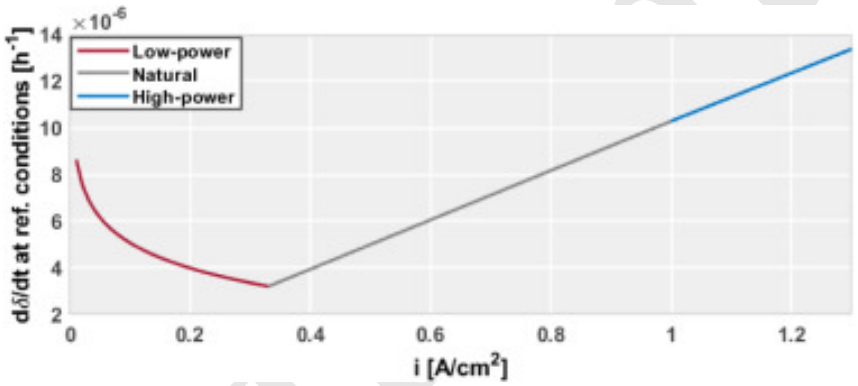

Fig. 4: Extension to a continuous degradation spectrum in PEM fuel cells [25] (reproduced under the terms of the Creative Commons license CC BY-NC-ND).

In conclusion, this section has identified the key characteristics governing fuel cell operations, highlighting the non-linear conditions that must be considered by the optimisation algorithm. The subsequent section will provide an in-depth examination of the literature related to optimal control of these hydrogen-based energy grids.

2.2 *Microgrid control strategies*

Achieving economical optimisation for the non-linear characteristics previously highlighted, necessitates employing intricate methodologies. Moreover, the decision-making process relies on system-level data inaccessible through direct decentralised means, hence making the optimisation impractical to perform frequently. This real-time control is outside the scope of the optimisation algorithm, although briefly addressed in the literature review in Appendix D. Consequently, this section will highlight methodologies designed to address high-level economical system optimisation, alongside the requisite solving routines.

2.2.a Energy management methodologies

Optimisation formulation Traditionally, Economic Dispatch (ED) has served as the method for determining power set points within grids consisting of multiple generators and loads regardless of the transmission network, with a focus on minimizing overall system costs. Conversely, the fundamental Power Flow (PF) problem addresses the division of power flows within a meshed transmission network at a given moment, independent of power generation specifics and lacking optimisation considerations. Optimal Power Flow (OPF) emerged as a means to combine both approaches, aiming to achieve comprehensive optimisation for power system management. This undertaking involves tackling a highly nonlinear problem, offering flexibility for single or multiple objectives such as minimizing losses, maximizing profits, reducing interruptions, or extending equipment lifespan [28].

The comprehensive formulation of OPF, known as AC-OPF, encompasses the entire set of electrical system equations without approximations or assumptions. Constraints imposed on the optimisation reflect the unique characteristics of the system at hand, encompassing inequality constraints, binary constraints, and stochastic variables, significantly impacting solving methodologies. Given the intricacies involved, numerous studies have proposed simplifications through assumptions or by disregarding certain effects to tailor the problem to specific scenarios [29]. One notable simplification is the DC-OPF, which, despite its name, doesn't exclusively handle DC flows but rather eliminates reactive power flow. This simplification arises from the following assumptions: power cable resistance is neglected, constant voltage at all nodes, and the voltage angle is very small [30]. Although the DC-OPF offers computational advantages due to its linear nature, it comes at the expense of power loss information. Alternatively, a linearization method for AC-OPF, proposed in [31], preserves power loss considerations and voltage information, as can be seen in Figure 5. The study observed that the computational times for DC-OPF, linear AC-OPF, and full AC-OPF were 0.4, 4.1, and 30.3 seconds respectively, for calculating optimal flows over a day in a given system.

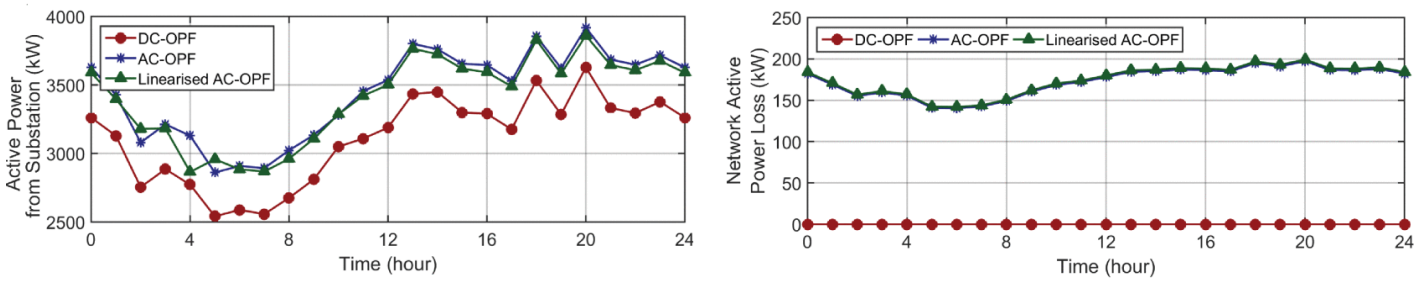

Fig. 5: Comparison of the performance of OPF formulations [31] (reproduced under the terms of the Creative Commons license CC BY 4.0).

Real-time energy management As discussed in the preceding section, the computational demands associated with intricate optimisation techniques present an obstacle to their real-time application in the control of microgrids. Additionally, the inherent uncertainties within forecasts of renewable energy sources and load demand necessitate real-time adjustments to the anticipated optimal conditions. These factors underline the significance of collaborative efforts between the local controller (as discussed in Appendix D) and the EMS algorithm. As previously noted, the EMS optimisation computes economically optimal set-points for a

designated time frame, subsequently implemented by the autonomous local controller on a ms timescale.

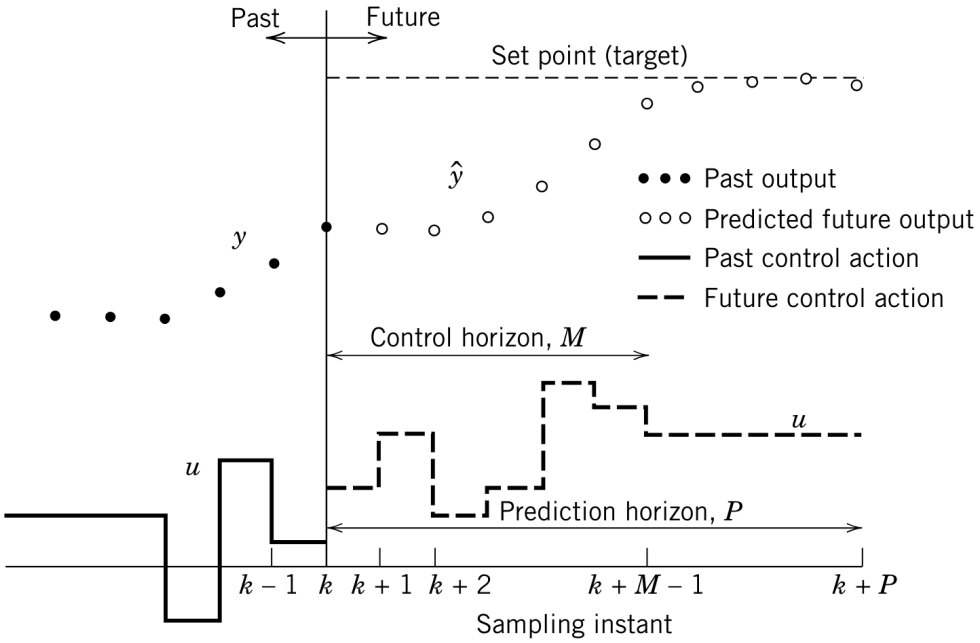

Fig. 6: Concept of a real-time MPC control structure [32] (copyright © 2017, IEEE).

An alternative approach to reconciling daily optimal control with local control is through Model Predictive Control (MPC), as also appeared in Section 2.2.b and Table 2. The MPC methodology involves a multi-time optimisation function characterised by a specified prediction horizon and control horizon. The fundamental concept entails incorporating system information spanning the prediction horizon into the optimisation process to derive optimal set-points. Consequently, how to arrive at the set-points, given the current system state, is optimally calculated within the control horizon. Notably, the controller applies solely the initial control action while disregarding future actions. Subsequently, in the second time step, the horizon regresses by one step, and the algorithm iterates, as illustrated schematically in Figure 6. This approach offers several advantages, including the multi-time integration of information, which proves highly advantageous in microgrid scheduling, while concurrently accommodating constant corrections for uncertain conditions. Moreover, within the optimisation step, there exists flexibility in defining a suitable objective function, as explored by [33], who included the OPF formulation within a MPC framework. However, a notable drawback lies in the predictive aspect, necessitating intricate insight into the system's dynamic behaviour. Furthermore, the methodology is computationally intensive, requiring a multi-time optimisation calculation at each time-step.

2.2.b Health aware fuel cell control strategies

The models in the previous Section describe the loss as a function of the input conditions. However, for the purpose of health-aware operations more sophisticated models are required with the possibility to find the most optimal deployment strategy. This section aims to shed light on the modeling approaches taken in literature to optimally schedule FC operation including lifetime consideration. Thereby, focussing on scheduling methods that include hydrogen technologies and its associated behaviour. The fundamental characteristics of PEM fuel cells and electrolyzers described by their minimum and maximum powers, and maximum allowed ramp rate are covered by all efforts. However, when looking more specifically into efficiency or the inclusion of degradation, many differences arise.

A proper example describing the different scheduling techniques is given in [34] comparing the potential of Economic Dispatch (ED) and Economic Model Predictive Control (EMPC) strategies. Both methods pose an optimisation problem where the latter is more sophisticated by solving the problem at any time step given a predetermined prediction horizon. The problem is consequently solved by either Dynamic Programming (DP)

or Mixed-Integer Linear Programming (MILP). The study concludes that solving the ED problem by DP is too computationally expansive while DP is preferred over MILP in terms of accuracy when solving the MPC problem. Since both solving routines require linear equations and constraints the non-linear effects of efficiency are hardly taken into account. [35] addresses the problem of non-linear plant dynamics, especially FC efficiency, by executing the non-linear equations outside the MPC loop, hence taking them constant in the optimisation.

In an effort to further develop the performance of the scheduling effort [36, 37] propose multi faceted MPC algorithms. The purpose is to separate the slow acting assets as the FC from the rapid acting assets as an BESS, for the sake of computational efficiency. Both models also include binary variables that determine the on/off state as to reduce the amount of start/stop cycles. Extending this binary variable principle, [38] introduces Mixed Logic Dynamic (MLD) for start/stop states and degradation state. The MLD framework allows for the introduction of the state variables which in turn is better suited for including certain degradation costs. The study suggests a MIQP solving routine since it was found that it is better able to reduce degradation compared to a MILP solver. Expanding on the MLD framework, [39] adds cold and warm intermediate states between on/off/standby for a more accurate representation of the timeline in the start-up process. Consequently costs are added to the state changes, however without taking into account how fast it changes. In a later study [40], the same authors go back to a three state system to alleviate the complexity and focus on a double MPC to better describe the fast acting assets.

Lastly, it is observed that the primary objective of these studies is to address the optimisation problem considering one or multiple days, often without regard for computational efficiency. However, to effectively assess algorithm performance or to evaluate a business case, a simulation period including seasonal effects is more appropriate, expanding the importance of computational effectiveness. The studies summarised in Table 2 report computational times ranging from 40 [39] to 120 s/day [37]. A significant contribution to the literature would be to reduce the computational effort, thereby enabling a wider range of applications.

Table 2: Overview of studies addressing hydrogen technologies in scheduling efforts focusing on degradation.

	Model Approach			**Degradation Characteristics**				
	Method	**Solver**	**Efficiency**	**Start/ Stop**	**Load change**	**Standby**	**High power**	**General Lifetime**
[34]	ED vs EMPC	DP vs MILP	Linear					x
[35]	Adaptive EMPC	MILP	Non-Linear					x
[36]	Multi-stage MPC	MILP	Constant	x				x
[37]	Multi-time MPC	MILP	Constant	x				x
[38]	Multi-time MLD-MPC	MIQP	Constant	x	x			x
[39]	MLD-MPC	MILP	Constant	x	x	x		x
[40]	MLD Cascaded MPC	MILP	Constant	x		x		x
[41]	Economic dispatch	MILP	Linear	x	x		x	x
	Hierarchical MLD-OPF	MILP	Multi-level	x	x	x	x	x

Although, many effective efforts regarding the scheduling of hydrogen assets in microgrids have been presented above, none of them includes sufficient degradation dynamics as discussed in the models from Section 2.1.c. Finally, [41] does include an empirical voltage degradation model aiming to prevent start/stop cycles, high power and fast ramping into an ED framework, however the scheduling accuracy lacks far behind the studies mentioned before. Table 2 clearly depicts the shortcomings of the previous work in this field. The gap that arises in this section can be described as the delicate balance between accuracy of degradation prevention in hydrogen assets and optimal scheduling of microgrids, without losing sight of computational effectiveness. The methodology of this research, as described in Section 3, aims to develop solutions to the literature gap identified above and how it is exploited in this research.

3 METHODOLOGY

The literature overview presented in the previous chapter highlights the efforts done in addressing the two main goals of this thesis: health aware fuel cell operation and robust control of semi off-grid systems. This chapter builds on the knowledge gained and consequently proposes multiple improvements. The chapter starts with elaborating on the proposed fuel cell model, incorporating the necessary dynamic behaviour and degradation prevention. Secondly, the proposed energy management system aimed at overcoming the challenges of the congested grid is presented.

3.1 Fuel cell model

Optimising hydrogen assets in real time applications requires an adequate model that searches for the right balance between accuracy and computational effort. The required accuracy is determined by the application, in this case the FCPB site. To become a feasible alternative to diesel generators the life time cost of operation is important. Therefore, the main cost contributions, such as component lifetime and hydrogen consumption are of increased interest. For that reason, the focus of the model in this section is aimed at including accurate efficiency values and degradation behaviour. The fundamental choices of this model are presented here while the mathematical details are delineated in Appendix A.

As presented in Section 2.1.b, the conditions causing degradation are fairly well understood in literature. On the other hand, Section 2.1.c highlights that only a limited amount of studies actually quantifies the degradation according to the identified degradation conditions. Allthough these studies are not most recent, they provide an initial reference input to start quantifying degradation. The efforts of literature to apply this degradation quantification is elaborated in Section 2.2.b, where Table 2 clearly highlights the shortcomings of literature to the focus of the fuel cell model mentioned before. Therefore, this section proposes a fuel cell model with a piece-wise constant efficiency including all identified degradation characteristics while still formatted as MILP equations for efficient solving routines.

The basis of the fuel cell model is derived from MLD systems framework [42] due to its excellent capability to describe interdependent physical operating constraints in a MILP format. Additionally, this format has already proven its advantages in describing advanced fuel cell characteristics [38, 39, 40]. Within the MLD structure binary variables are introduced that adopt their own characteristic features distinguishing between specific operating conditions, referred to as states throughout this thesis. Building on the binary state variables, the MLD formulation allows for binary variables that describes the switch between two states, referred to as state switches. These quantities are leveraged to develop an accurate fuel cell model from an operational and degradation perspective.

From the literature overview in Section 2.1 the key fuel cell characteristics are derived. The continuous efficiency curve introduces non-linear equations hence the inability of linear programming to solve the system. Therefore, all studies proposing hydrogen EMS algorithms in Table 2 apply a constant efficiency to their model input at each optimisation step which is a strong assumptions given the actual efficiency curve. A solution is presented by Huang et al. [35], who applies a non-linear efficiency equation to update the efficiency between consecutive optimisations according to the previous measured power. However this approach is only valid when the ramp rate is severely limited which is not the case for modern PEMFC systems [11]. Another solution is found in MILP where the full power range of the fuel cell is segmented in bins where the efficiency is set accordingly. In theory, by applying infinite bins the original profile is retrieved, obviously at the cost of the calculation effort.

Degradation is, similar to efficiency, a function of power, as illustrated in Figure 7. Noticeable is the fact that the efficiency is lowest at point where degradation is highest. This inverse relationship arises due to the underlying electrochemical mechanisms that drive both phenomena. The proposed model takes advantage of this correlation by defining three power generating states: Low Power (LP), Medium Power (MP) and High Power (HP), specifically tailored to the experimental degradation data in Table 1. The boundaries of the

proposed power states are depicted in Figure 7, alongside general efficiency and degradation curves found in literature.

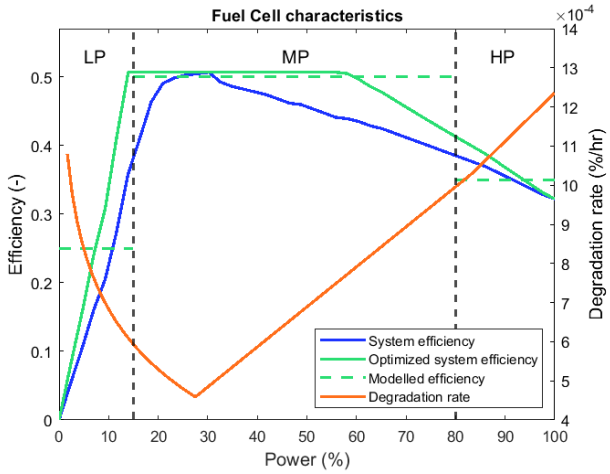

Fig. 7: Typical efficiency [5] and degradation [25] curves along with the proposed state classification (own work).

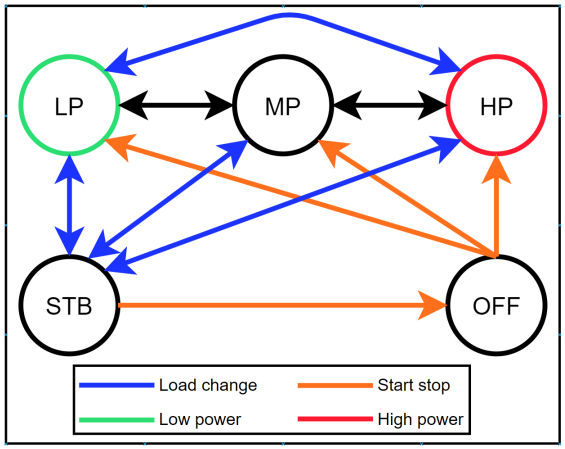

Fig. 8: Schematic of the adopted states, along with the applied degradation costs in the optimisation model (own work).

Table 3: Proposed state parameters of the fuel cell.

State	**Min power (% of max power)**	**Max power (% of max power)**	**Efficiency (%)**	**Depreciation cost (€/hr)**	**Degredation Cost (€/hr)**
OFF	0	0	0	0	0
STB	-1	-1	0	CAPEX / lifetime	0
LP	5	15	25	CAPEX / lifetime	CAPEX · 8.7e-6 / EoL
MP	15	80	50	CAPEX / lifetime	0
HP	80	100	35	CAPEX / lifetime	CAPEX · 10.2e-6 / EoL

Besides the power production states, an OFF and Standby (STB) state are introduced to model the degradation associated with start stop and load change cycles. The standby state serves as an intermediate step between power production and off where the system is maintained at operational temperature without consuming hydrogen, thereby providing the option to prevent frequent start-stop cycles. The cost related to load change degradation which occurs as a result of gas starvation and the place-exchange mechanism (detailed in Section 2.1.b) is applied to state transitions between the power production states and standby as well as between low and high power states. Similarly, the cost associated with start-stop cycles is applied between the off state and all other states.

An additional feature of the introduced state switch variables is the possibility to constrain specific state switches. In this model, switches from power production to off are prohibited as to simulate the shutdown procedure and allow for potential purging. Furthermore, based on experimental findings, the switch from off to standby was forbidden as to prevent the fuel cell from consuming power during negative market prices. A graphical summary of the degradation characteristics of the states and state switches is presented in Figure 8, while the corresponding numbers are summarised in Table 3. The remaining assumptions regarding the fuel cell model are summarised below.

Assumptions

- The efficiency is constant within a state (see Table 3, based on [6]).
- The hydrogen inlet pressure and temperature are considered constant and regulated by the fuel cell manufacturer.
- The ramp up and down rates are 20 %/s [11], rendering it irrelevant for the 15-minute time interval.
- The assumed CAPEX is 1000 €/kW with a lifetime of 25000 hours under ideal operating conditions [43].
- The STB power consumption is 1 % of the maximum power [40].
- The fuel cell is in OFF state at the start of every simulation.

3.2 FCPB model

This section establishes the characteristics and assumptions for the remaining assets within the FCPB microgrid, according to Figure 9, while the mathematical background is presented in Appendix A.

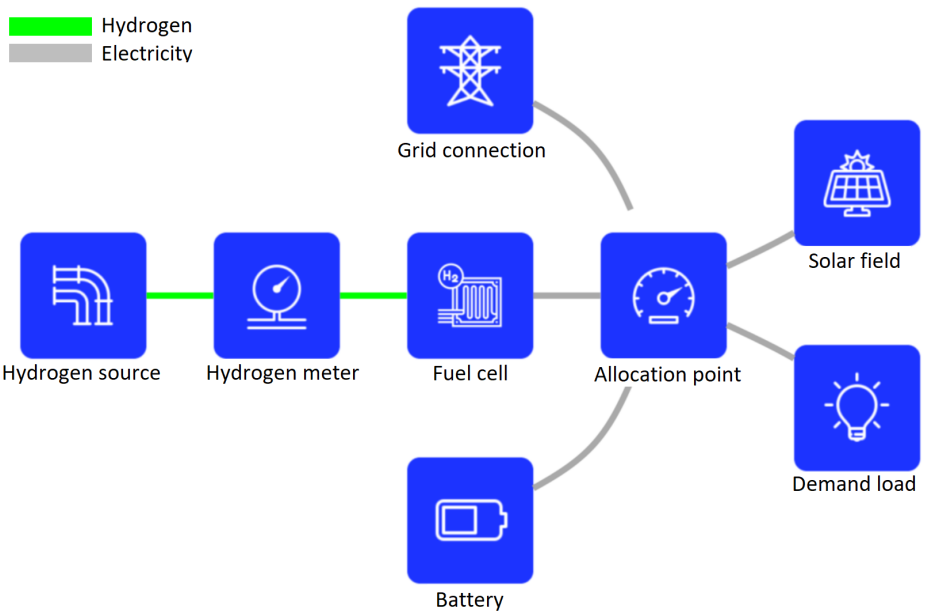

Fig. 9: Schematic visualisation of the FCPB microgrid (own work).

3.2.a Battery

The battery asset is the backbone of the system providing several functions guaranteeing continuous operation of the system. The rapid response in both providing and consuming electricity compensates for the limitations of other assets, which proves beneficial for degradation prevention in the fuel cell. Moreover, the peak shaving capability of the battery mitigates the congestion in energy deficit systems, thereby improving the overall system economy. Furthermore, the battery allows for uncertainty to happen without an immediate shortage or surplus of power. Battery systems, compromising of electrochemical cells, are prone to all kinds of degradation as well (see the literature study in Appendix D), however for this thesis this behaviour is out of scope. As a result the battery is modeled as a fast acting asset without any restrictive constraints other than mentioned in the following assumptions.

Assumptions

- The SoC at the start of the simulation is 50 %.
- The battery SoC is kept within 10 and 90 % for degradation and efficiency purposes. No other degradation measures are taken.
- The battery has a 95 % (dis)charge efficiency [44] and no additional storage losses.
- The depreciation cost for usage is 50 €/MWh, determined by the CAPEX and lifetime [45].

3.2.b Grid connections

An important attribute of the FCPB is its capability to operate in a semi off-grid mode. That is, a limited or congested grid connection is still available, but cannot solely fulfill the demand. Depending on the load profile and magnitude, this ya result in either an energy deficit or a power deficit. The former entails that the cumulative load over a specified period exceeds the aggregate of the possible grid offtake, while the latter induces that the peak power exceeds the grid power. The allocation point in Figure 9 serves as the measuring asset that aggregates the total power that flows into the system.

Given the remote location and temporary nature of the system, hydrogen pipelines are not a feasible solution. As a viable alternative, hydrogen is supplied through tanks on a periodic basis frequent enough to be irrelevant to the EMS. Similarly to the allocation point, the hydrogen meter illustrated in Figure 9 measures the flow and applies the corresponding costs. All other assumptions regarding the hydrogen and electricity sources are detailed below.

Assumptions

- The available grid connection corresponds to the maximum available for building sites of 55 kW where feed-in is not allowed.
- The system operates on the Dutch electricity market with a dynamic contract. An additional energy supplier fee fee of 20 €/MWh is added to the market spot price.
- Hydrogen is delivered from large tanks that are resupplied in time and is instantaneously supplied to the fuel cell.
- The hydrogen off-take price is taken as the average over 2024 from the German green hydrogen index, valued at 220 €/MWh [46].

3.2.c Solar park

In addition to grid connections, the FCPB facilitates the usage of local renewable sources such as solar and wind. In the context of this study, only solar is incorporated in the energy mix. The effective utilisation of intermittent solar energy requires adequate energy storage as well as proper energy scheduling, which will be thoroughly investigated in Chapter 4. The underlying assumptions for the solar field are listed below.

Assumptions

- Solar generation is fetched from actual historic irradiance data in Delft of the year 2022 [47].
- The output power is determined by the maximum output power of the plant, assuming optimal tilt and azimuth, including 7 % additional system losses [48].
- The solar panels can be curtailed individually when required.

3.2.d Demand load

The demand load is comprised of daily charge patterns for various electrified construction vehicles. The fleet includes 20 smaller pieces of equipment, such as forklifts, wheel loaders, and small cranes, as well as five larger vehicles including supply trucks and large excavators. Based on each vehicle's individual characteristics as runtime, operational pattern, battery capacity and charge power two randomised scenarios were created by a previous intern as depicted in Figure 10. The choice for two distinct patterns arises from the uncertainty in the actual site demand, where a deviation in maximum power (300 vs 260 kW), total energy (1.9 vs 1.8 MWh) and timing of peak power (10 PM vs 12 PM) is chosen for maximum robustness. For the purpose of simulations, the annual demand patterns are established according to the assumptions below.

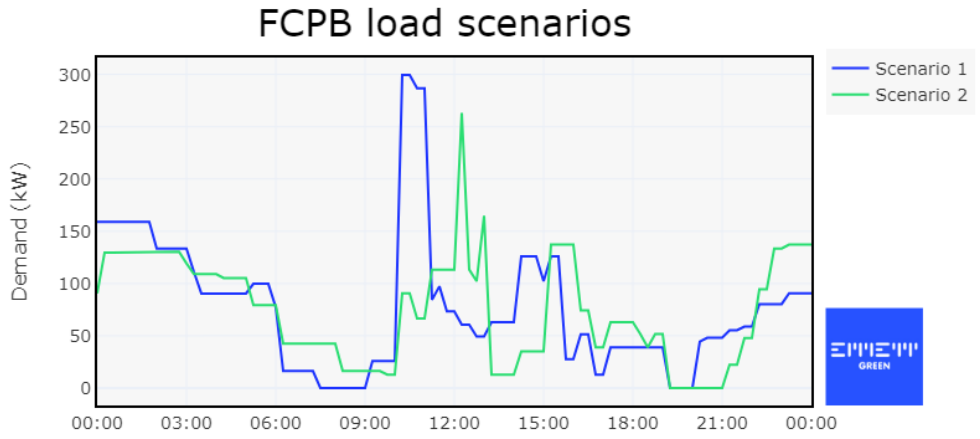

Fig. 10: Two scenarios of vehicles charging during the day (own work, based on fellow intern).

Assumptions

- The demand load is compromised of two semi-random scenarios of vehicles charging, as proposed by a previous intern.
- Every consecutive day is different, every 2 weeks the pattern repeats and the weekends are free of load.
- The load must be fulfilled at all times.

3.3 Optimisation formulation

The previous section delved into the characteristics of specific assets and described the overall system configuration. This section develops the optimisation algorithm that is applied to this system for the dual purpose of economical optimisation and health-aware operation. It starts with formulating the optimisation problem, continues with the MPC scheduling approach applied by numerous studies in Table 2, and finishes with a novel scheduling approach aimed at improving the computational burden of the former.

The literature overview highlights several optimisation formulations that are adopted in literature. Among these, ED, DC-OPF and AC-OPF are the most recognised formulations. ED simplifies the problem by disregarding power flows between assets yielding in lower accuracy compared to OPF formulations. DC-OPF is derived from AC-OPF by assuming no cable losses, constant voltage at all nodes and a negligible voltage angles to eliminate reactive power flow. Since it is assumed that the local controller handles voltage and current values, the application of AC-OPF is redundant. The implementation of DC-OPF instead of AC-OPF greatly reduces the computational complexity converting a quadratic nonlinear problem into a linear formulation.

Moreover, it should be noted that as a result of the MLD formulation for the fuel cell states the overall system is transformed into a MILP formulation. The MILP OPF is constructed as a classical optimisation problem seeking the minimum of a cost function dependant on the set of continuous variables $\boldsymbol{P}(t)$ and the set of binary variables $\boldsymbol{\delta}(t)$, subject to a set of linear constraints, as shown in Equations (3) and (4). In these equations the set of all timestamps T and the functions f and $\boldsymbol{g}$ depend on the optimisation approaches outlined in Sections 3.3.a and 3.3.b. For a comprehensive description of the mathematical formulation, the reader is referred to Appendix A.

$$\min \sum_{t \in T} f(\boldsymbol{P}(t), \boldsymbol{\delta}(t)) \tag{3}$$

$$\text{s.t.} \quad \boldsymbol{g}\left(\boldsymbol{P}(t), \boldsymbol{\delta}(t)\right) \leq 0 \tag{4}$$

3.3.a Rolling horizon approach

The principles of MPC, as discussed in Section 2.2.a provide a perfect framework for energy scheduling purposes due to the combination of real time implementation and future forecasting at the same time. Many studies have adopted this approach and show its increased performance over Newton and heuristic based algorithms [33] as well as rule based algorithms [37] in solving OPF problems. In addition, the inclusion of the prediction horizon increases the renewable utilization [35] while decreasing the hydrogen consumption [34]. Additionally, it is proven that an MPC can handle uncertainties without being overly conservative [37]. However, the increased performance is affected greatly by the prediction horizon [34] which is the major cause of the increased computational burden. Erazo-Calceda et al. even found that increasing the prediction horizon length by 25 % the solution time increased by 50 %, where it should be noted that a quadratic problem formulation was used [33].

Albeit computationally expensive, the MPC approach is well suited to apply the previously proposed fuel cell model aimed at degradation reduction. Furthermore, the integration of the MLD formulation with states and state switches should perfectly showcase the added benefit of the prediction horizon and its magnitude. The assumptions applicable to this rolling horizon approach are listed below.

Assumptions

- The rolling horizon optimisation includes several timestamps in the prediction horizon.
- A dynamic timestep is applied in an effort to reduce the computational time.
- The complete fuel cell model as proposed in Section 3.1 is applied over the full prediction horizon.

3.3.b Fixed schedule approach

The computational expense is the primary drawback associated with MPC approaches. Therefore this section aims to adopt a novel scheduling solution combining the benefits of an MPC while reducing its computational effort. The integration of forecasting and real-time application is essential and should be included in the novel approach.

Within the MPC framework, 95 % of the calculated results remain unused, as only the result of the first timestamp is implemented. This is the predominant factor contributing to the increased computational costs. An evident solution would be to reduce the prediction horizon and thereby the unused results. However, the accompanied reduction in performance [33] is undesirable. As a first solution, the previous section applies a dynamic timestep to sustain the prediction horizon, albeit with a coarser perspective. Subsequently, it is proposed to get rid of the rolling optimisation and perform a daily single scheduling optimisation with the full model for forecasting purposes. Consequently, the results of the fuel cell states and battery SoC are communicated to a single timestep optimisation that handles the real time implementation with the actual realised powers. This approach retains the predictive capabilities and real time implementation while avoiding redundant calculations.

As a result of the scheduling optimisation, the real time optimisation can be simplified to increase computational speed. Most notably, the fuel cell model is constrained to solely the scheduled state, changing the optimisation to a linear program. Without multiple timestamps in the optimisation, the battery requires a different strategy to encourage charging at the correct times. This has been solved by introducing a (linear) penalty to deviating from the scheduled SoC, as suggested by Bidi et al. [49].

A fundamental drawback of this approach is the necessity of accurate forecasting since the time between optimisation and implementation is greatly increased as compared to the MPC. To overcome the discrepancies between forecasted and actual loads and generation two distinct safety margins are introduced in the scheduling optimisation. First, the minimum SoC limit of the scheduling optimisation is increased to always maintain some reserve capacity for unforeseen circumstances. Second, the load prediction can be overestimated by a certain factor to promote the scheduling of reserve power. Since these safety quantities are system specific and not well covered in literature, their values are experimentally tuned and their impact assessed in the results Section. A summary of this section is given in the assumptions listed below, while a schematic overview of the MPC and fixed schedule approach is provided in Figure 11.

Assumptions

- The scheduling optimisation is performed well before the start of the next day.
- The complete fuel cell model as proposed in Section 3.1 is included in the scheduling optimisation.
- In the short-term optimisation the fuel cell state is fixed according to the schedule. Degradation costs are not applied in this optimisation since that information is provided by the schedule.
- In the short-term optimisation the battery follows the SoC schedule, where a linear penalty is introduced for deviating from the schedule [49].
- The scheduled SoC in the short term optimisation is calculated as the weighted average of the previous and next hour.
- In the scheduling optimisation the minimum SoC is increased in order to provide a safety margin in the real time optimisation.
- An additional margin is taken on top of the predicted load in order to provide a safety margin in the real time optimisation.

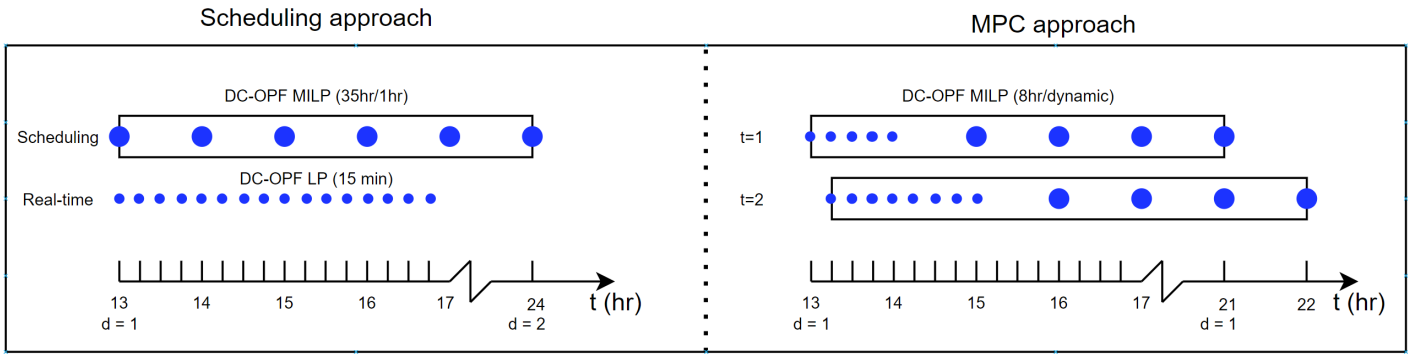

Fig. 11: Schematic of the proposed scheduling approach and the dynamic MPC approach displaying the timesets and models used in the optimisations (own work).

3.4 Simulation approach

This section describes how the adequacy of the proposed models in reaching the two-fold goal of this thesis is investigated. In addition, several hypotheses are drafted regarding the impact of the proposed models.

Upon completion and integration of the models into the existing Emmett Green EMS structure, the initial steps involved validating the correct configuration of the models. To this end, a unit test matrix was created that evaluated the impact of specific features one by one. For a detailed account of the validation analysis, the reader is referred to Appendix C.

The first objective of this study is to provide a health-aware optimisation framework, accounting for the key issues of fuel cell degradation. The fuel cell degradation framework of Desantes et al. [25] (see also Figure 4) based on the experiments of Pei et al. [27], is inversely applied in the proposed model outlined in Section 3.1. By incorporating degradation factors associated with start-stop cycles, dynamic loads, and power-dependent phenomena, this model calculates the State of Health (SoH) as a function of operational conditions. Consequently, this model can be utilised to evaluate the performance of the optimisation framework by providing a quantitative measure of its adequacy.

The second objective is to assess the robustness of the optimisation algorithm in ensuring the security of the load supply. Particularly, in the congested microgrid where energy and power deficits prevail the method of optimisation, the guarantee of load fulfillment raises a challenge. Unlike most hydrogen EMS papers [34]-[41], which typically simulate a day to a maximum of a week, this study simulates the FCPB site over the entirety of 2023 to include all extreme events. The results of these simulations will be evaluated according to several KPI's including simulation duration, utility costs, fuel cell SoH, battery SoH and solar and grid utilization.

The thesis starts with comparing the two proposed optimisation methods, and benchmarks them against a Rule-Based Strategy (RBS) proposed by Huang et al. [50] and scenarios lacking the MLD formulation or forecasting capabilities. The hypothesis is that the MLD formulation enhances the lifetime of the fuel cell albeit at the cost of the utility bill (electricity and/or hydrogen). Furthermore, the prediction capability is expected to increase the battery and solar utilisation, thereby reducing utility costs.

Subsequently, both optimisation methods are exposed to a sensitivity analysis that should provide insights in the relevant parameters and design choices. Especially, attention is given to the effectiveness of forecasts and the length of prediction horizons. The hypothesis is that extending the horizon and increasing the forecast accuracy results in better economical choices as the optimisation benefits from improved inputs. Finally, an economic system sizing analysis is conducted. Naturally, it is hypothesised that increasing battery and fuel cell size increase the system economy. However, the point at which the investments outweigh the increased economy is unknown.

4 RESULTS

This section describes the results of the multiple analyses proposed in in Section 3.4. The simulations are performed on the FCPB system, according to the numbers described in Section Appendix B, over the entirety of 2023. As a reference for the simulation time the hardware configurations is as follows: a laptop with an Intel core I7 at 2.2 GHz and 16 GB RAM is used. The EMS program is written in Python and the optimisation is solved with the mixed-integer CBC solver in OR tools.

4.1 Rolling horizon vs fixed schedule approach

The asset power distributions calculated by the rolling horizon optimisation are depicted for a solar-deprived and solar-rich day in Figures 12 and 13 respectively. A prediction horizon of 12 hr is adopted in these figures based on the findings of Section 4.2. In both figures, the top plot displays the costs for electricity and hydrogen in 2023 where it is established that hydrogen is a factor 1.5 to 8 more expensive, considering a 50 % conversion efficiency. Notably, negative prices do not even occur on these days. Consequently, the fuel cell serves as back-up power to cover the energy deficit over the entire day (or week). Throughout this thesis, the following convention is adopted: positive power denotes generation while negative power denotes consumption. The figures reveal the ability of the rolling horizon optimisation to distribute the power and reduce the grid and fuel cell utilization as more solar generation is available. The multi-timestamp MILP is solved in around 80 seconds per day, amounting to 8 hours of computational time for a single year.

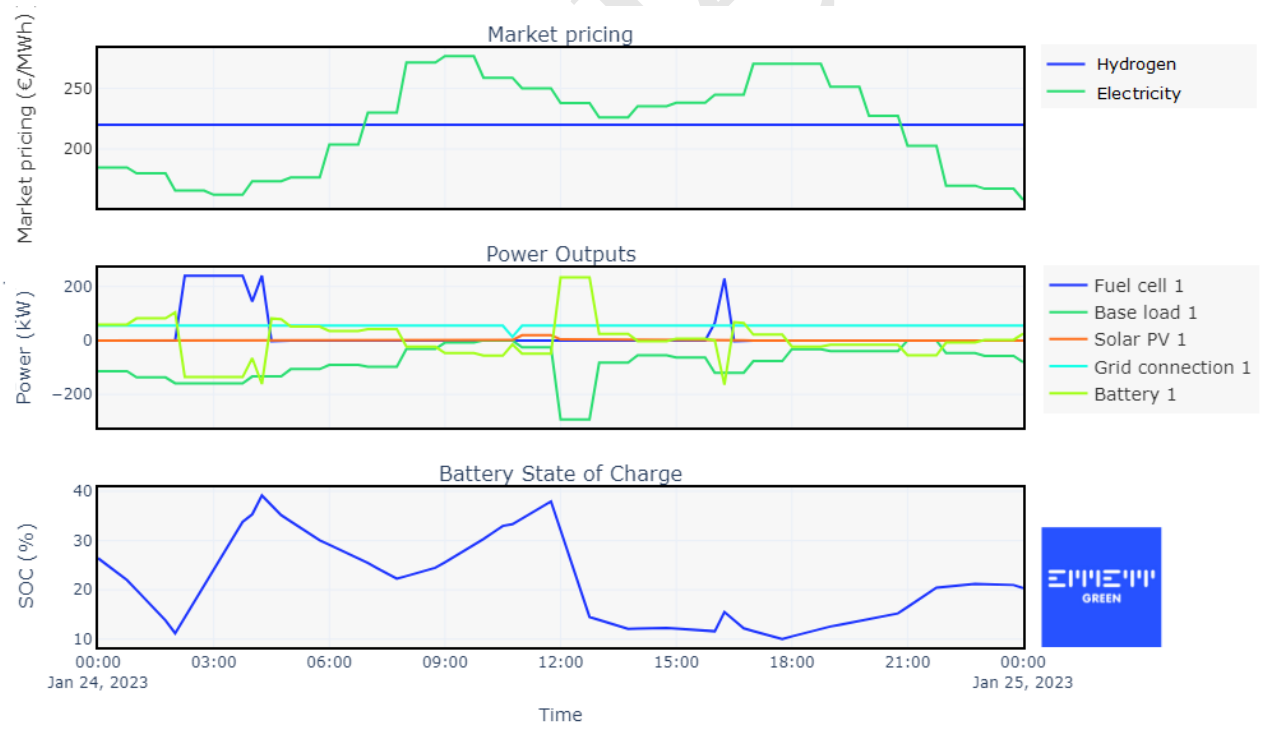

Fig. 12: Simulated results on a winter day with the rolling horizon approach (own work).

The results over the same 2 days as calculated by the fixed schedule approach are depicted in Figures 14 and 15. The fixed schedule approach requires some tuning depending on the site, forecast accuracy and year of operation. This analysis is covered in Section 4.3, while the optimal outcomes are presented here. Several observations are done while comparing the fixed schedule and rolling horizon approach.

Foremost, as the key driver for the implementation of the fixed-schedule approach, the computational time has been reduced to merely 3 s/day, representing a reduction of 96 %. This improvement results in an annual simulation of 25 min, down from 8 hr, proving particularly beneficial when many simulations

have to be completed. There is no established relation between problem size and solving time, due to the branch-and-bound algorithm [51]. Additionally, the inclusion of modern techniques like presolving, heuristics and parallelism, designed to accelerate large problem solving, further complicates the establishment of this relation. An example, of these improved routines is observed over the weekend where many zero-values occur and the simulation time drops by almost 50 %. Still, in the optimisations the amount of variables scale linearly with the amount of timestamps increasing from 50 to 800 in the fixed schedule and rolling horizon optimisations respectively. Besides the increased solving time, constructing the problem also requires progressively more time. Overall, the fixed schedule proves highly effective in reducing the computational burden.

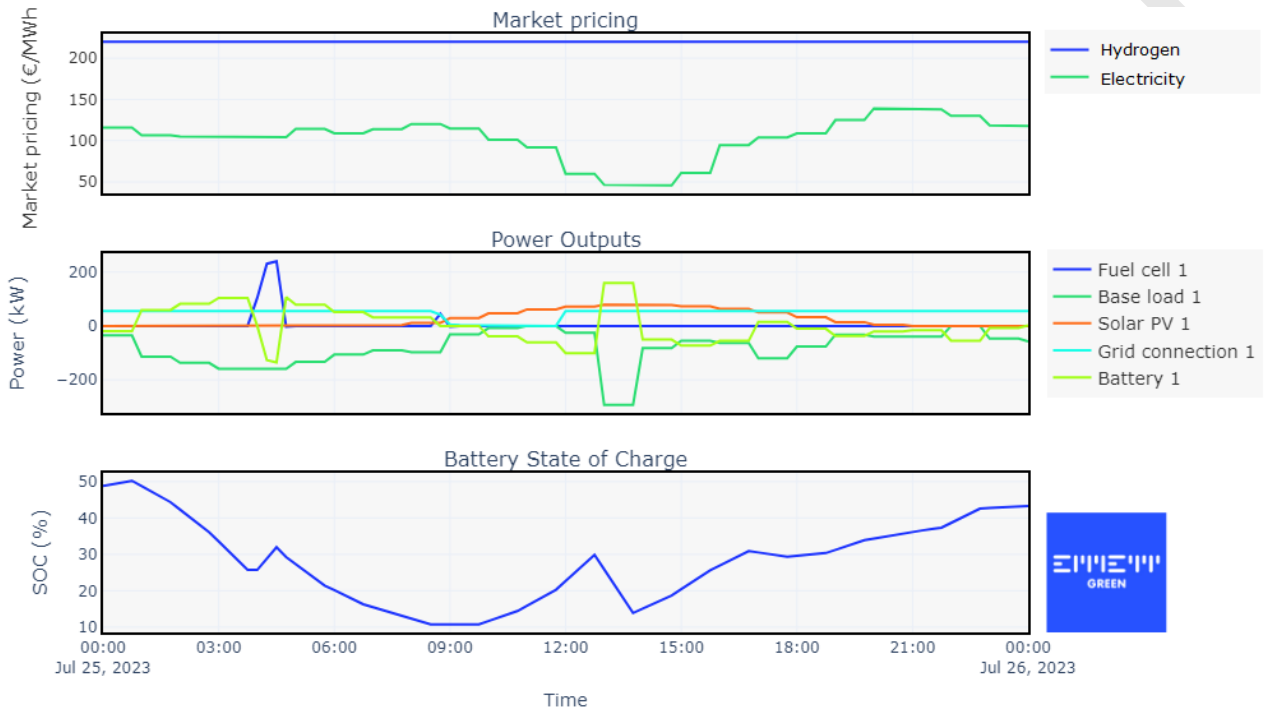

Fig. 13: Simulated results on a summer day with the rolling horizon approach (own work).

Another interesting observation is depicted in the bottom graph of Figures 12 to 15, depicting the SoC profiles of the battery during the day. In the rolling horizon approach the battery tends to charge only when a load peak (or negative prices) occurs within the horizon, resulting in many days starting with a relatively low SoC. The fixed schedule approach on the other hand oversees the full day hence it ensures a higher SoC at the start of the day, resulting in a lower fuel cell usage. In addition, the SoC margin accounted for in the scheduling approach allocates more energy to the battery to accommodate inaccurate predictions, as it cannot rely on the fuel cell when it is scheduled off. Leading to reduced fuel cell degradation albeit at the expense of battery degradation (indeed this is verified by the KPIs in Table4).

The impact of the proposed MLD framework is clearly reflected in the operational profile of the fuel cell. The amount of start-stop and load cycles is reduced to a minimum with the fuel cell predominantly operating at the maximum allowed power in the MP state. Moreover, throughout the entire year, not a single LP and HP state incident occurred due to the reduced conversion efficiency. Interesting is the profound difference in fuel cell activation times between both optimisations. Given that the battery has sufficient power to cover the load the rolling horizon uses the fuel cell when the battery is depleted. Figure 13 clearly demonstrates that the fuel cell charges the battery precisely 12 hours in advance, providing just enough energy to serve the load that arises at the prediction horizon. The downside of this approach occurs in this figure as well since the fuel cell is required to start up again at 9 AM due to the inaccuracy in load forecast, increasing the degradation. This raises the questions whether to include prediction margin in this optimisation as well. In contrast, the fixed schedule approach prefers activation of the fuel cell during high anticipated loads. Note that the prediction of

the load is taken as the average over both load profiles hence the offset in Figure 15. The scheduling difference is even more evident in the annual heatmaps displayed in Figures 16 and 17. Using the fixed schedule approach the operation of the fuel cell is concentrated around peak load hours for longer periods of time due to the scheduling optimisation interval. Whereas the rolling horizon approach has the freedom to start and stop more frequently.

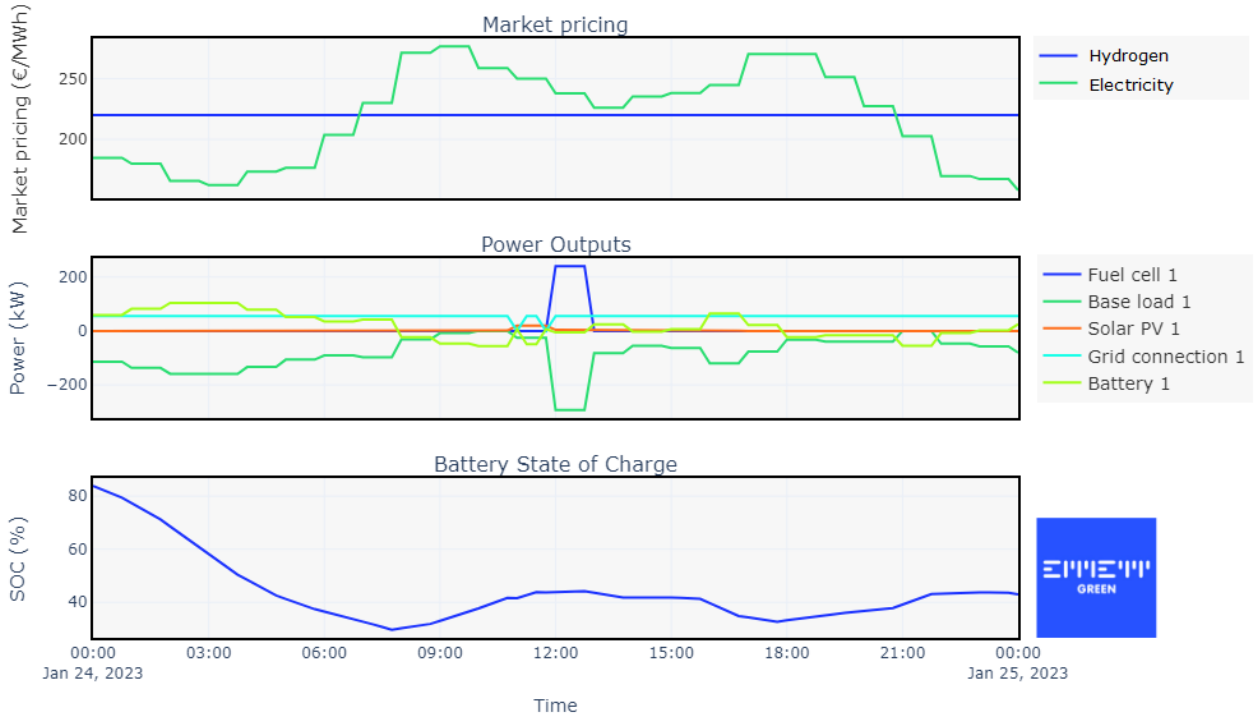

Fig. 14: Simulated results on a winter day with the fixed schedule approach (own work).

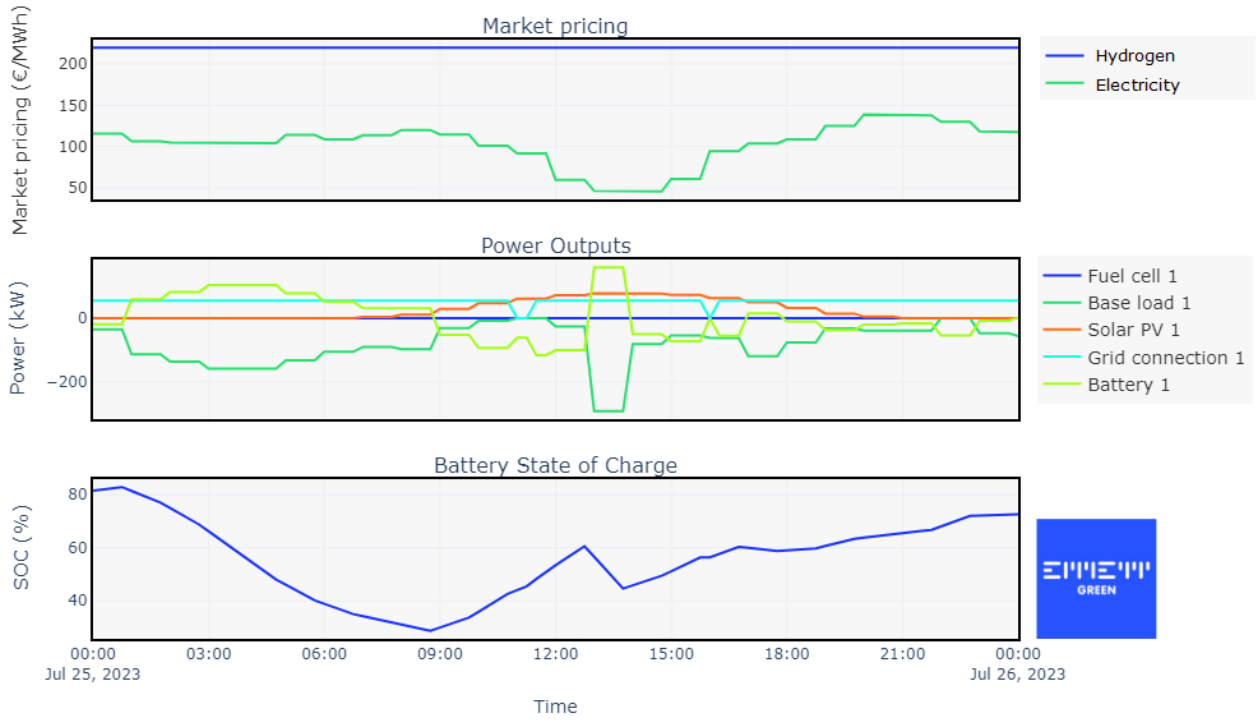

Fig. 15: Simulated results on a summer day with the fixed schedule approach (own work).

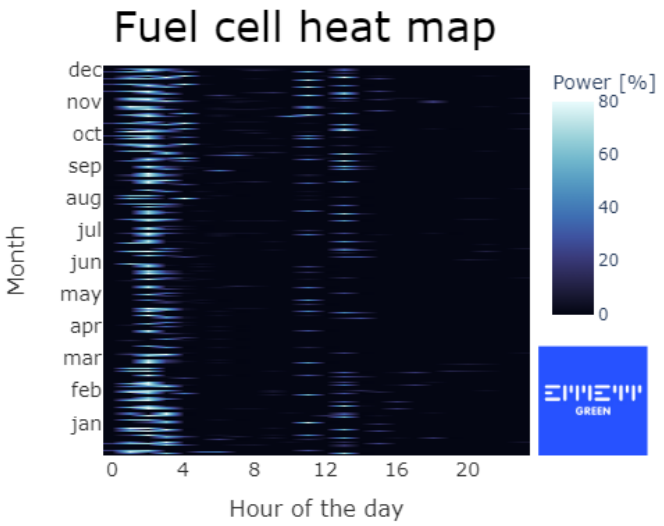

Fig. 16: Fuel cell power over the year with the rolling horizon approach (own work).

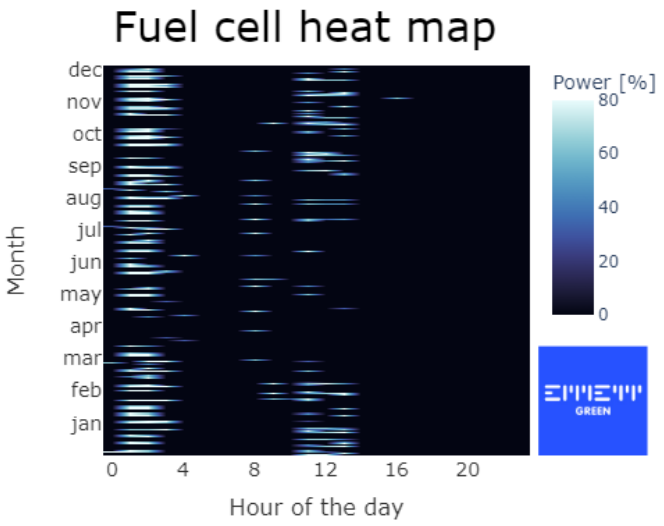

Fig. 17: Fuel cell power over the year with the fixed schedule approach (own work).

Looking critically at the initial results it was observed that solar generation was occasionally curtailed during the day even though the battery was not fully charged. This issue arose because the actual SoC being above the scheduled SoC, due to an underprediction of solar. Being not economically optimal, it was proposed to only apply the SoC penalty when the actual SoC falls below the scheduled SoC. As a result, solar utilisation increased from 65 % to 88.9 %. Although disallowing curtailment would maximise this value, it would render the system infeasible during solar-rich weekends.

4.1.a Benchmarks

The previous section proves the adequacy of the proposed models in managing the congested FCPB site. This section benchmarks the two main additions, the MLD framework and the forecasting approaches, by comparing a scenario without multiple timestamp optimisations and without the MLD framework. The former is achieved by simulating the site with only single timestep optimisations while the latter is achieved by removing all binary state and state switch variables, and assuming a constant efficiency over the entire power range. Additionally, a straightforward, non-optimisation-based strategy serves as the last benchmark. The RBS, as proposed by, [50] follows a hierarchical power distribution approach: solar energy is prioritised for load supply, followed by the grid, battery and fuel cell. Furthermore, the battery is consistently charged when solar or grid power is available and the fuel cell only switches on with a depleted battery and off when the battery is fully charged.

In the previous section, a daily power distribution has been examined to verify the behaviour during short periods. This section on the other hand revises only the cumulative results over the entire year, which are presented in Figure 18. In this figure the costs for hydrogen and electricity are retrieved directly from the measuring assets in the output data. The depreciation costs are calculated according to:

$$C^{FC}_{depreciation} = \text{CAPEX} \cdot \frac{SoH_{loss}}{SoH_{EoL}} \tag{5}$$

$$C^{BAT}_{depreciation} = \text{CAPEX} \cdot \frac{SoH_{loss}}{SoH_{EoL}} \tag{6}$$

where SoH_{EoL} is the end-of-life criterion, set to 10 % of OCV at nominal power, corresponding to 0.07 V [25] for the fuel cell. The battery end-of-life criterion is determined by the maximum number of cycles allowed. SoH_{loss} refers to the voltage degradation observed calculated by the extended lifetime model of Desantes et al. [25] in the case of the fuel cell. While it refers to the number of cycles for the battery, calculated by energy

throughput, where one cycle consists of 0 to 100 to 0 % SoC. The depreciation costs of the assets, combined with the costs of contracted electricity and hydrogen, are subsequently used for the calculation of the LCOE, as described by [52]:

$$LCOE = \frac{C^{FC}_{depreciation} + C^{BAT}_{depreciation} + C_{electricity} + C_{hydrogen}}{E_{load}} \tag{7}$$

where all costs are according to the annual total of 2023 and E_{load} is the sum of supplied energy over the same period, equal for all scenarios. The calculated LCOE's of the benchmarks simulations are depicted in Table 4, ranging from 227 to 327 €/MWh. This range is comparable to the results found by Fontava et al. [52] for a similar system, and estimates by NREL [53]. It should be noted that this is a simplification of the complete system and that the LCOE is highly dependent on system configuration, location and economic conditions.

The figure reveals several key observations. Firstly, the scenarios with only single timesteps perform worse in electricity and hydrogen costs aspects, while scoring better in depreciation (not all assets simultaneously) and calculation time. The reduced utilization of the battery in the first two scenarios is explained from the associated costs of its usage which typically do not result in a profit within one timestep. The addition of the MLD fuel cell model effectively reduces fuel cell degradation even without incurring higher hydrogen or electricity costs. Contrasting, the RBS approach stimulates the usage of the battery when its not fully charged, shifting the depreciation from the fuel cell to the battery. The outcomes are expected since the algorithm has the least amount of information available for decision making, therefore having to rely on the back-up fuel cell more often. Consequently, all these single timestep scenarios fail to serve the load demand when the power deficit increase. This was experimentally proven by reducing the fuel cell maximum power. Therefore, while it can be used as a benchmark given this system layout, that is where its functionality ends. As a result, no further attention is given to this approach, while it is anticipated that there are improvements to be made.

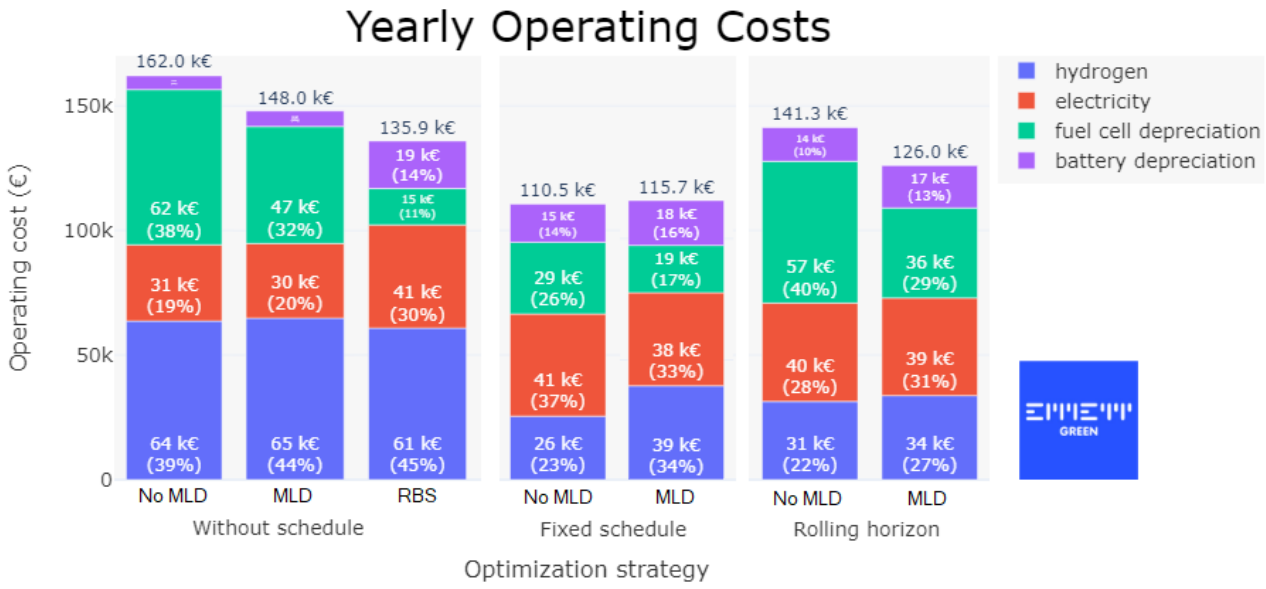

Fig. 18: Cost comparison for the proposed solutions and a benchmark (own work).

Regarding the fixed schedule results, a vast reduction of costs is achieved by reducing the fuel cell and hydrogen usage. By taking into account the upcoming day and hours this approach capitalises on inexpensive energy whenever the battery SoC permits it. Within this approach, the introduction of the MLD model substantially extends the fuel cell life, although it does not offset the increased hydrogen costs. This characteristic is explained by the simulation approach, which dictates the fuel cell state for an hour, whereas the stateless model can operate the fuel cell more flexible at 15 minute intervals. The rolling horizon approach shows a similar trend

when it comes to resource usage; however, the prediction horizon is deemed to short to fully leverage the MLD framework in reducing fuel cell depreciation. Conversely, in this scenario, the extended fuel cell life does offset the increased hydrogen costs.

Figure 19 depicts the source of energy for all scenarios, providing a deeper understanding of their behaviour. Firstly, it confirms that the fuel cell plays a more significant role in the single timestep scenarios. Secondly, it emphasises that the share of free solar energy is increased with the inclusion of longer optimisations. RBS specifically falls far behind in terms of solar utilisation since it fails to reserve battery capacity. Furthermore, increased hydrogen usage does not necessarily correlate with greater degradation, as evidenced by comparing scenarios with and without MLD framework. Moreover, it is observed that the MLD framework necessitates the battery to compensate for the fuel cell, which aligns with the expected roles of fast and slow-acting assets. It is also noteworthy that while the sum of solar, grid and fuel cell power appears to always be 100 %, the actual sum is slightly higher due to the 95 % efficiency of both charging and discharging, depending on the extent of battery usage. A comparison of the charging and discharging contributions verifies that 10 % of the energy is lost during battery storage.

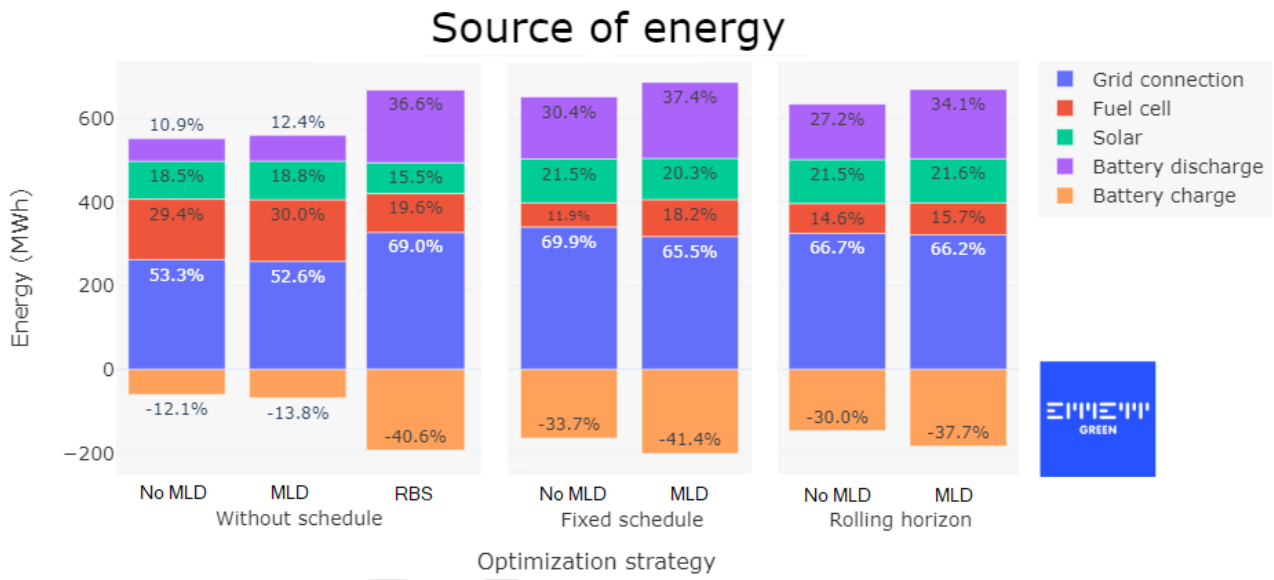

Fig. 19: Origin of energy that serves the load demand for the proposed solutions and a benchmark (own work).

Figure 20 dives deeper into the causes of degradation for the presented scenarios. It is highlighted that the applied degradation model, as proposed in [25]), is derived from an experimental fuel cell study in [27]. While this model is representative, it is important to acknowledge that commercial fuel cell degradation can deviate.

The strategy incorporated in the MLD framework specifically targets the degradation components from this model by reverse engineering the costs related to the identified degradation conditions. The resultant behaviour after applying the MLD model is evident across all optimisation scenarios. Low- and high-power degradation are entirely avoided by raising the minimum power, benefiting both the degradation costs as well as the operating hours. The RBS approach is effective in reducing the number of fuel cell operating hours, however neglecting the notion of high power degradation. Furthermore, the model aims to reduce the number of start-stop cycles, a goal achieved in the fixed schedule and rolling horizon approach. It can be concluded that without the information from future timesteps the model is not able to avoid unnecessary start-stop cycles.

Besides the calculated SoH according to the operation profile, the number of operating hours, as presented in Table 4, provides a complimentary measure for assessing SoH. Given the assumed lifetime of 25.000 hr [43], and an EoL criterion of 10 % [25] there is a profound gap between both SoH indicators. The cause of the mismatch is found in the application of back-up power which is paired with frequent start-stop cycles and short power producing periods. The impact of the MLD formulation remains evident, reducing the amount of operating hours by a factor of 2 and 3 for the fixed schedule and rolling horizon approaches.

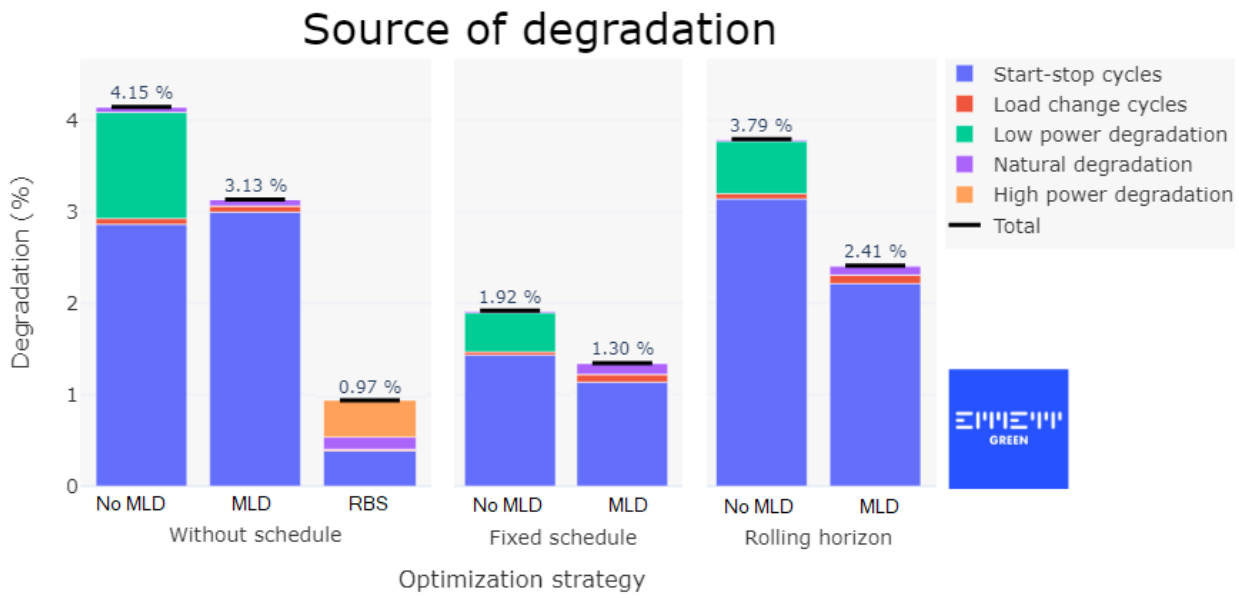

Fig. 20: Contributing factors in fuel cell degradation for the proposed solutions and a benchmark (own work).

On the other hand, degradation related to changing the power level is slightly increased by the MLD framework. According to the applied model, the magnitude of load change degradation is determined by the delta of power as well as the frequency of power fluctuations, where the reference degradation per cycle is a factor of 35 lower than with start-stop cycles. In scenarios without health-aware operation, there are more load fluctuations but their magnitude is insignificant. In contrast, the scenarios that include the MLD framework exhibit larger deviations caused by switching between states or from the minimum to maximum values within a state. Lastly, a notable feature of the proposed model is the ability to set the device in STB mode to avoid a cold start. Over the year, given this specific system layout, no instances were observed where it was more economical to avoid a start-stop cycle by temporarily switching to STB. This outcome can be attributed to the battery's capability to supply the maximum power required by the load. To conclude the benchmark tests, an overview of the most important performance indicators is depicted in Table 4.

Table 4: Summary of KPI's for all benchmark simulations.

optimisation approach	**Calc. time (s/day)**	**FC SoH (%)**	**FC usage (hr)**	**Bat SoH (cycles)**	**Utilization solar (%)**	**Utility cost (k€)**	**LCOE (€/MWh)**
No schedule	0.5	95.8	2465	55	82.0	94.2	327
+ MLD	1.5	96.9	1887	63	83.4	94.8	299
+ RBS	1.5	99.0	407	190	69.3	102.3	274
Fixed schedule	0.8	98.1	1014	152	94.9	66.5	227
+ MLD	3.0	98.7	477	184	91.5	77.7	234
Rolling horizon	9	96.2	1283	136	94.7	70.8	285
+ MLD	80	97.6	416	169	94.9	72.8	254

4.2 Rolling horizon sensitivity

The rolling horizon approach proves to be highly effective in controlling the FCPB site, especially in terms of reducing the utility costs. However, as already pointed out the in the previous section, in terms of fuel cell degradation prevention it lacks behind the fixed schedule approach. A possible explanation is found in the reduced prediction horizon between the two approaches. The literature presented in Table 2 heavily utilises a rolling horizon, however none of the studies include an analysis on how long this horizon should be. Therefore, this section investigates the impact of the prediction horizon length. Three scenarios are presented in Figure 21, where the second part of the dynamic timestep is extended by four hours. The results of all KPI's are summarised in Table 5.

Table 5: Summary of KPI's depicting the impact of the prediction horizon.

optimisation approach	Calc. time (s/day)	FC SoH (%)	Bat SoH (cycles)	Utilization solar (%)	Utilization grid (%)	Utility cost (k€)	LCOE (€/MWh)
4	50	96.9	155	94.9	83.8	83.4	294
8	65	97.5	164	94.9	91.1	75.9	262
12	80	97.6	169	94.9	93.8	72.8	254

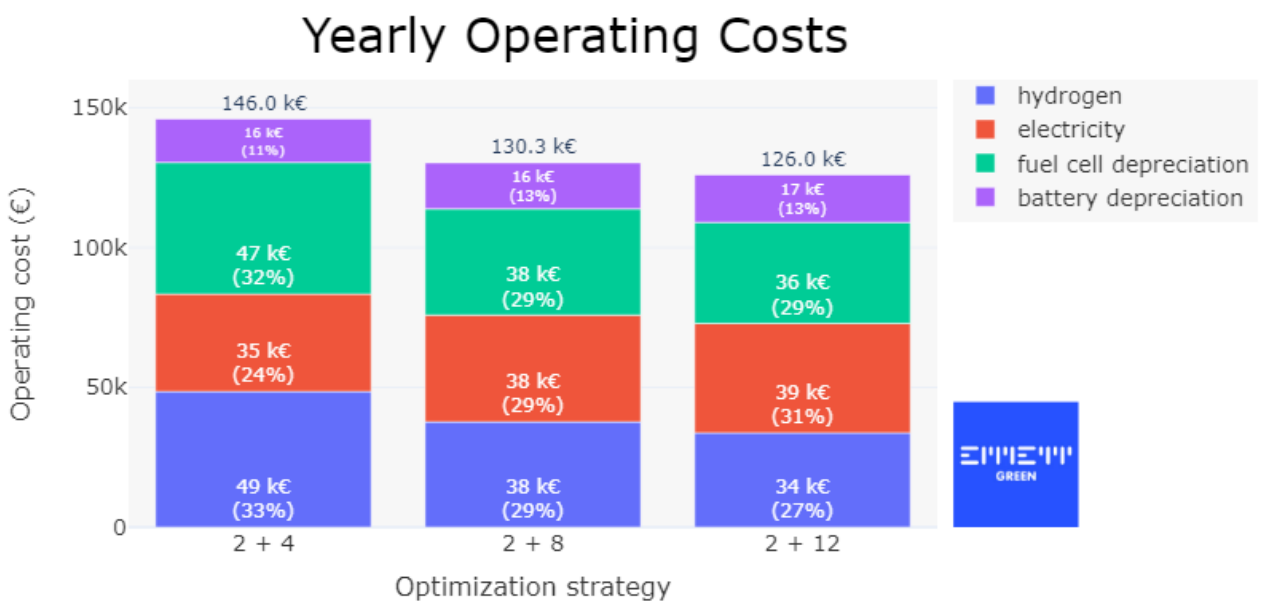

Fig. 21: Cost sensitivity given various prediction horizons (own work).

First, the computational time of these scenarios increased linearly from 50 to 80 s/day, while the cost reduction did not follow a linear pattern. The diminishing added benefit together, combined with the inclusion of unknown electricity prices in the prediction window, prevents the extension of the horizon beyond 12 hr. As expected, providing more information to the optimisation results in better economic decisions. However, the added benefit of more information diminishes with an increasing prediction horizon. For the MLD framework, scheduling as far in the future as possible is deemed particularly relevant, leading to considerable improvement in fuel cell lifetime.

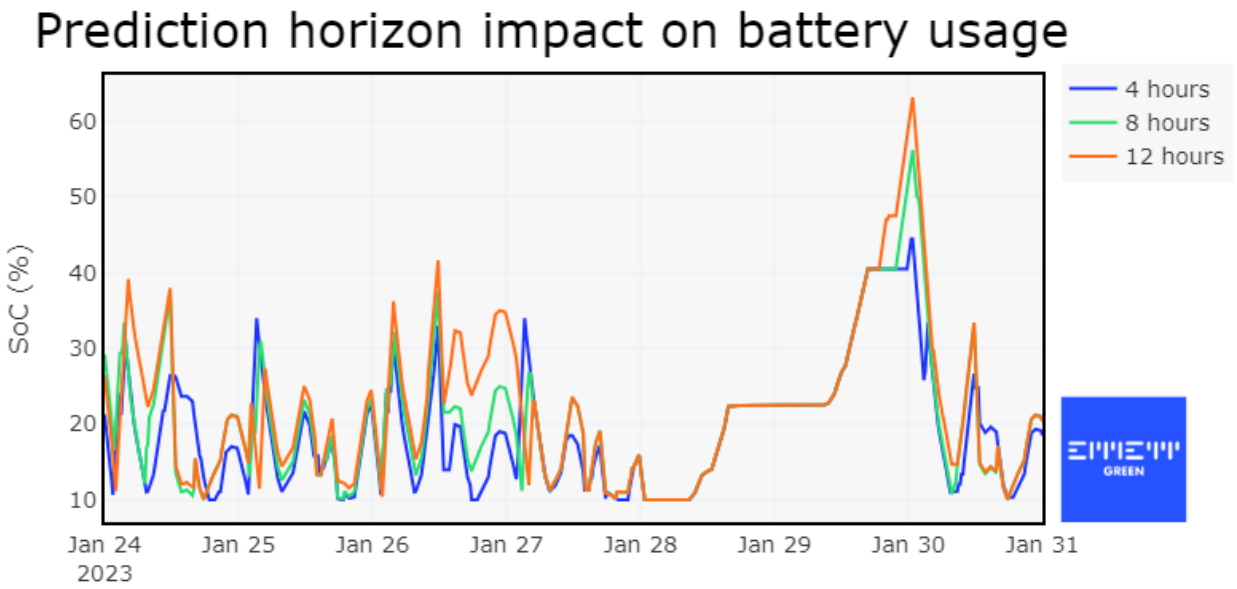

Fig. 22: Battery usage given various prediction horizons (own work).

Anticipating the load by charging the battery, especially in power-deficit configurations, is the primary reason for the reduction in hydrogen usage for longer horizons. This effect is clearly demonstrated by the SoC curves in Figure 22. During a winter week with low solar generation the battery is not fully charged over the weekend. Consequently, to fulfill the demand on Monday without resorting to the fuel cell, the algorithm starts charging the battery as soon as the load appears on the horizon. This process is more effective with a longer lead time. In Table 5 it is indeed verified that the grid utilisation increases when extending the horizon. This behaviour is reflected in the reduction of operational cost, and the slight increase in battery usage. Secondly, it is interesting to note that the solar utilization is exactly equal in all horizons, indicating that solar energy is only curtailed when the battery is fully charged during solar-rich weekends.

4.3 Fixed schedule sensitivity

Similar to the rolling horizon approach, the fixed schedule optimisation benefits from future predictions. The importance of anticipating future behaviour has been demonstrated in previous sections. This insight can be applied to extend the scheduling horizon to, for example, two or three days, resulting in a rolling optimisation approach with a relatively coarse interval. It should be noted that since the optimisation is performed only once a day, after the electricity prices for the next day are known, the horizon can be extended to 36 hours without requiring price predictions. However, extending the horizon to include more days would necessitate the estimation of electricity prices, similar to the estimation of solar generation and demand load. As these forecast are not available and the simulations are performed in the past, perfect foresight is assumed in these simulations. The outcomes of extending the scheduling horizon are presented in Figure 23 and Table 6.

The outcomes align with the expectations based on the rolling horizon results. Incorporating additional information into the decision-making process enhances the results, albeit at a diminishing rate. Again, the extended horizon is effective in applying the battery to prolong the fuel cell life and increase the grid utilization. One outlier was identified in the table: a reduced solar utilization accompanied by an increased utility cost for the two-day simulation. No concrete explanation for this behaviour has been found, however due to the small deviations, it is be considered as a simulation error. Additionally, computational effort has increased significantly, particularly since only one of the 97 $(24 \cdot 4 + 1)$ simulations has been adjusted. It can be concluded that the increased computational time and the necessity for proper energy forecasts do not justify the marginal performance improvement.

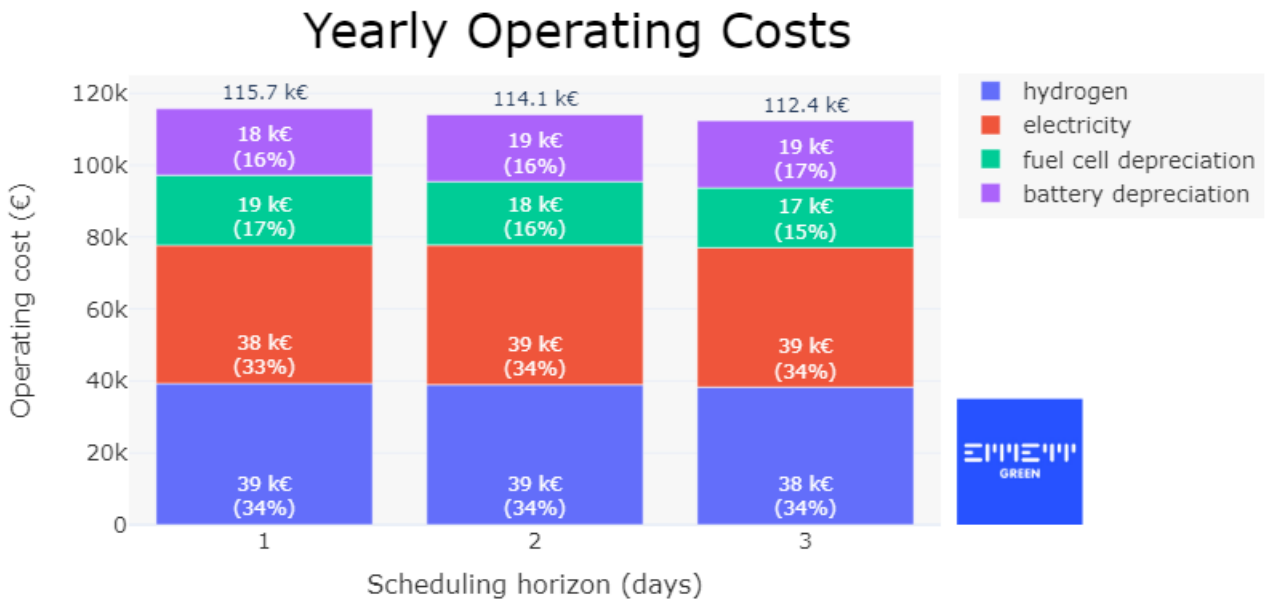

Fig. 23: Cost sensitivity given various scheduling horizons (own work).

Table 6: Summary of KPI's depicting the impact of the scheduling horizon.

optimisation approach	Calc. time (s/day)	FC SoH (%)	Bat SoH (cycles)	Utilization solar (%)	Utilization grid (%)	Utility cost (k€)	LCOE (€/MWh)
1	3.0	98.70	184	91.5	91.3	77.7	234
2	4.5	98.82	186	88.9	92.5	77.8	230
3	7.0	98.89	187	90.2	92.7	77.0	227

4.3.a Safety margins

As mentioned in Section 3.3.b, the fixed schedule approach requires additional parameters to take uncertainties into account. These parameters are referred to as the safety margins and are present as load margin and soc margin. The former introduces an overestimation of the load into the scheduling optimisation, thereby scheduling the fuel cell more aggressively. While the latter decreases the SoC window in the scheduling optimisation, keeping energy in reserve to be used when energy deficits occur in real time. In addition, to track the reference SoC a penalty is introduced which determines the amount of slack permitted. This section describes a short analysis on the impact of the different margins performed on the FCPB site with a 500 kWh (0.5 C) battery.

To develop insights into the different strategies that account for scheduling uncertainties, an analysis has been performed in where full credit was attributed to a single strategy. The resulting impact on different cost contributions in the system is depicted in Figure 24, where all percentages are relative to the total cost of the most effective strategy. The analysis aimed to determine the lowest possible margin (with increments of 5 %), which allowed the system to operate without becoming infeasible. The resulting combination of feasible margins, as shown in Table 7, correspond to the outcomes of Figure 24. From the results, it can be derived that both margin strategies can individually solve the uncertain scheduling issue. However, the chosen approach severely affects the operating cost of the system.

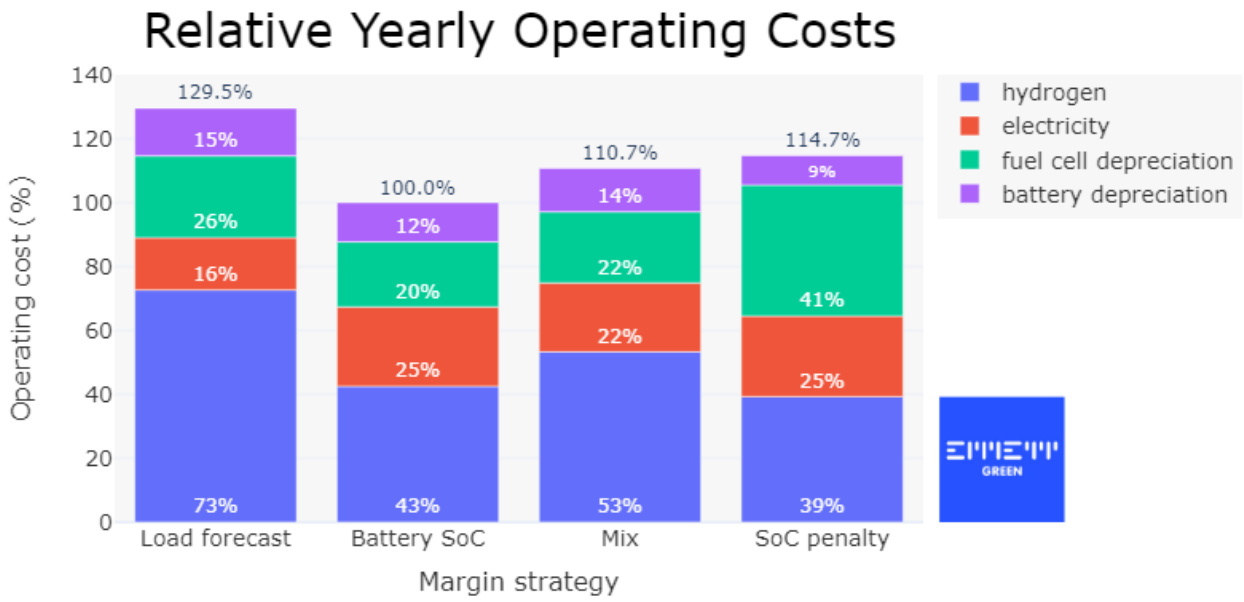

Fig. 24: Impact of applying different margin strategies to the system economy (own work).

By inflating the expected load, the scheduling optimisation resorts to the fuel cell to compensate the energy deficit, as the grid connection and solar inputs are already at maximum capacity. According to the MLD methodology the fuel cell state remains unchanged in the real-time optimisation, where it encounters less load than expected, leading to increased fuel cell and battery usage. Moreover, an increased share of solar power is curtailed due to the battery reaching full capacity. In contrast, when the minimum battery SoC limit is increased during scheduling, the grid and fuel cell primarily cover the load, while the reserved battery capacity manages the mismatch in scheduled and actual load. Within the latter approach, it is important to note that the SoC margin has an upper bound related to the size of the battery and other components. Specifically, the other energy sources should be able to recover the SoC from a low value to the minimal scheduled SoC value within a single timestep. If this criterion is not met, a combination of margins should be applied.

Lastly, the impact of the SoC deviation penalty was assessed by adjusting its value. An effective value was determined to be 2.5 €/% (0.5 €/kWh for the given battery). The operating cost of the battery is valued at 0.05 €/kWh, making this a strict penalty. Gradually lowering the penalty does not result in different behaviour until it decreases to 1 €/%. The non-continuous behaviour can be explained by the optimisation formulation, where decisions are typically binary, determined by a certain threshold. Once the deviation penalty was sufficiently reduced, the battery made more short-term oriented decision in the real-time optimisation, necessitating other margins to increase, thereby diminishing the potential cost savings. From Table 7 and Figure 24 it is clear that the possible benefits of a reduced deviation penalty are offset by the increase in the other two margins and a significantly increased fuel cell depreciation.

Table 7: Value of margin parameters applied in the comparison.

Margin Strategy	**Load forecast margin (%)**	**Scheduled battery SoC margin (%)**	**SoC deviation penalty (€/%)**
Load forecast	55	0	2.5
Battery SoC	0	50	2.5
Penalty	60	60	1
Mix	25	25	2.5

4.3.b Demand forecast

The primary goal of the FCPB site is to accommodate reliable charging of electric construction vehicles. Inherent to this objective is a degree of uncertainty regarding the timing and type of vehicles being charged. Section 3.2 presents two distinct daily charging profiles that can be anticipated, where the aggregation of a numerous vehicles already provides a degree of smoothing. When the scheduling optimisation is performed, a prediction of the load must be included. Three important features indicating the prediciton's accuracy are the total daily consumed energy, the peak load magnitude and the peak load timing. As the previous section demonstrates that applying a SoC margin is most profitable, the impact of the chosen load forecast is assessed based on the battery SoC, as depicted in Figure 25.

For reference, a simulation with perfect foresight has been plotted, along with one assuming the 'other' day (Figure 10), and one using the average. For readability, only the scheduled SoC of the perfect foresight case is plotted, as all scenarios behave similarly. For this specific week the SoC margin was set to 25 %, observable at the start of the weekend where all schedules aim to deplete the battery by the end of the day. The main observation from this graph are the 24-hr scheduling horizon, which explains the lack of solar usage on Saturday, and the correlation between prediction accuracy and required SoC margin. The alternating load profile results in days of underestimation (even days) and overestimation (odd days) which is immediately reflected in the SoC profile of the predicted scenario. Vast downward deviations occur on the 24th, 26th and 30th while upwards deviations occur on the 25th and 31st.

Taking the average of both profiles as a prediction mitigates one of the three inaccuracy measures, specifically the timing of the peak load. This average demand profile has two peaks of significantly reduced magnitude. Consequently, the resulting SoC profile shows a reduction in the downwards SoC deviations, suggesting that the magnitude of the peak is less critical in the prediction. This conclusion is supported by the state scheduling of the fuel where the freedom of selecting its power remains, as long as it is scheduled in a power producing state. Due to the increased performance while keeping uncertainty, the average of the demand load has been equipped throughout this thesis as the load prediction.

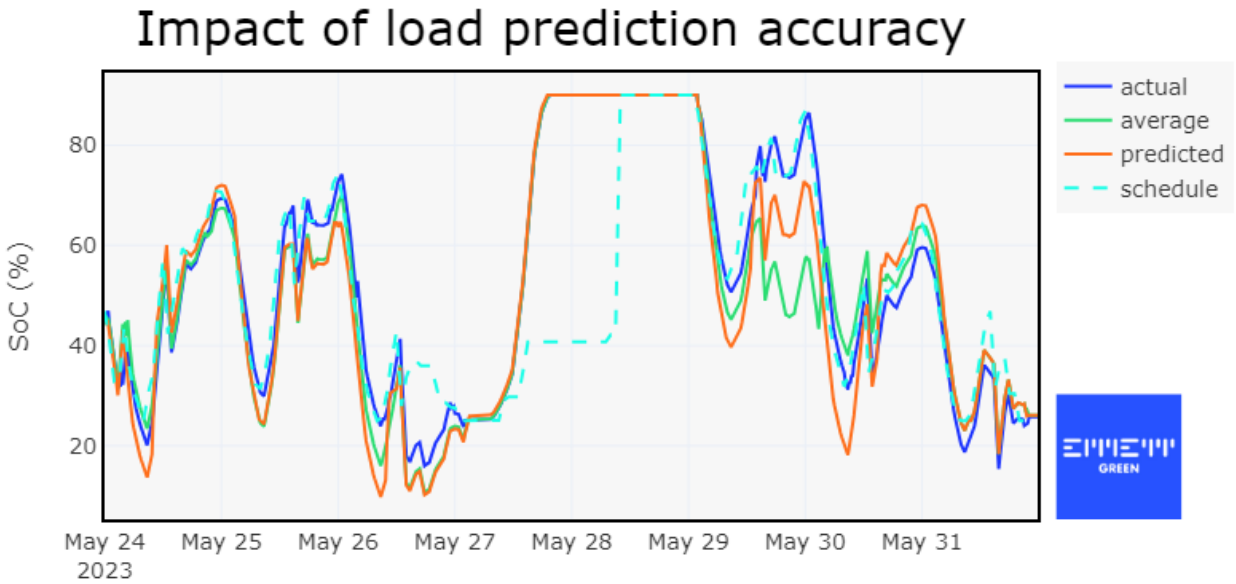

Fig. 25: Observed battery slack as a result of the applied load forecast (own work).

4.4 Site sensitivity

With the efficacy of the methods validated and their sensitivities identified, an economic analysis of the FCPB site is performed. To this end, the scheduling approach is employed for its rapid computational time. The optimisation parameters include a scheduling horizon of 1 day, a SoC deviation penalty of 0.5 €/kWh, a preference

for using only a SoC margin, a load margin when required, and the average of the load profiles as a prediction.

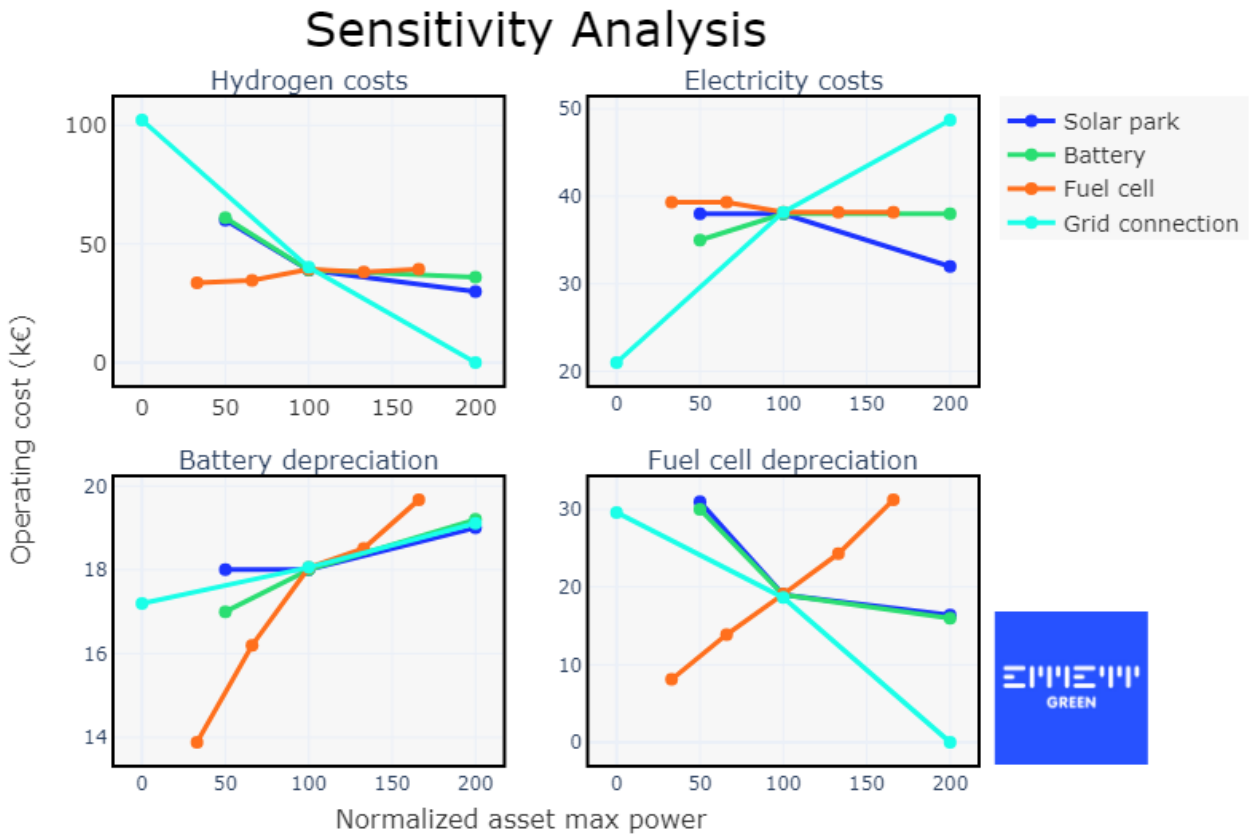

Fig. 26: Summary of the sizing analysis performed (own work).

While keeping all other assets constant, the economical impact of the maximum power of the solar park, battery, fuel cell and grid connection is investigated. As before, the contributors to the operating cost are the electricity and hydrogen usage, as well as the fuel cell and battery depreciation. Although, larger grid connections and solar parks are paired with higher investment costs as well, it is assumed that the operational pattern does not impact the lifetime or costs of these assets.

4.4.a Fuel cell power

Figure 26 presents the costs per contributor as a function of the asset's maximum power for all investigated assets. As the backup power asset, the optimisation aims to minimise hydrogen costs without excessively impacting the fuel cell's lifespan. The cost impact as a function of the fuel cell power, ranging from 100 to 500 kW, is highlighted in orange. The top two graphs show that the impact on energy sources is minimal. A minor shift from electricity to hydrogen is attributed to the increased minimal power of the larger fuel cell.

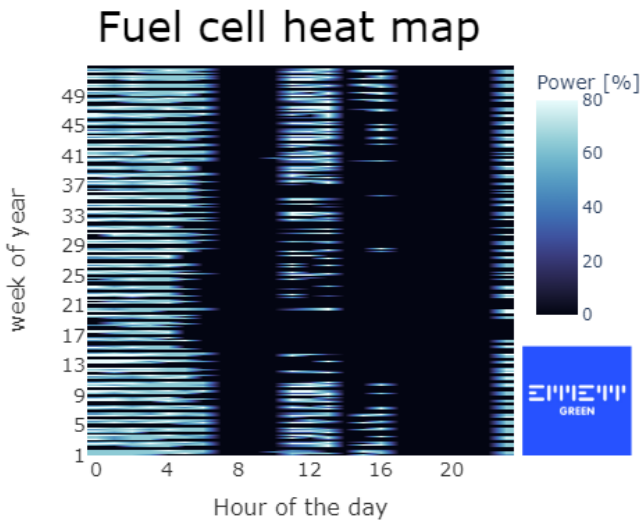

Fig. 27: Heatmap of a 100 kW fuel cell, showing the daily and seasonal patterns (own work).

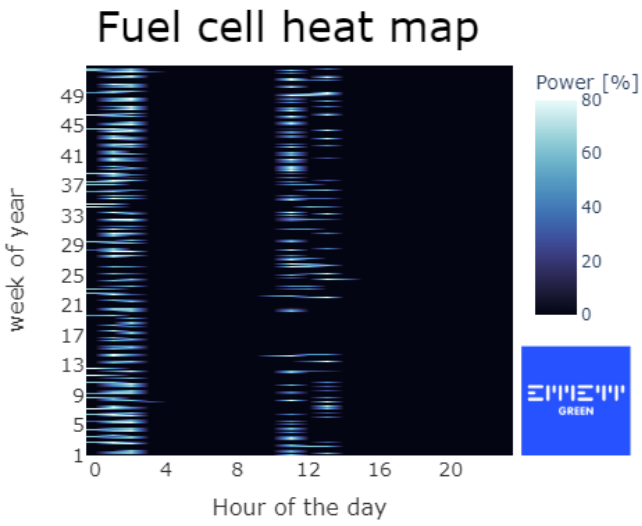

Fig. 28: Heatmap of a 500 kW fuel cell, showing the daily and seasonal patterns (own work).

Conversely, from a depreciation perspective, considerable changes occur. As indicated by Equation (5), both degradation and initial CAPEX influence the total depreciation cost. Increasing the fuel cell size allows the optimisation to reduce operating hours, as shown in Figures 27 & 28. However, as Figure 20 demonstrates, start-stop cycles are the primary contributor to the total degradation, especially after the MLD framework implementation. The heatmaps reveal that while the number of start-stop cycles decreases, it is not substantial, resulting in a SoH improvement from 97.8 % to 98.8 % for the smallest and largest fuel cell, respectively. This roughly doubles the fuel cell's lifespan, but increases the investment cost five-fold. In addition, the sensitivity analysis indicates an accompanied steep increase in battery depreciation. This increase is directly caused by the reduction of fuel cell operating hours at an increased power level. Overall, it can be concluded that over-sizing the fuel cell negatively affects the systems economy by increasing both battery and fuel cell depreciation.

4.4.b Battery capacity

The green lines in Figure 26 depict the influence of battery capacity on the economic performance of the system. In the semi off-grid configuration the battery is the key in flexible operation and the selection of the preferred energy source, as is elaborated in Figure 29.

Initially, the priority is given to free solar energy, with the 2 MWh battery capable of utilizing 100 %, compared to 78.3 and 88.9 % for the 0.5 and 1 MWh batteries respectively. Secondly, the grid utilization increases from 80.9 % to 92.5 % for the smaller batteries and decreases again to 91.1 % for the large battery. This reduction for the largest battery is attributed to the increased solar contribution, although it was expected that grid utilization would increased further toward 100 %, thereby mitigating hydrogen usage. A further increase in grid utilization could be realised by extending the scheduling horizon; however, reaching 100 % is heavily dependent on the load profile. The above described shift in energy sources is evident in Figure 29 and the associated energy costs in Figure 26.

Consequently, fuel cell depreciation is reduced while a slight increase in battery depreciation is observed. Unlike the case with increasing fuel cell size, the increase in battery size has a lesser impact on the depreciation cost. The battery lifetime is determined by the amount of cycles underwent, which is a function of total energy throughput and capacity. As shown in Figure 29, the energy throughput is only marginally increased, while the capacity is doubled. Therefore, the batteries undergo 347, 187 and 97 cycles respectively. Therefore it is concluded that the battery throughput is a site specific variable only slightly affected by the battery size.

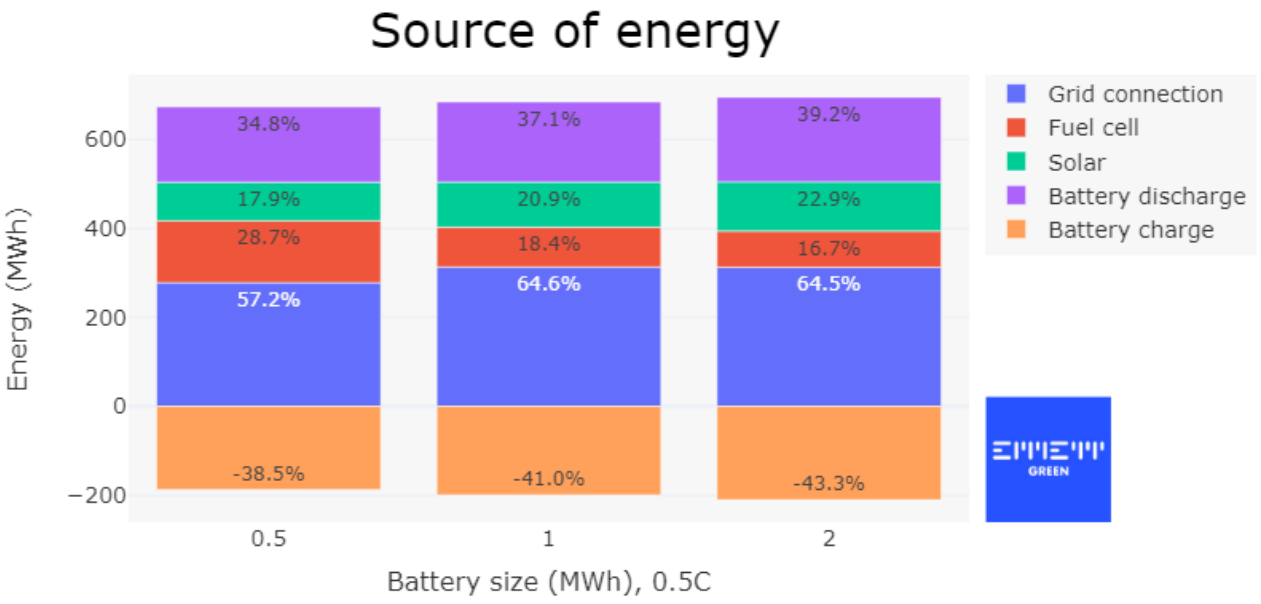

Fig. 29: Influence of battery sizing on the energy source distribution (own work).

4.4.c Grid connection

The limited grid connection heavily influences the characteristics of the FCPB site, both from a simulation and technical perspective (See the literature study in Appendix D). Under current legislation in the Netherlands, a maximum connection of 55 kW is allowed for building connections, resulting in a 30 % energy deficit for the applied load profiles. Nonetheless, it is important to evaluate the proposed optimisation framework in fully, semi and off-grid configurations. The cost impact is displayed in Figure 26, with the fully off-grid scenario omitted to maintain readability. In addition, the distribution of energy sources is shown in Figure 30.

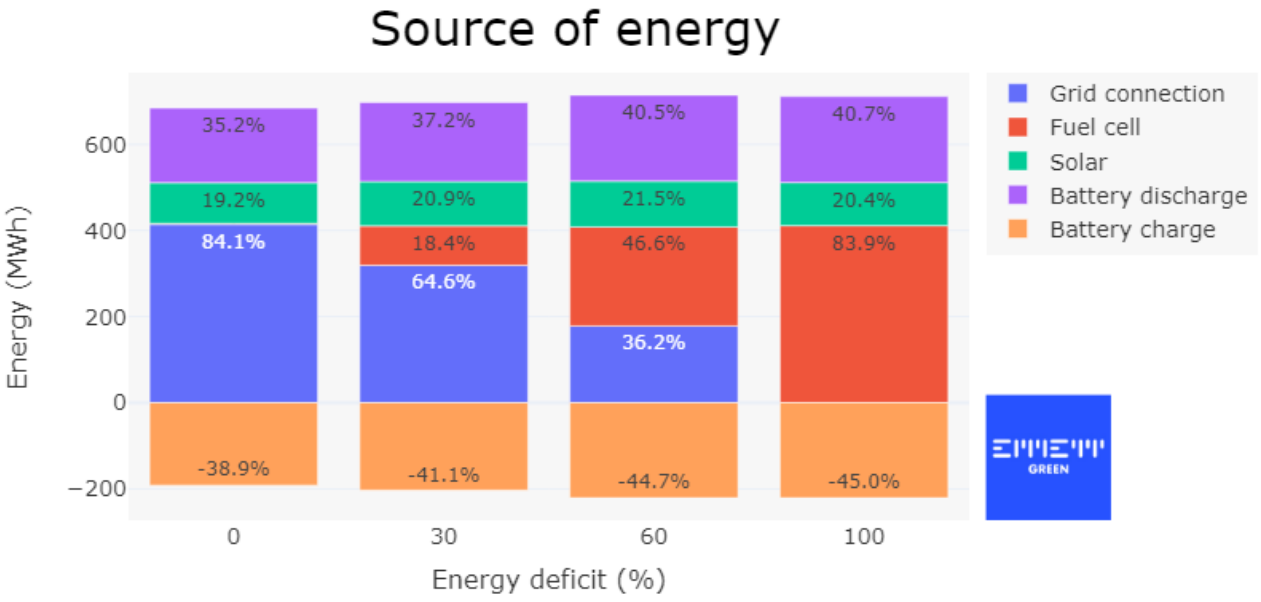

Fig. 30: Influence of grid configuration on the energy source distribution (own work).

The energy deficit measure is defined as 100 % minus the ratio of maximum grid offtake to total load during all weekdays. Therefore, in the 30 % deficit scenario, a maximum of 70 % of electricity can be sourced from the grid if weekend are not taken into account. The power plots show that the grid is minimally engaged in the

weekend except for days with negative prices. In practice, maximum grid utilization is not reached due to the inclusion of solar power and the specific load profile shape. The cost analysis reveals a major impact of the grid connection size, due to the cost difference between electricity and hydrogen. Furthermore, it is observed that the importance of the battery increases as the grid size is reduced, resulting from the increased fuel cell usage. Moreover, the absence of fuel cell usage when no energy deficit exists, indicates that the power deficit is simultaneously resolved for this specific system configuration. In conclusion, the grid connection has the largest influence on the system's economical perspective and the proposed model's performance is insensitive to the grid configuration.

4.4.d Solar power

Lastly, the influence of the solar park is examined. For every semi off-grid location, local generation and appropriate management of intermittency are crucial for self-sufficiency. Therefore, increasing the size of the solar park should be beneficial for the system economy, as confirmed by Figure 26 for all costs except battery depreciation. Figure 31 demonstrates the shift in resources for several solar park sizes.

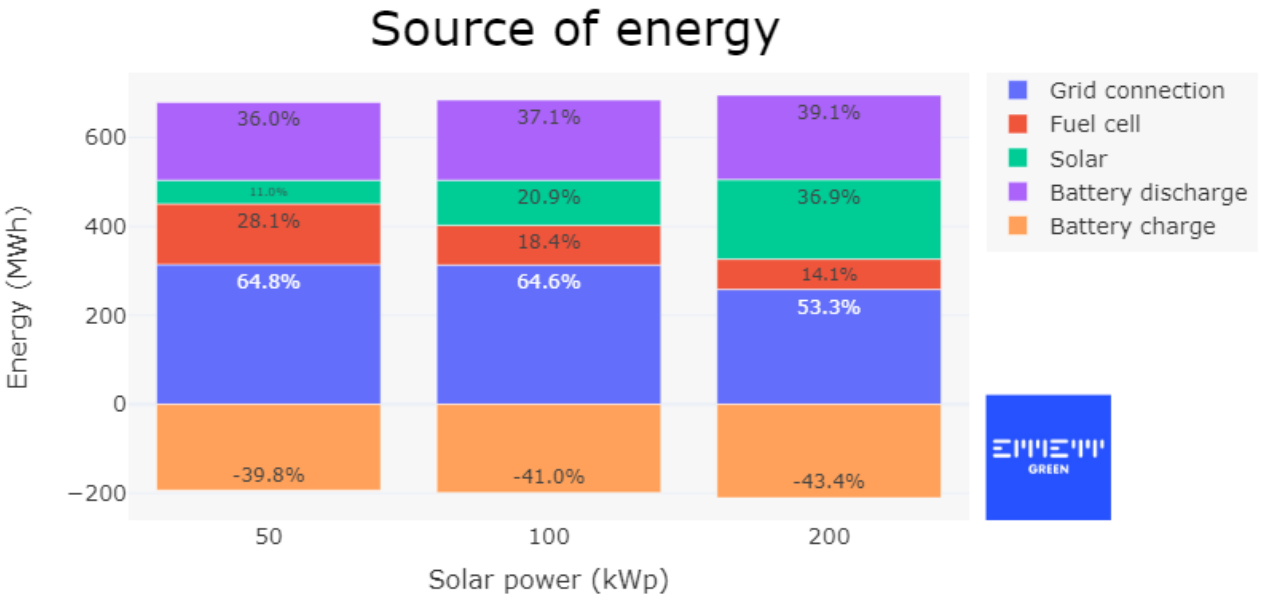

Fig. 31: Influence of solar park on the energy source distribution (own work).

In the 50 and 100 kWp solar parks configurations, near maximum grid utilization is observed (30 % energy deficit), hence the reduction of solar is compensated by the fuel cell. Conversely, the fuel cell cannot fully benefit from the increase to a 200 kWp installation due to the timing mismatch between peak powers. Instead, the additional solar power replaces a combination of fuel cell and grid power. Solar utilization rates are 96.0, 91.5 and 80.7 % for the 50, 100 and 200 kWp plants respectively. Since the investment cost of the solar park is not included in the analyses, it raises the question whether the decrease in total operating cost justifies this higher investment. From Section 4.4.b it is evident that the solar utilization is influenced by the battery size, suggesting that a larger solar park is more advantageous when the battery size is increased accordingly.

5 GENERAL DISCUSSION

This section discusses the previous results in a broader context and compares them to related literature. The first part provides an overview of all KPIs, followed by the discussion in the second part.

5.1 Simulation overview

Table 8 depicts the KPI's for all simulations concluded over the year 2023. The row 'Fixed schedule + MLD' shows the reference case, with a 1-day scheduling horizon, a SoC margin, a 300 kW fuel cell, 1 MWh battery, 30 % energy deficit and 100 kW solar power. In the rolling horizon sensitivity analysis, the reference case is 'Rolling horizon + MLD' with a 2 + 12 hr horizon. The margin analysis is performed on a 0.5 MWh battery.

Table 8: KPI overview of all performed simulations.

Config	Calc. time (s/day)	FC SoH (%)	Bat SoH (cycles)	Utilization of solar (%)	Electricity cost (k€)	Hydrogen cost (k€)	Total cost (k€)	LCOE (€/MWh)
Benchmarks								
No schedule	0.5	95.9	55	81.3	30.6	63.7	162.0	327
+ MLD	1.5	96.9	62	81.2	29.9	64.8	132.9	299
+ RBS	1.5	99.0	190	66.9	41.4	60.8	135.9	274
Fixed schedule	0.8	98.1	170	94.9	40.9	25.5	110.5	227
+ MLD	3.0	98.7	184	91.5	38.4	39.2	115.7	234
Rolling horizon	9.0	96.2	136	94.7	39.5	31.3	141.3	285
+ MLD	80	97.6	169	94.9	39.1	33.7	126.0	254
Rolling horizon sensitivity								
2 + 4 (hr)	50	96.9	155	94.9	34.8	48.5	146.0	294
2 + 8 (hr)	65	97.5	164	94.9	38.2	37.6	130.3	262
Fixed schedule sensitivity								
2 (days)	4.5	98.8	186	88.9	38.8	38.9	114.1	230
3 (days)	7.0	98.9	187	90.2	38.7	38.2	112.4	227
Fixed schedule margins								
Load forecast	3.0	97.3	415	85.2	17.5	113	192.3	388
Mix	3.0	97.7	392	82.6	27.5	82.6	163.8	331
SoC penalty	3.0	96.5	259	77.3	34.1	53.9	153.9	311
Fuel cell sizing								
100 (kW)	3.0	97.8	156	93.1	36.2	45.2	108.1	219
200 (kW)	3.0	98.1	179	93.4	35.1	49.7	121.7	246
400 (kW)	3.0	98.8	196	91.5	38.2	40.7	123.3	249
500 (kW)	3.0	98.8	201	92.1	37.8	41.6	129.3	261
Battery sizing								
0.5 (MWh)	3.0	98.0	347	78.3	34.6	61.3	143.1	289
2 (MWh)	3.0	98.9	97	100	37.8	35.7	109.5	221
Grid sizing								
0 (%)	3.0	99.9	171	92.0	48.1	2.1	100.7	204
60 (%)	3.0	97.6	201	89.5	21.0	103.3	172.8	349
100 (%)	3.0	96.9	207	85.1	0.0	181	220.4	446
Solar sizing								
50 (kWp)	3.0	97.9	179	96.0	38.2	60.0	147.7	299
200 (kWp)	3.0	98.9	194	80.7	31.9	30.0	98.0	198

5.2 Discussion

Firstly, the principal objective of this thesis -robust management of the FCPB site- has been effectively achieved using two distinct approaches. The rolling horizon strategy, commonly cited in literature (see Table 2), has proven its resilience to uncertainties, at the expense of simulation duration. Conversely, the proposed fixed schedule approach, designed to reduce the computational burden, proved highly effective, resulting in a 96 % reduction in simulation time. Where the calculation time of the rolling horizon approach is comparable to that reported by Shen et al. 120 s/day [37] and Abdelganhy et al. 40 s/day [39].

From an economic perspective (refer to Figure 18), the introduction of multiple timestep optimisation proved beneficial, reducing the total operating costs per year by 13 % and 5.2 % for the fixed schedule and rolling horizon strategies respectively. The hypothesis in Section 3.4, stating that increased solar and grid utilization made possible by adequate battery scheduling would enhance system economy, was confirmed (refer to Figure 19). In this comparison it should be noted that further optimisation of the single timestep simulations was not pursued, as these approaches proved to be non-viable solutions in heavily congested grids.

Secondly, health-aware fuel cell operation has been incorporated through an extensive MLD model, able to describe all known degradation phenomena. As a result, the lifetime of the fuel cell has been increased significantly, by 32 % and 36 % for the fixed schedule and rolling horizon approach respectively. The integration of low power, high power and load change degradation, along with varying efficiency levels is unprecedented within an OPF formulation, narrowing the described literature gap. However, judging from Figure 20, a major part of the degradation reduction is realised by avoiding low power operation, which could be similarly avoided by adjusting the lower power limit within a simpler model formulation.

The hypothesis in Section 3.4, which stated that increased fuel cell life would offset increased utility cost, was rejected for the fixed schedule approach. This is attributed to the hourly scheduling interval of the fixed schedule, resulting in longer operating hours than required. At the same time, even without MLD formulation, the fixed schedule approach delivers a close to optimal solution, rendering improvements more challenging. Finally, it is observed that the stateless optimisation exhibits low power operation for extended periods of time, where a constant efficiency is not justified. Therefore, the actual hydrogen utilization and costs are expected to be higher than displayed in Figure 18.

Sensitivity analyses on scheduling and prediciton horizons initially show contradicting results. However, it should be noted that the three rolling horizon cases are considerably shorter than those of the fixed schedule. In that perspective, it is observed that initially extending the horizon increases the performance while at some point the benefits plateau, exactly in line with the conclusions from Rezaei et al. [54].

Where the proposed fixed schedule approach greatly outperforms the rolling horizon approach in computational time, it falls short in robustness to uncertainties, as was also advocated by Shen et al. [37]. To resolve this issue several margins strategies are introduced to create a more conservative schedule. Although their individual impact is evident in the case study (refer to Figure 24), it remains uncertain whether these parameters behave similarly in other system configurations. Additionally, parameter refinement is likely required for real-world applications presenting a disadvantage compared to the rolling horizon approach.

Another important matter that has been mainly outside the scope of this thesis are the forecasts for system parameters. Hydrogen and electricity market prices are known a day in advance, posing no considerable issue. It is the prediction of solar and load that contribute to system uncertainties. A naive solar forecast has been applied in this thesis, resulting in solar utilization of over 90 % in most scenarios, where the full capacity is not utilised due to the restriction of battery capacity and no grid feed-in. Therefore investing resources in improving solar predictions is likely not worthwhile. In contrast, as discussed in Section 4.3.b, load forecasts accuracy strongly impacts system performance. The section concludes that the better the forecast the fewer margins are required, contributing to an improved economy. Leading to the conclusion that in absence of sufficiently accurate predictions a rolling optimisation approach is advised, aligning with Fang et al.'s conclusions [36]. The results show that accurate load prediction efforts should focus on predicting the timing of load peaks instead of the magnitude, particularly caused by the state scheduling method. This conclusion is supported by Lima et al. [55], who analogously found that when predicting imbalance prices a predictive distribution (when

is the highest change of the peak) is more beneficial than a point forecast (predicting the magnitude) when optimising for revenue.

With the proposed models a sizing analysis on the FCPB site has been conducted, providing practical insights into their effect on the system economy. Other than hypothesised, increasing the fuel cell size negatively impacts the system economy, as the five-fold increase in investment does not justify the two-fold increase in lifetime. Moreover, larger fuel cells necessitate the battery to compensate more for limited dynamic behaviour, contributing to higher costs. Therefore, it can be confidently said that the fuel cell size should be reduced to a minimum, only compensating for the power deficit.

An optimum battery size was confirmed to exist, as mentioned by [56], however without identifying the determining parameters. The battery size analysis indicated that optimal battery capacity correlates directly with load and solar magnitudes at the site. A further analysis, in the range between 1 and 2 MWh, should conclude the optimal sizing for the given FCPB site.

Contrary to [40], the proposed models effectively manage semi- and fully off grid configurations without the need for changing the optimisation. The economic impact of altering grid connections is crucial, due to the current high price of hydrogen. Future projections suggest a decrease in hydrogen price from 7 €/kg to 1.5 €/kg by 2050 [2], which could drastically change this outlook. Grid connection size, however, remains beyond the circle of influence, due to regulatory restrictions.

Lastly, adding more locally sourced renewables improves the system economy. Cheap energy replaces hydrogen first, depending on battery capacity and power deficit. Although the system economy improves, the solar utilization share decreases, indicating an imminent trade-off between investment and cost reduction.

Furthermore, several general limitations are to be discussed. Firstly, solar generation data from 2022 was apprehended since it was the most recent data available. While at the same time the electricity prices of 2023 were utilised due to the war-inflated 2022 prices. This introduces a correlation discrepancy between price and solar generation. Future research should avoid applying these conflicting datasets.

Another important factor in the SoH analysis is the absence of recent fuel cell degradation data. The reference degradation values date back to an experimental PEMFC in 2015, while modern commercial fuel cells likely have increased lifetimes, especially given the US's department of energy target of 30.000 hr lifetime [57].

The EMS optimises the system in 15-minute time intervals, similar to all studies in Table 2, in order to bound the computational burden. In real time applications, only a single optimisation has to be performed, allowing for timestep refinement and prediction horizon extension. Alleviating this time restriction also opens the door to a rolling horizon approach with a 24 hr prediction horizon.

In this analysis, the equipment charging demand was assumed to follow a set profile. However, in practice, equipment may remain plugged in overnight without requiring the entire time for charging. This introduces another optimisation variable, allowing flexibility in selecting the optimal charging time. For example, only the battery can be charged over the weekend while equipment could be charged in advance as well.

Finally, fixed safety margins were applied throughout the year. It was observed that larger soc deviations occur in summer, requiring more conservative margins. In real applications, adopting dynamic safety margins, would optimise performance based on seasonal requirements.

6 CONCLUSION

6.1 Conclusions

The research questions stated in the introduction have been addressed to provide a solution for Optimal Energy Management for Semi Off-Grid Systems with Health-Aware Hydrogen Asset Operation. For the answers to the initial four questions it is referred to the literature study, the remaining questions are answered below:

5. How to combine the robust optimisation and health-aware operation into a single integrated optimisation algorithm?

By combining the insights from the literature review, a novel method for robust energy management of semi off-grid sites with health-aware fuel cell operation was proposed. Robust and economical optimisation was achieved by applying an OPF formulation within a dynamic timestep rolling horizon framework. In an effort to reduce computational cost and extend the prediction horizon, the rolling horizon was replaced by a fixed schedule framework, at the cost of simulation robustness. Secondly, benefiting from the MLD formulation, a binary variable model able to describe start-stop cycles, load change cycles, low power and high power degradation as well as multiple efficiency values was introduced. The performance of the hierarchical MLD-OPF optimisation is evident from the results and discussion: a reduction of 96 % in computational time compared to common rolling horizons, a total operating cost reduction of 13 % compared to the benchmark, a 32 % increase in fuel cell lifetime compared to a formulation without MLD framework and independence of accurate solar predictions.

6. What are the decisive parameters within the optimisation framework?

The results and discussion highlight multiple parameters of interest. Most importantly, it was found that extending the optimisation horizon beyond a day does not contribute to vastly increased performance, even when weekend patterns are observed. Secondly, in order to cope with uncertainties it was found that scheduling reserve battery capacity is most economically friendly. The inclusion of safety margins is a drawback of the proposed model due to their requirement of system dependent fine-tuning. Furthermore, the accuracy of load predictions is worthwhile investigating further, laying the focus on predicting peak times instead of magnitudes. Moreover, it turned out that by providing the right incentives, solar utilization is virtually independent of prediction accuracy.

7. Given the proposed EMS algorithm what is the impact of asset sizing within the FCPB system?

Foremost, being the backbone of off-grid operations, it was concluded to minimise the PEMFC size since the lifetime increase of larger systems does not justify the increased investments. The analysis shows that start-stop cycles are responsible for the largest share of inflicted degradation. Maximum fuel cell power amounting to a third of the peak load power is deemed sufficient for the investigated case. Secondly, the optimum battery capacity was found to be correlated to the system's energy throughput as well as the installed solar capacity. Although being architecturally different, the optimisation algorithm does not require a differentiation between fully and semi off-grid site. Varying the contracted grid capacity depicts an evident impact on operational expenditure, concluding that hydrogen is currently a highly uneconomic solution. Finally, it was found that increasing installed solar capacity positively influences the cost, although the full potential is limited by the battery capacity.

In summary, the above answers provide a comprehensive view of the contributions of this thesis. The identified literature gap—integrating a sophisticated EMS algorithm with comprehensive fuel cell degradation characteristics while maintaining computational efficiency—has been addressed. The results show that the semi off-grid site can be robustly optimised throughout a year with a 13 % decrease of operating costs and a 33 % improvement of lifetime, all while requiring only 5% of the computational effort, thereby successfully narrowing of the gap. Closing the literature gap would be achieved by incorporating the insights from the subsequent section.

6.2 Recommendations

Based on the conducted research, valuable insights have been discovered in the field of health-aware operations as well as microgrid optimisation. Especially, during the implementation of the models new findings and ideas arose that could be part of future research. First, with respect to the MLD model of the fuel cell, several refinements could be implemented. In this thesis, three distinct power producing states are applied, while judging from their continuous profile, the degradation and efficiency are more accurately modelled within, for example, ten states. This extension would also allow for a better incorporation of load change degradation since it is dependent on the fluctuation magnitude. Additionally, it is recommended to study the applied degradation costs, where the focus should be on applying costs that avoid unwanted behaviour instead of being accurate.

Moreover, since the proposed models are based on somewhat outdated degradation values, it is strongly advised to validate these characteristics for the implemented system.

Thirdly, due to the focus being on fuel cells, the degradation characteristics of the battery should be taken into account more prominently. Factors like DoD, C-rates and storage SoC do influence the lifetime. The proposed MLD framework could similarly be applied for this purpose.

Resulting from the findings in this thesis, it is strongly advised to shift the research attention to predicting the load demand of charging construction vehicles. Or alternatively, it would be advised in real-time operation to steer charging to certain time windows, thereby improving the prediction accuracy.

When it comes to accounting for uncertainties this study proposed several strategies for safety margins. The magnitude of these margins were experimentally tuned to the worst day in the year. Future research could be focused on adaptive margins improving the economical results on less demanding days.

In order to optimise computational burden, the scheduling optimisation applies a time interval of an hour. The system's hydrogen usage and fuel cell degradation could benefit from a smaller interval, reducing the operating hours of the fuel cell.

Furthermore, in real-time applications when calculation windows allow for it, it should be advised to include information to the fullest extent in the decision making. There is no evidence presented in this study that show reduced benefit of including more information. Therefore, a rolling optimisation approach with a horizon of at least 24 hours is always advised.

Finally, the successful implementation of the EMS into an semi off-grid system relies on local stable control of the actual power flows. To this purpose, the literature review provides an extensive background suggesting multiple solutions. Future research should validate the adequacy of these solutions, especially in terms of stability.

REFERENCES

1. S Colleen, History of Fuel Cells, (2017).
2. PWC, The green hydrogen economy Predicting the decarbonisation agenda of tomorrow, (2023).
3. J Zhao and X Li, A review of polymer electrolyte membrane fuel cell durability for vehicular applications: Degradation modes and experimental techniques, *Energy Conversion and Management*, (2019), 199:112022.
4. V Malik, S Srivastava, M K Bhatnagar, and M Vishnoi, Comparative study and analysis between Solid Oxide Fuel Cells (SOFC) and Proton Exchange Membrane (PEM) fuel cell – A review, *Materials Today: Proceedings*, (2021), 47:2270–2275.
5. A Ramírez-Cruzado, B Ramírez-Peña, R Vélez-García, A Iranzo, and J Guerra, Data from Experimental Analysis of the Performance and Load Cycling of a Polymer Electrolyte Membrane Fuel Cell, *Data*, 5 2020, 5(2):47.
6. A Saeedmanesh and J Brouwer, *Dynamic Modeling of a Solid Oxide Electrolyzer System under Two Different Thermal Control Strategies*, 7 2018.
7. CellKraft, Fact sheet fuel cell systems, (2018).
8. J Nordlund, A Ocklind, and P Gode, On the startup reliability of fuel cell systems, In: *Proc. , INTELEC 2008 - 2008 IEEE 30th International Telecommunications Energy Conference*, (2008), 1–3.
9. A Oyarce, E Zakrisson, M Ivity, C Lagergren, A B Ofstad, A Bodén, and G Lindbergh, Comparing shut-down strategies for proton exchange membrane fuel cells, *Journal of Power Sources*, (2014), 254:232–240.
10. J Fan, Y Yang, T Ma, D Zhu, and X Xu, Investigation on a Shutdown Control Strategy with Residual Oxygen Rapid Elimination for Proton Exchange Membrane Fuel Cell System, *Energies*, 1 2023, 16(3):1285.
11. K Nikiforow, J Pennanen, J Ihonen, S Uski, and P Koski, Power ramp rate capabilities of a 5kW proton exchange membrane fuel cell system with discrete ejector control, *Journal of Power Sources*, (2018), 381:30–37.
12. A Loskutov, A Kurkin, A Shalukho, I Lipuzhin, and R Bedretdinov, Investigation of PEM Fuel Cell Characteristics in Steady and Dynamic Operation Modes, *Energies*, (2022), 15(19).
13. Y Haseli, Maximum conversion efficiency of hydrogen fuel cells, *International Journal of Hydrogen Energy*, (2018), 43(18):9015–9021.
14. P Ren, P Pei, Y Li, Z Wu, D Chen, and S Huang, Degradation mechanisms of proton exchange membrane fuel cell under typical automotive operating conditions, *Progress in Energy and Combustion Science*, (2020), 80:100859.
15. M Chandran, P Karthikeyan, K Babu NB, and O Das, A study of the influence of current ramp rate on the performance of polymer electrolyte membrane fuel cell, *Scientific Reports*, 3 2022, 12:21888.
16. J Kim, J Lee, and Y Tak, Relationship between carbon corrosion and positive electrode potential in a proton-exchange membrane fuel cell during start/stop operation, *Journal of Power Sources*, (2009), 192(2):674–678.
17. F Nandjou, J.-P. Poirot-Crouvezier, M Chandesris, J.-F. Blachot, C Bonnaud, and Y Bultel, Impact of heat and water management on proton exchange membrane fuel cells degradation in automotive application, *Journal of Power Sources*, (2016), 326:182–192.
18. Y Li, P Pei, Z Ma, P Ren, Z Wu, D Chen, and H Huang, Characteristic analysis in lowering current density based on pressure drop for avoiding flooding in proton exchange membrane fuel cell, *Applied Energy*, (2019), 248:321–329.
19. C Qin, J Wang, D Yang, B Li, and C Zhang, Proton Exchange Membrane Fuel Cell Reversal: A Review, *Catalysts*, (2016), 6(12).
20. E Wallnöfer-Ogris, F Poimer, R Köll, M Macherhammer, and A Trattner, Main degradation mechanisms of polymer electrolyte membrane fuel cell stacks – Mechanisms, influencing factors, consequences, and mitigation strategies, *International Journal of Hydrogen Energy*, (2024), 50:1159–1182.
21. A Topalov, S Cherevko, A Zeradjanin, J Meier, I Katsounaros, and K Mayrhofer, Towards a comprehensive understanding of platinum dissolution in acidic media, *Chemical science (Royal Society of Chemistry)*, 3 2014, 5:631–638.
22. X Yang, J Sun, X Meng, S Sun, and Z Shao, Cold start degradation of proton exchange membrane fuel cell: Dynamic and mechanism, *Chemical Engineering Journal*, (2023), 455:140823.
23. M Whiteley, S Dunnett, and Jackson, Failure Mode and Effect Analysis, and Fault Tree Analysis of Polymer Electrolyte Membrane Fuel Cells, *International Journal of Hydrogen Energy*, (2016), 41(2):1187–1202.
24. H Chen, P Pei, and M Song, Lifetime prediction and the economic lifetime of Proton Exchange Membrane fuel cells, *Applied Energy*, (2015), 142:154–163.
25. J M Desantes, R Novella, B Pla, and M Lopez-Juarez, A modeling framework for predicting the effect of the operating conditions and component sizing on fuel cell degradation and performance for automotive applications, *Applied Energy*, (2022), 317:119137.
26. Y Ao, S Laghrouche, D Depernet, and K Chen, Lifetime prediction for proton exchange membrane fuel cell under real driving cycles based on platinum particle dissolve model, *International Journal of Hydrogen Energy*, (2020), 45(56):32388–32401.
27. P Pei, Q Chang, and T Tang, A quick evaluating method for automotive fuel cell lifetime, *International Journal of Hydrogen Energy*, (2008), 33(14):3829–3836.
28. E Obio, S Ali, I Oyebanjo, D Abara, F Suleiman, P Ohiero, D Oku, and V Ogar, Comparison of Economic Dispatch, OPF and Security Constrained-OPF in Power System Studies, *Journal of Power and Energy Engineering*, 8 2022, 10(08):54–74.
29. E Mohagheghi, M Alramlawi, A Gabash, and P Li, A Survey of Real-Time Optimal Power Flow, *Energies*, (2018), 11(11).
30. L Mones, A Gentle Introduction to Optimal Power Flow, (2021).
31. A Soleimani, V Vahidinasab, and J Aghaei, A Linear Stochastic Formulation for Distribution Energy Management Systems Considering Lifetime Extension of Battery Storage Devices, *IEEE Access*, (2022), 10:44564–44576.
32. F Alsaleem, M Tesfay, P Arunasalam, and A Rao, Adaptive-model predictive control of electronic expansion valves for evaporator superheat minimization, In: *Proc. , 2017 IEEE International Conference on Electro Information Technology (EIT)*. IEEE, 5 2017, 159–165.
33. D Erazo-Caicedo, E Mojica-Nava, and J Revelo-Fuelagán, Model predictive control for optimal power flow in grid-connected unbalanced microgrids, *Electric Power Systems Research*, (2022), 209:108000.

34. Q Li, X Zou, Y Pu, and W Chen, Real-time Energy Management Method for Electric-hydrogen Hybrid Energy Storage Microgrids Based on DP-MPC, *CSEE Journal of Power and Energy Systems*, (2024), 10(1):324–336.
35. C Huang, Y Zong, S You, and C Træholt, Economic model predictive control for multi-energy system considering hydrogen-thermal-electric dynamics and waste heat recovery of MW-level alkaline electrolyzer, *Energy Conversion and Management*, (2022), 265:115697.
36. X Fang, W Dong, Y Wang, and Q Yang, Multi-stage and multi-timescale optimal energy management for hydrogen-based integrated energy systems, *Energy*, (2024), 286:129576.
37. W Shen, B Zeng, and M Zeng, Multi-timescale rolling optimization dispatch method for integrated energy system with hybrid energy storage system, *Energy*, (2023), 283:129006.
38. F Garcia-Torres and C Bordons, Optimal Economical Schedule of Hydrogen-Based Microgrids With Hybrid Storage Using Model Predictive Control, *IEEE Transactions on Industrial Electronics*, (2015), 62(8):5195–5207.
39. M B Abdelghany, M F Shehzad, D Liuzza, V Mariani, and L Glielmo, Optimal operations for hydrogen-based energy storage systems in wind farms via model predictive control, *International Journal of Hydrogen Energy*, (2021), 46(57):29297–29313.
40. M B Abdelghany, V Mariani, D Liuzza, and L Glielmo, Hierarchical model predictive control for islanded and grid-connected microgrids with wind generation and hydrogen energy storage systems, *International Journal of Hydrogen Energy*, (2024), 51:595–610.
41. C Dall'Armi, D Pivetta, and R Taccani, Health-Conscious Optimization of Long-Term Operation for Hybrid PEMFC Ship Propulsion Systems, *Energies*, (2021), 14(13).
42. A Bemporad and M Morari, Control of systems integrating logic, dynamics, and constraints, *Automatica*, (1999), 35(3):407–427.
43. M Wei, Reversible Fuel Cell Cost Analysis and Megawatt PEM Cost Analysis for H2 Grid Storage Systems, Technical report, Lawrence Berkeley National Laboratory, 5 2022.
44. E Redondo-Iglesias and S Pelissier, On the Efficiency of LFP Lithium-ion Batteries, In: *Proc. , 2022 Second International Conference on Sustainable Mobility Applications, Renewables and Technology (SMART)*. IEEE, 11 2022, 1–5.
45. TenneT, Adequacy Outlook: A TenneT study exploring the future of resource adequacy in a net-zero emission Dutch and German energy system, Technical report, 5 2023.
46. EEX, Green HYDRIX index Germany, (2024).
47. S Pfenninger and I Staffell, Long-term patterns of European PV output using 30 years of validated hourly reanalysis and satellite data, *Energy*, (2016), 114:1251–1265.
48. A Veiga, Ultimate guide to utility-scale PV system losses, 12 2022.
49. F K Bidi, C Damour, D Grondin, M Hilairet, and M Benne, Optimal fuel cell and electrolyser Energy Management System for microgrid, In: *Proc. , IECON 2019 - 45th Annual Conference of the IEEE Industrial Electronics Society*. IEEE, 10 2019, 2197–2202.
50. C Chunjun, C Huang, Y Zong, S You, and C Træholt, *Optimal Operation of Multi-Energy System Integrated with an Alkaline Electrolyzer Dynamic Power-to-Hydrogen&Heat (P2H2) Model*, 2 2022.
51. Gurobi, Mixed-Integer Programming - A Primer on the Basics, (2023).
52. V.M. Fontalvo, G. J. Nelson, O. Pupo-Roncallo, M. E. Sanjuan, and H. A. Gómez, A techno-economic assessment for fuel cells hybrid systems in stationary applications, *International Journal of Sustainable Energy*, 12 2023, 42(1):889–912.
53. NREL, Best Research-Cell Efficiency Chart, (2023).
54. A Rezaei and J B Burl, Effects of Time Horizon on Model Predictive Control for Hybrid Electric Vehicles, *IFAC-PapersOnLine*, (2015), 48(15):252–256.
55. L M Lima, P Damien, and D W Bunn, Bayesian Predictive Distributions for Imbalance Prices With Time-Varying Factor Impacts, *IEEE Transactions on Power Systems*, 1 2023, 38(1):349–357.
56. M Sufyan, N Abd Rahim, C Tan, M A Muhammad, and S R Sheikh Raihan, Optimal sizing and energy scheduling of isolated microgrid considering the battery lifetime degradation, *PLOS ONE*, 2 2019, 14(2):e0211642–.
57. HFTO, Hydrogen and Fuel Cell Technologies Office - Multi-Year Program Plan, Technical report, US Department of Energy, (2024).

B SYSTEM SPECIFICATION

This appendix provides an overview of all system parameters used in the optimisation problems. The values stated here correspond to the standard system layout, used in the benchmark study. In the sensitivity analysis values may deflect as is be stated in the main body of the thesis. Parameter values based on a source have already been mentioned in Section 3.

Table B.1: Overview of all system parameters, the quantities that change over time are indicated with a *.

Parameter	**Value**	**Parameter**	**Value**	**Parameter**	**Value**
Battery		*Fuel cell*		*Solar*	
P_{max}	500 (kW)	P_{max}	300 (kW)	P_{max}*	100 (kW)
P_{min}	-500 (kW)	P_{min}	-3 (kW)	P_{min}	0 (kW)
λ_ϕ	see Eq (B.1) (€/kW)	λ_ϕ	0 (€/kW)	λ_ϕ	0 (€/kW)
E_{cap}	1000 (kWh)	η	see Table 2 (%)	η_{loss}	7 (%)
η_{ch}	95 (%)	P_{ru}	20 (%/s)		
η_{disch}	95 (%)	P_{rd}	20 (%/s)		
CAPEX	600 (€/kWh)	CAPEX	1000 (€/kW)		
Lifetime	6000 (cycles)	Lifetime	25000 (hr)		
		C_ϕ^{state}	see Eq B.2 (€/hr)		
		C_ω^{switch}	see Eq B.3 (€/cycle)		
Electricity grid		*Hydrogen grid*		*Demand load*	
P_{max}	0 (kW)	P_{max}	0 (kW)	P_{max}*	-300 (kW)
P_{min}	-55 (kW)	P_{min}	$-\infty$ (kW)	P_{min}*	-300 (kW)
λ_ϕ *	20 + day ahead price (€/kW)	λ_ϕ	220 (€/kW)	λ_ϕ	0 (€/kWh)

The cost assigned to the operation of the battery (both charge and discharge) is equal to its depreciation costs according to:

$$\lambda_\phi^{BAT} = \frac{\text{CAPEX} \cdot \Delta t}{2 \cdot E_{cap} \cdot \text{Lifetime}} (€/\text{kW}) \tag{B.1}$$

where Δt is the time between simulation steps, equal to 0.25 or 1 hr and the factor 2 arises from a full charge and discharge cycle. The degradation costs of the fuel cell states and switches are recovered from the reference values ξ_{ref} in the literature (see Table 1 and 2) with a unit of μV/hr or μV/cycle. These have been converted to €/hr and €/cycle, assuming an EoL criterion of 10 % (or 0.07 V) at nominal power (see Section 4.1.a, by the following equations:

$$C_\phi^{state} = \text{CAPEX} \cdot \left(\frac{1}{\text{Lifetime}} + \frac{\xi_{ref}}{0.07} \right) \quad (€/\text{hr}) \tag{B.2}$$

$$C_\omega^{switch} = \text{CAPEX} \cdot \frac{\xi_{ref}}{0.07} \quad (€/\text{cycle}) \tag{B.3}$$

C VALIDATION

The objective of unit tests is to systematically validate the behaviour of the proposed methods. This is achieved by visual inspection of the output as well as manual calculations to verify the correctness. These tests will be performed on the last week in May 2022 due to some exceptional prices and weather conditions. All required code changes to simulate the unit tests are documented separately and all system parameters are present in special configuration files; see, for example, Figure C.1. This approach ensures the repeatability of the experiments. Table C.1 shows the conducted unit tests, the measured variables and expressions and the intended goals. The detailed analysis of each test is intentionally left out for clarity, however, it should be noted that all experiments were successfully finished.

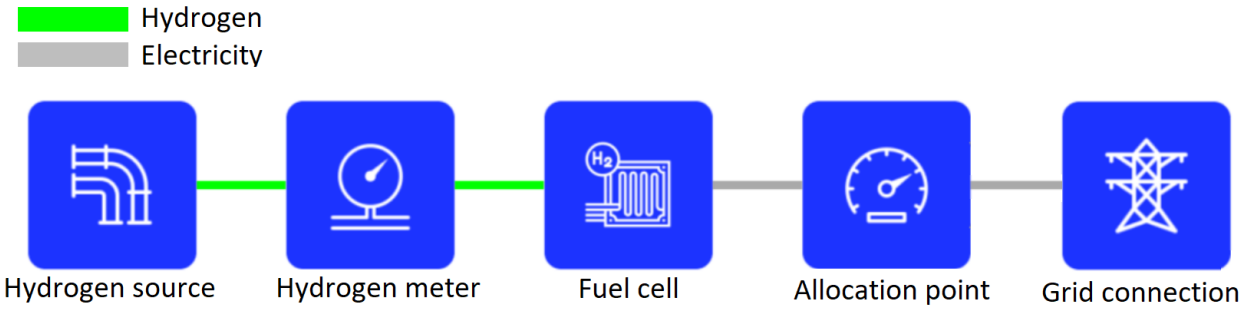

Fig. C.1: Asset configuration of unit test 1 (own work).

Table C.1: Summary of performed unit tests, their measurements and goals.

Configuration	Recorded expressions	Goals
1. Simple FC with dynamic contract	electricity and hydrogen power utility and asset cost	Validate ramp rates, efficiency, cost of hydrogen and cost of asset
2. MLD FC with dynamic contract	states, state switches, powers	Validate states, state switches and efficiencies.
3. MLD FC with demand load	electricity and hydrogen power, states, state switches, asset cost	Trigger all states and state switches, check efficiency and ramp rates
4. MLD FC with imbalance contract	electricity power, utility cost	Validate principles work for other electricity markets as well
5. MLD FC with fixed schedule	scheduled and actual powers, scheduled and actual utility cost	Schedule and actual power should match when perfect foresight is included for a dynamic contract
6. Battery with fixed schedule	electricity power, asset cost scheduled and actual SoC	Validate battery SoC tracking and implementation of deviation penalty
7. Solar with fixed schedule	scheduled and actual powers	Validate no unnecesary curtailment and predicted values
8. Demand load with fixed schedule	scheduled and actual powers	Validate predicted values
9. Battery with rolling horizon	electricity power, SoC, asset cost and utility cost	Validate rolling horizon strategy with a battery alone
10. MLD FC with rolling horizon	electricity power, utility cost, states and state switches	Validate states and switches and compare with tests 2 and 5.

D LITERATURE REVIEW

See next page.

ABSTRACT: The recent past has shown an increased interest in DC microgrids, addressing the need of effective local integration of renewables. Along with green hydrogen fueled back-up power these microgrids provide a CO_2-free alternative for congestion areas or remote locations. This literature review aims to identify the challenges related to asset safety, DCMGs design and PEMFC degradation. Consequently, insights into optimal optimisation algorithms is provided, taking these characteristics into account. The findings indicate that isolated DCMGs are prone to stability issues, adequate safety devices are scarce, PEMFC degradation cannot be ignored and optimal optimisation is computationally expensive. Nevertheless, this literature review provides an extensive foundation to develop a robust EMS for hydrogen backed semi off-grid sites.

CONTENTS

1 INTRODUCTION

With the rapidly increasing housing demand and decreasing building permits due to NOx emissions, the need for emission-free building sites arises. A semi-off grid battery and fuel cell combination or in short the FCPB (Fuel Cell Power Bank) is targeted as a promising solution for this purpose. With restricted access to grid energy on these locations the FCPB is able to provide a continuous supply of renewable energy for charging electric equipment. The main assets of the system are currently known and a first technical design has been made. As a next step, an optimisation of several designs aspects should be carried out and a robust control strategy should be applied. The optimisation at hand will be addressed in this thesis where the major focus is on guaranteeing safe autonomous operation.

The flexible FCPB platform asks for a sturdy EMS that is able to cope with the different renewable energy profiles, asset combinations and user demands. Obviously, a user asks for the best economical usage of the system that might overlook safety concerns. Therefore, the need for a reliable fundamental layer of safe operation arises. The goal of this thesis is to develop the aforementioned fundamentally safe operation layer and integrate it with the (adapted) EMS system of Emmett Green. The outcomes of the thesis should aid a rapid implementation of the FCPB

for emission-free construction sites, relieving the Dutch housing and nitrogen crises on top of reducing the greenhouse gas emissions.

The structure of this literature review comprises four distinct chapters, each dedicated to addressing specific research questions. Chapter 2 will focus on identifying the risks associated with the assets. Following this, Chapter 3 will delve into discussions concerning the safe architecture of a microgrid. Subsequently, Chapter 4 will center its attention on exploring the relevant fuel cell characteristics, while Chapter 5 will undertake the analysis of control strategies. Pertaining to the integration of insights from the preceding findings multiple strategies for a robust control algorithm of the FCPB are proposed and compared in the final thesis document.

2 ASSET RISK ANALYSIS

As an initial step in the development of a safety-conscious design for a microgrid predominantly powered by Fuel Cells (FCs) and batteries, this section undertakes a thorough examination of the interconnected assets. The objective is to grasp the safety implications inherent in such systems and the corresponding methods of mitigation or regulation. The outcomes of this section offers insights into the critical parameters that necessitate consideration in both the design and control phases of the microgrid.

2.1 Battery risks

Sony was the first to commercially introduce the public to Lithium-ion Battery's (LiBs) in 1991. Undoubtedly, a lot of effort has been invested into increasing battery performance, safety, ease of manufacturing and lifetime. The conquest to the most optimal cell lead to an explosion in variety while the working principle stayed the same. Each lithium-ion battery exists out of a negatively charged anode and positively charged cathode separated by a liquid electrolyte. The electrolyte is an electrical insulator and an ionic conductor, hence a current is generated in the external circuit. Based on the uncomplicated anode-separator-cathode researchers began experimenting with various exotic materials to adjust the performance of the battery. An important consequence of the materials selection, is the voltage potential delivered by the cell, which directly influences the specific energy density [1]. In addition, factors as material abundance, costs, environmental impact and predominantly safety should be considered. Safety enhancement, prevention of thermal runaway incidents, and mitigation of toxic exhaust emissions are prominent priorities within the current research agenda. Figure 1 presents an overview of the performance characteristics depending on the materials chosen. Noticeable is the fact that each chemistry excels in one or two Key Performance Indicators (KPIs) but never in all. The graphite NMC cells, that dominate the recent demand, seem to have found the right balance between all KPIs. However, the cobalt used is controversial in terms of material abundance and socio-economic impact which should also be considered [2].

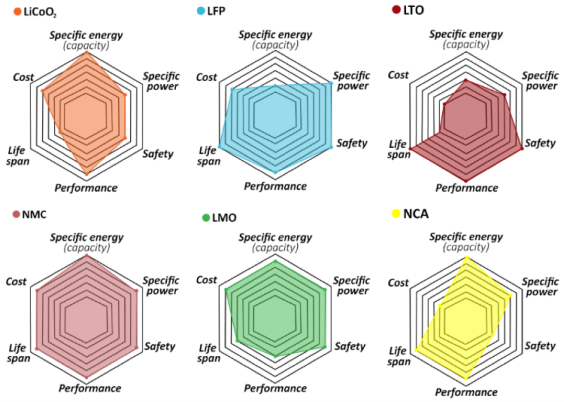

Fig. 1: Performance characteristics of different LiB chemistry's [3]

2.1.a Degradation and safety

It is for a reason that the notion of safety is included in the top five KPIs; spontaneous explosion and fire hazards are intrinsically part of the introduction of LiBs. Thermal runaway is the main contributor to this imminent explosion hazard which can be triggered due to a variety of events. Significant research has been spent to investigate and mitigate this behaviour [5]. Degradation of the internal parts due to (mal)operational are considered to accelerate the chance of thermal runaway. Solid Electrolyte Interphase (SEI) layer growth, lithium plating, electrode decomposition and particle fracture are among the primary mechanisms followed by a longer list of consequent secondary mechanisms, as schematically shown in Figure 2 [4]. [6] presents an overview of the influence of design, production and application to the independent mechanisms.

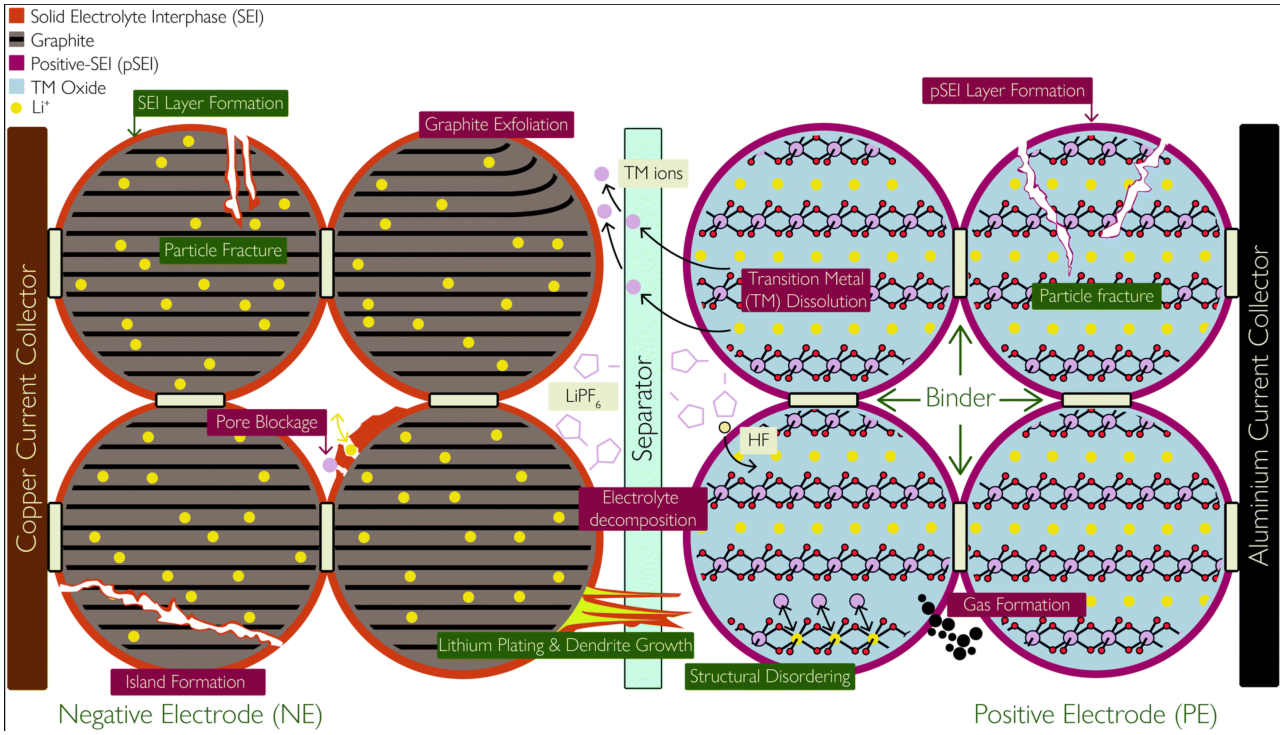

Fig. 2: LiB degradation mechanisms [4]

As safety and material selection are closely related an increased interest in Lithium Titanate Oxide (LTO) and Lithium Iron Phosphate (LFP) chemistry' is observed. LFP cathodes are characterised by excellent thermal stability due to the strong covalent P-O bonds [7] and absence of exothermic redox reaction between cathode and anode at high temperatures [8]. Both effects contribute to the reduction of severance in the case of thermal runaway. Contrastingly, LTO type batteries offer a complete different approach to safe operation by selecting a different anode material. The LTO anode does not exhibit any volume change during the lithium insertion process due to the constant lattice parameters [9], significantly reducing the mechanical stress and accompanied degradation. In addition, the increased voltage plateau to lithium (≈1.55 V) compared to conventional graphite anodes (≈0.25 V) reduces the risk of lithium plating and dendrite growth and prevents the build-up of a thick SEI Layer [10]. Dendrite growth is associated with separator puncture and consequent short-circuit while SEI layer growth is associated with higher resistance and capacity fade.

2.1.b Safe design of battery systems

As the technology matures the safety considerations of LiBs are more adequately addressed. In the recent past many authors have applied FMEA methodology on LiBs in a variety of different applications. Utility scale Electrical Energy Storage (EES) in combination with Renewable Energy Sources (RES) are critically scrutineered in [11, 12] where a distinction is made between controllable and uncontrollable events on the system level. On the LiB cell level, the impact on safety of the previously mentioned degradation mechanisms is addressed in detail by [13]. This analysis provides good insights in how to mitigate hazards by improving design and correlating usage with degradation. An example of how to mitigate hazards based on knowledge of degradation mechanisms is presented in [14]. The study was able to reduce the severity of 191 out of 289 identified risks from unacceptable to as low as reasonably possible leaving only one risk as unacceptable (human error) by applying adequate monitoring and battery management. Lastly, it is important to include the use case of the LiB at hand as [15] demonstrated the increased amount of risks associated with LiBs in automotive applications. As a result of the continued efforts to safer LiBs several standards and design codes have been published to guarantee a worldwide consensus on EES systems, as conveniently grouped in [16]. Noteworthy is that the IEC 62933-5-1 and IFC Chapter 12 do not mention a vast list with requirements but instead require the designer to perform a hazard identification and risk assessment & mitigation analysis. In conclusion, in

terms of safety LiBs present a unique case due to their tendency of catastrophic thermal runaway triggered by numerous possible events. Mechanical, electric and thermal abuse as well as degradation can trigger thermal runaway through a cascade of events. Recent advances in cell chemistry, monitoring systems and battery management, together with established design codes and standards path the way to intrinsically safe LiBs.

2.1.c Safe operation

The studies presented above outline the design and operational requirements that should be adhered to. The design of LiBs is outside the scope of this study, however the operational constraints are a fundamental part of safe control. As was concluded in the previous section the degradation of the internal cell structure is one of the major causes of thermal runaway. The state of degradation is often referred to as the State of Health (SoH), and is an important feature in safety and performance as the control limits should be adjusted accordingly. The primary control parameters that affect the SoH are, State of Charge (SoC), Depth of Discharge (DoD), (Dis)Charge rate ((D)C-rate), and temperature. On top of the controllable parameters there are uncontrollable events as well, like time and the historical amount of cycles endured. The estimation of SoH is a hot research topic where a variety of non-destructive methods is outlined by [17]. Hence, from a control perspective it can be concluded that the control parameters SoC, DoD, (D)C-rate and temperature should be within their respective limits, according to the specific LiB at hand and the current SoH.

2.2 Fuel cell risks

Although the first working fuel cell was demonstrated in 1839 by Sir William Grove the commercialisation of the technology has only been accelerated in recent years [18]. High costs related to the production of hydrogen and low oil prices are the main contributors to this slow introduction. However, with the renewed interest in emission free electricity generation the attention has shifted away from combustion engines, paving the way for hydrogen technology. A Proton Exchange Membrane Fuel Cell (PEMFC), being a electrochemical cell, has a lot of similarities to a LiB when it comes to the working principle. It consist out of a positive and negative electrode separated by an ionically conductive membrane that is an electric insulator, pushing the electrons to the external load (see Figure 3). At the anode hydrogen is supplied which travels through the diffusion layer and reacts with the catalyst (usually platinum) in the catalyst layer. The oxidation reaction that occurs, $H_2 \rightarrow 2H^+ + 2e^-$, splits the hydrogen molecules into protons and electrons. The distribution plates collects the electrons while the protons diffuse through the membrane. At the cathode side oxygen is supplied to react with the protons and electrons, $\frac{1}{2}O_2 + 2H^+ + 2e^- \rightarrow H_2O$, forming water and completing the electrical circuit.
An effective PEMFC requires several systems to sustain the reaction in the chemical cell. First of all, the hydrogen should be supplied at a conform pressure requiring valves, pumps and a control system. Secondly, proper water saturation is challenging but vital to avoid drying or flooding of the membrane, mainly caused by the attraction of water to the anode due to polarization [19]. Hence a humidifier, its associated pumps and control should be included in the design. As a result, a FC system has significantly more components than a LiB that can suffer failure.

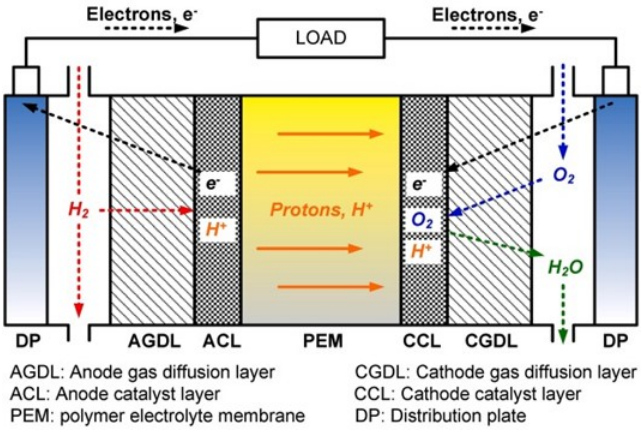

Fig. 3: Schematic overview of the PEMFC working principle with its components [20]

2.2.a Safe design of PEM Fuel Cell systems

Equivalent to the journey of LiBs, the long history of PEMFCs has led to numerous studies into safety aspects of these systems. The primary difference in safety originates from the fact that a LiB is a storage device while a PEMFC is only converts chemical energy into electrical energy. Hence the catastrophic thermal runaway that follows from the release of the stored energy is not observed in a PEMFC. However, the energy storage medium, in this case the hydrogen tank, is still a major safety concern.

As is the case for LiBs, PEMFC are prone to degradation caused by thermal, chemical and mechanical cycles experienced during their operational life [21], which will be further discussed in Section 4. The key difference is that this degradation only results in a reduction in efficiency and power [22], or in severe cases it can cause a controllable fire [23]. Multiple studies have applied a FMEA analysis on PEMFC to outline the associated risks. The stationary PEMFC in a microgrid is addressed in [24] together with the applicable SAE, ISO and NFPA standards and design guidelines. In their FMEA the hydrogen storage and valves are given the highest risk priority. Interestingly, [25] applied a risk analysis to conclude that the refuelling process actually involves higher risks due to higher change of failure. A significant portion of the guidelines originate from the automotive industry where a vast amount of effort is spent in creating a safe environment for hydrogen fuel cell vehicles. The National Highway Traffic Safety Administration (NHTSA) published an extensive report with a 26 page long FMEA table together with standards that should cover each failure mode [23]. They conclude that almost all failure modes, except for tank rupture, can be adequately monitored and therefore the risks are acceptable. [26] underlines this conclusion with the statement that fuel cell vehicles do not pose a greater danger than conventional ICE vehicles. More recently, [27] compared the risk matrices of a PEMFC with and without safety measures to conclude that risks associated with onboard hydrogen storage and supply systems have been reduced to levels that are as low as practically possible. The remaining issues related to uncontrollable explosions due to fires or accidents can be mitigated by requiring sufficient distance between hazardous hydrogen containing assets as described in the Dutch 'Publicatiereeks Gevaarlijke Stoffen' [**?**].

The risks assessments described above present a positive outlook for PEM Fuel Cells. It is underlined by most studies that by applying existing safety devices the risks involved can be reduced to acceptable levels. Multiple renowned organisations describe codes and standards in order to guide designers to a system that mitigates most risks. Explosion of pressurised hydrogen storage facilities is identified as the most prominent failure mode due to the uncontrollable situations that can cause it. However, guidelines exist to mitigate the severity of these events as well. The above discussion highlights the design aspects that contribute to a safe PEMFC, the discussion on safe operation is highlighted in more detail in Section FC.

2.3 PV risks

The earliest solar photovoltaic (PV) cell was created in 1883 by Charles Fritts, achieving 1% efficiency with Selenium. The technology was later boosted by a publication of Einstein and the unlimited financial resources during the space race to become a cost effective alternative to fossil fuel powered generators [28]. Current PV panels usually consist of a negatively and positively doped silicon semiconductor under a glass plate. When solar rays are incident they knock an electron free from the atoms. The doping results in a build-up of electrical charge creating a potential. When a circuit is connected the free electrons recombine with a free spot (hole) on the other side of the material sandwich. This process is continually repeated with a highest reported energy efficiency of 26.1% [29]. The relatively low efficiency is a combined effects of losses like the atmosphere and front contacts blocking light or silicon only allowing certain wavelengths of light. Significant research has opted a variety of solutions to these problems which increase electrical efficiency up to 47.1% [29], usually at the cost of cost efficiency. Besides efficiency the increase in safety is also a major research topic as will be discussed in the following section.

2.3.a Safe design of PV installations

The introduction of intermittent renewable power sources as PV into small DC-microgrids brings several challenges regarding stability and reliability to the table. Although being a mature technology that is prone to failures [30] claims to be the first attempt at creating an extensive (public) FMEA of PV systems. The study concludes that the grounding system and inverter possess the highest RPN number. [22] describes the fault universe that is observed in a PV dominated DCMG and concludes that the failure modes merely result in a decreased power input to the DCMG. A similar list of faults is identified by [31] together with fault detection techniques. The study advocates a fault detection method that is robust to changes in the micro-grid and PV configuration. The list of faults is further developed by [32], who categorised them in a schematic overview. Lastly, [33] performed an in-depth analysis on component level of

the DC-DC boost converter that connects the panels and grid since they identified the boost converter as dominating factor in system reliability.

In addition to the perceived fault mechanisms the literature discusses field data of the occurrence of these faults as well. [34] presents an elaborate overview of failure data that is directly suitable for applying in an FMEA. An example of this data is provided by [35] who reported several interesting conclusions from 63 small to large scale PV plants in Spain and Italy. For example, proper maintenance reduced the amount of failures irrespective of the plants age, smaller plants (<750 kW) endure twice the amount of failures per panel compared to larger installations and the highest amount of failures is observed in the monitoring systems, communication systems and inverter. All this input was used by [36] in an up-to-date FMEA, assigning the highest safety priority to hidden cracks in hot spots, isolation faults of underground cables and poor welding during manufacturing. Ultimately, it should be noted that the roll-out of large scale PV-arrays has not been hindered due to safety issues as was the case for hydrogen technologies. This is mainly due to the vast amount of standardization and design codes that are developed by respectable institutions (ASTM, NEC, IEEE, IEC, SEMI, UL), as is neatly summarised in [37].

It can be concluded from the above analysis that the mechanisms behind PV faults are well understood. Although the studies do not present an unambiguous answer to the dominant failure mechanisms, converters and grounding issues are mentioned most frequently. Due to presence of sufficient field data trustworthy FMEA results are available. With the integration of abundant design standards, the outlook for safe photovoltaic (PV) installations appears exceedingly promising

2.4 Conclusion

The purpose of this section was to identify the risks associated with the assets that could hinder the safe implementation of the FCPB. Regarding LiBs it was found that controlling the SoC, DoD, (D)C-rate and temperature within their respective limits, taking into account the current SoH, should prevent catastrophic thermal runaway. Furthermore, the risk analysis performed on PEMFCs identified the explosion of pressurised hydrogen tanks as the highest priority risk, with the notion that guidelines mitigating the occurrence and severity exist. Especially when adhering to the PGS guidelines, the implementation of hydrogen power for the FCPB application is feasible. It is referred to Section 4, for the safe operational limitations of controlling a PEMFCs stabilised DCMG. Lastly, the widespread acceptance of solar PV plants have lead to extensive understanding of PV failure mechanisms and adequate prevention. Given the unidirectional power flow the introduction of PV plants into the DCMG does not append significant challenges.

3 SAFE DESIGN OF THE DCMG

3.1 System design

Physical design of microgrids plays a crucial role in the safety characteristics of the realised system. Although the relative recent flourishing of microgrid implementations due to the introduction of locally produced renewable energy extensive research has been conducted on potential design improvements. Microgrids are often assessed on their stability, power quality, reliability, flexibility and resource utilization [38, 39], as well as suitability to the FCPB project and cost effectiveness. This section will present an overview of literature efforts to characterise the possibilities and challenges in DCMG design.

3.1.a DC vs AC microgrids

Alternating current (AC) has dominated electricity distribution networks for years due to numerous advantages over Direct Current (DC) distribution. However, the rise of localised renewable DC energy sources (PV, fuel cells) and DC energy storage techniques have opened the door to the re-introduction of DC distribution in microgrid applications. This section will discuss the (dis)advantages of a DC microgrid (DCMG) over its AC counterpart according to several reviews.

Starting with an observed efficiency increase due to the reduced amount of AC/DC converters required related to DC renewable generation sources, storage and loads [40]. This effect is amplified by the DC nature of most electric loads, that are often equipped with AC/DC rectifiers to comply with AC sources. Moreover, a rectifier can conveniently switch its operation mode allowing a DC input, diminishing the need for new equipment [41]. In addition, a DCMG does not suffer from traditional AC shortcomings as frequency

Table 1: Advantages and disadvantages of AC and DCMGs

	Advantages	**Disadvantages**
DCMG	Less required converters	Absence of inertia results in decreased stability
	Suitable for most AC as DC loads	Inclusion of CPLs leads to instability
	Easier power quality control	Fast fault current dynamics due to capacitive in/output filters
	Economically a better technical solution	Underdeveloped safety regulations
	High power transfer capabilities	Underdeveloped electrical design standards
ACMG	Zero current crossing assisting in arc extinguishing during faults	Requires frequency modulation
		Reduced efficiency due to skin effects
	Lower system cost	Inrush currents due to transformers

regulation, skin effects and inrush currents caused by transformers [42]. Finally, the power density in an equivalent cable is a factor $\sqrt{2}$ higher in DC compared to AC [43].

Undoubtedly, not only advantages are observed. Concerns about the safety and stability of the DCMG are the fundamental incentives of this research into renewables DCMGs. Stability issues are related to the negative incremental impedance of Constant Power Loads (CPL), that can cause current spikes [44]. While safety concerns arise due to a lack of inertia and the accompanied fast fault currents, tightening the response-time requirements for safety devices [45]. Moreover, the underdeveloped standards and protection techniques pose a limitation for widespread implementation [41]. A summary of the above analysis among other effects is depicted in Table 1.

3.1.b Topologies

A DCMG can be designed to match the characteristics of a certain application by changing the topology of the busses. In real-world applications there are infinitely many configurations, nevertheless a simple classification method is presented in literature. This section will shortly discuss the different classes and present a summary of the previously mentioned performance characteristics at the end.

The single bus, or radial bus, is the most simple method of connecting the different assets in a DCMG. This lay-out allows for a directly connected Energy Storage System (ESS), despite not being required. Connecting an ESS directly results in inherent stability at the cost of not being able to control the voltage and ESS charging cycles [38]. A single bus can be characterised as low maintenance and cost effective [41], while the reliability can be increased by adding more assets [39]. Although being simple the inclusion of several parallel converters might result in uneven loading and circulating currents [46]. Lastly, the lack of redundancy is paired with easy fault detection at the cost of a lower availability [47].

A straightforward extension of the single bus topology by adding supplementary busses is referred to as the multi-bus topology. The main merit lies in the increased redundancy and accompanied availability due to effortless fault isolation, increasing the operational cost efficiency [48]. Multiple busses can be mounted in series or in parallel opting for a high design flexibility [41]. For example, an appliance can be connected to two parallel busses with auctioneering diodes for increased reliability [38]. In an attempt to increase the stability and reliability the multi-terminal structure is proposed which adds more than one grid-connection [39]. Fundamentally this addition is not tied to a distinct topology, however an application that requires this level of reliability is matched to the advanced topologies mentioned below [38].

An interesting variant of a multi-bus topology is the ring-bus, creating a closed loop with the busses.

Table 2: DCMG topology characteristics

	Cost	**Reliability**	**Redundancy**	**Inherent Stability**	**Protection strategy**	**Suitability**
Single	Very Low	Low	Very Low	When ESS directly connected	Easy	High
Multi-bus	Low	Low	Low	No	Easy	Moderate
Multi-terminal	Moderate	High	Moderate	No	Moderate	Very Low
Ring	Low	High	Moderate	No	Difficult	High
Ladder	High	Very high	Very high	No	Difficult	Low
Zonal	High	High	High	No	Moderate	Low

Again the main merit is the increased reliability during faults at the cost of increased cost and complexity [38, 41]. The possibility of bidirectional power flow poses some complexities in the safety and control design of the grid, however numerous studies propose a solution for it [39].

Extending the complexity even further one would arrive at the mesh-bus topology. The redundancy and availability are significantly increased by connecting several single and ring-busses together to form a ladder structure, as applied in crucial application like datacentres and naval ships [39]. This system eliminates the changes of single point failure due to open circuit faults when coupled with Intelligent Electronic Devices (IED) [48]. However, limited applications are demanding enough to justify the associated difficulties in design of control and protection strategies [45, 47].

Lastly, a subvariant of the mesh topology is classified as the zonal-bus topology where several generators, loads and a grid connection are grouped in zones and zones are connected by multiple busses [38]. This would be preferred when many assets are combined over larger physical area while achieving a high reliability [48]. As is the case with the other elaborate topologies the demerits are found in challenging coordination and control [47].

In conclusion, literature presents a concrete classification of DCMG topologies, where the application is crucial in deciding a distinct design. As mentioned before several performance characteristics are applied to assess a design topology. A convenient summary of these characteristics is presented in Table 2, and a schematic overview in Figure 4. The suitability column is related to the FCPB application employing a limited single grid connection, ESS, PEMFC and PV array.

3.1.c Unipolar and bipolar configurations

Besides the topology of the DCMG another important design aspect is the configuration, which distinguishes between unipolar and bipolar variants. A unipolar DCMG is the conventional choice where the DC bus consists of a positive and a neutral wire while a bipolar configuration adds a third negative wire. The introduction of the third wire has several advantages over the 2 wire configuration, as discussed in [39, 46, 47, 49]. Most importantly, it offers the possibility for different voltage levels, where assets can be installed between neutral and positive/negative, or between positive and negative, allowing more assets to be integrated with reduced losses and of-the-shelf converters [50]. With that the maximum potential to ground reduces as well and the fault clearance capacity increases due to the neutral line. Furthermore, the reliability of the system increases due to the partial continued operation under fault of one of the lines. Finally, existing 3-phase AC systems are easily retrofitted as the same 5 conductor cables can be utilised.

On the downside, the system comes with additional cables and an asymmetrical implementation of the loads cause an imbalance between the lines. The latter is considered as the main drawback as it requires supplementary devices and more complex control. The concerns can be addressed by either adding a voltage balancing device or connecting one of the loads or generators, preferably an ESS, to all three poles. Fortunately, the wide availability of voltage balancing devices for multiple applications alleviate the restric-

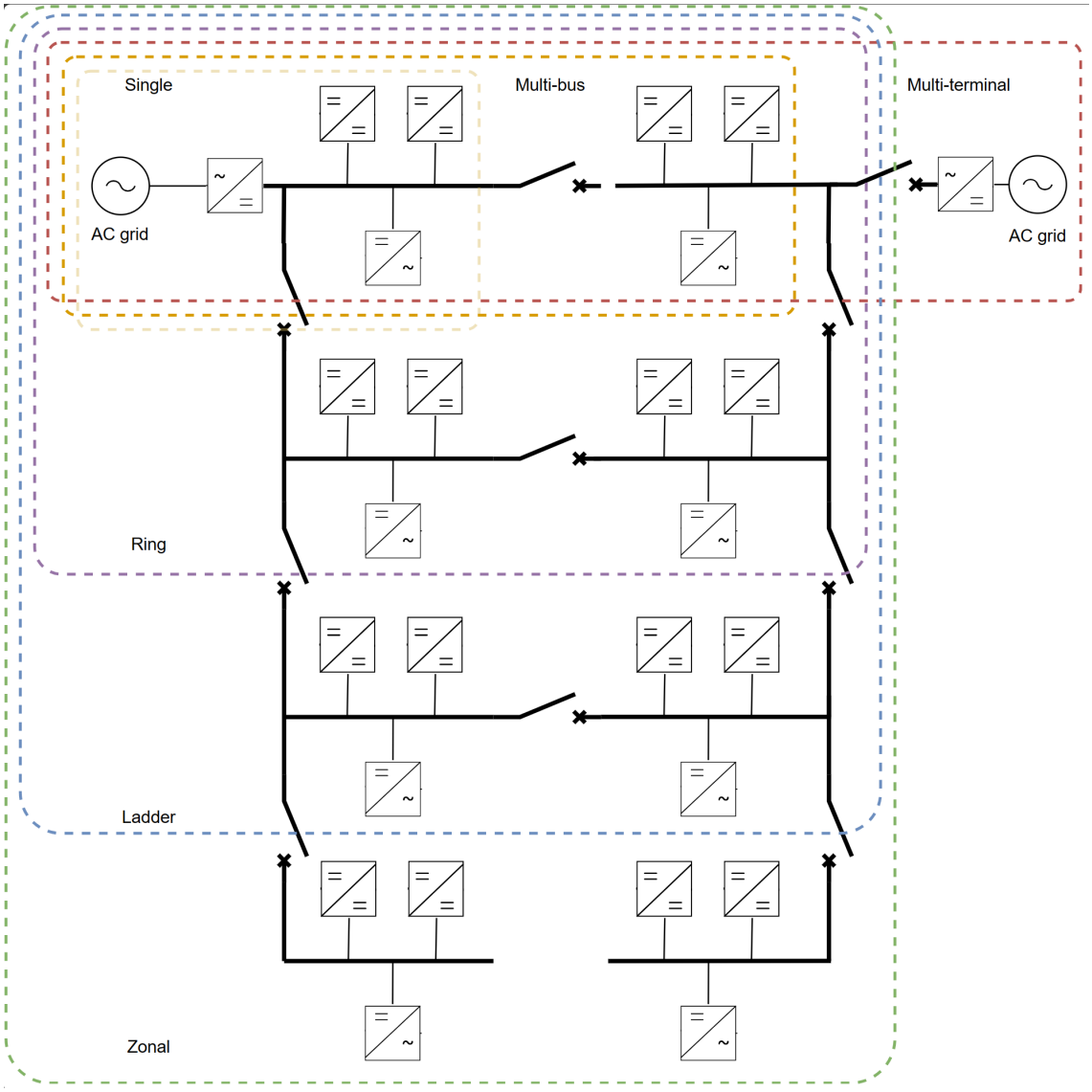

Fig. 4: Overview of various DCMG topologies (own work)

Table 3: Properties of the grounding devices [38, 45, 46, 51, 52]

	Stray current	**Touch potential**	**Fault detection**	**Fault ride-through**	**Reliability**
Ungrounded	Negligible	High	Difficult	Yes	Low
Solid grounding	High	Negligible	Easy	No	Low
Resistance grounding	Low	Low	Adequate	Yes	High
Diode grounding	Moderate/ Low	Moderate/ High	Easy	No	High
Thyristor grounding	Moderate/ High	Moderate/ Low	Easy	No	High

tion of this configuration [50].

3.1.d Grounding methods

Grounding of DC distribution networks is an important design variable due to the high impact on safety

and stability. The suitability of a grounding method is influenced by the system architecture, protective design (which is discussed in Section 3.2.c) and AC grid grounding arrangement [51]. Primary properties of an effective grounding design are minimizing stray current and its associated corrosion, guarantee safety to humans by minimizing the touch potential and facilitate Pole-to-Ground (PG) fault detection [53, 52], as well as secondary features as fault ride-through and immunity to network noise [51].

When it comes to grounding in DCMG applications a distinction between system grounding which refers to the busses and equipment grounding which refers to conductive component enclosures should be made [52]. In addition, the notions of grounding configuration (where is the connection made) and grounding devices (how is the connection made) are introduced [46]. The standardised name convention for the grounding configuration is described in IEC 60364. This code prescribes the first letter, either T or I, to the system grounding meaning connected or not connected to earth respectively. Likewise, the second letter, either T or N, refers to the conductive parts being connected to earth or neutral respectively. For the TN configuration a couple of sub-classes have also been mentioned in literature to increase the performance, especially in bipolar DCMGs, namely TN-S, TN-C and TN-C-S [40]. TN-S is proposed to increase the Electromagnetic Compatibility (EMC) by adding a separate Protective Earth (PE) line, while TN-C opts cost efficiency by combining the PE and Neutral line into a PEN line. Adopting the benefits of both, the TN-C-S is the most elaborate configuration, as schematically shown in Figure 5.

The unavoidable trade-off between stray current and Common Mode Voltage (CMV) is a matter of open discussion for DCMGs due to the lack of maturity and standardization [38]. The solid earth connection in TT and TN configurations result in leakage currents, inducing corrosion in the nearby metal objects. Yet, ground faults are easily detected by current monitors and systems disturbances are better absorbed [51]. An important remark, with solidly grounded DC sides is that the AC side cannot be solidly grounded as this would imply a short circuit path, hence the need for isolation transformers [54]. Ungrounded (IT) systems on the other hand suffer from potentially dangerous touch potentials (<60 V), difficulties of fault detection due to absence of leakage currents and underdamped voltage transients [51]. In addition, IT systems are unaffected by an initial ground fault providing exceeding reliability. Still, a rapid fault clearance is required because a second ground fault can create a short-circuit with considerable accompanied damage.

An alternative to the binary choice between grounded and ungrounded systems are meant to combine the advantages, or alleviate the disadvantages of both systems. For example, high resistance grounding enables continued operation during initial faults with safe but measurable ground current for effortless detection [54]. Another extension to solid grounding scheme is the inclusion of a diode which allows current to flow only from the ground into the system. If the CMV is above a threshold stray currents are prevented, however in practice low voltages are observed resulting in bidirectional conductive diodes [52]. Lastly, a bidirectional thyristor scheme is proposed where the IT system is grounded after a voltage limit has been observed. The reconfigurable grounding scheme ungrounds the system again upon sensing a reduction of stray current or trips the circuit breakers when the fault current persists [38]. The properties of the above mentioned grounding devices are categorically shown in Table 3. With respect to DCMG applications several studies have proposed to apply high resistance mid-point grounding due to the increased safety (half the voltage), ease of detection, primary fault ride-through and low stray currents [53, 55].

3.1.e Electrical standards

Standardization is mentioned as a major hurdle that prevents the widespread introduction of DCMGs according to the reviews presented above. However, a classic case of “who was first, chicken or egg” can also be identified here. At the time of writing, both standardization and research efforts are one the rise. The Dutch standardization office (NEN), is the first to introduce a guideline for implementing renewables oriented DCMGs, proposing a safety zone framework [**?**]. A schematic representation of this framework is presented in Figure 6, where the required incorporated safety measure are shown. The standard proposes TN-S based grounding for zones 1 to 3 , as well as galvanic isolation of the grid connecting ACDC converter. In addition, it recommends protection gear and the associated disconnection times for each zone sep-

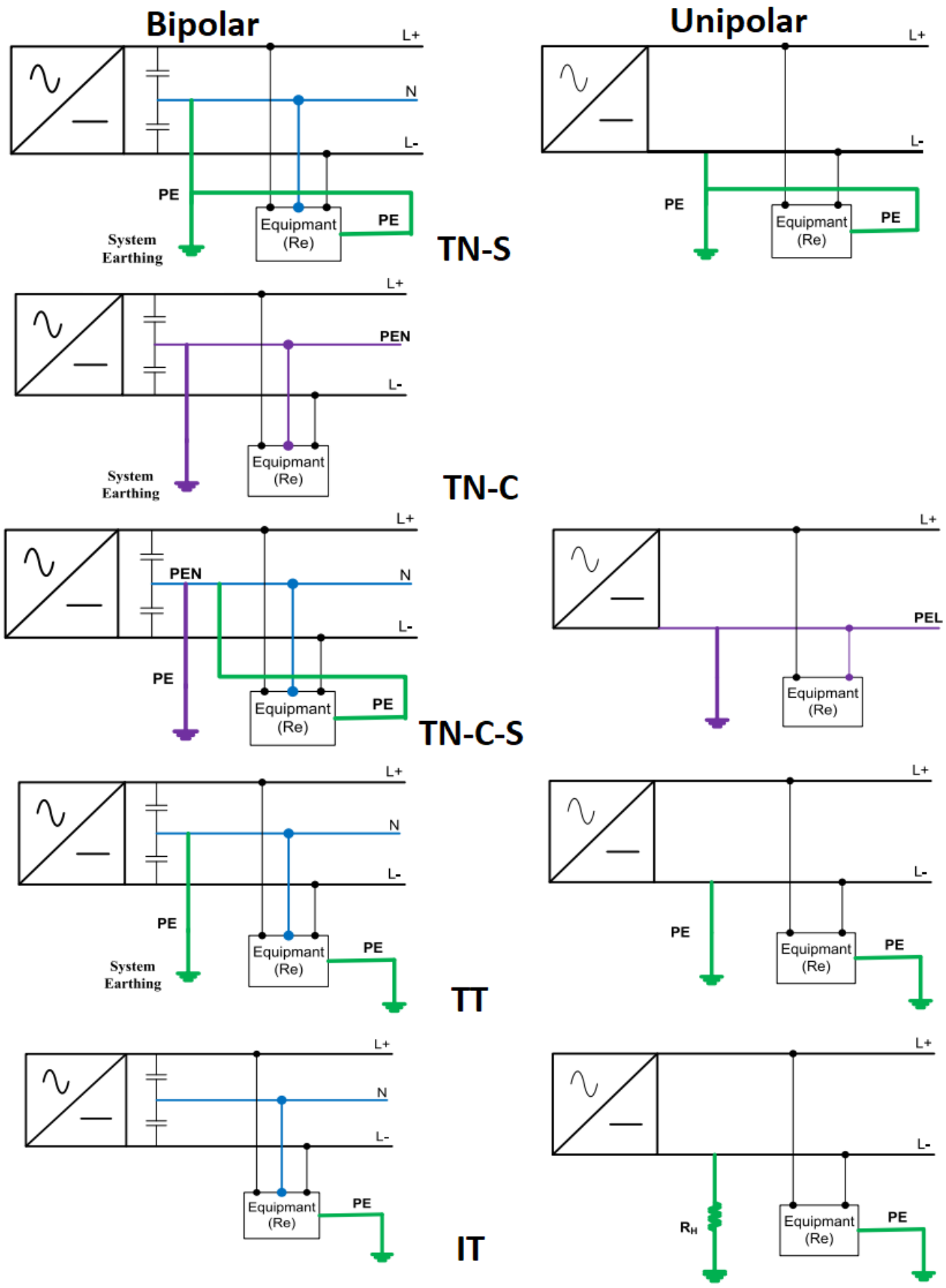

Fig. 5: The different grounding configurations according to IEC 60364 (adapted from [40])

Table 4: Overview of standardization efforts of several institutes

	Applications	Description
Emergence Alliance DCMG	DCMG	Recommends architectures and control in DCMG
IEC SEG 4	LVDC	Describes standardization measures up to 1500 VDC
IEC SEG 6	Microgrids	Assess aspects of microgrids in islanding mode
IEC 61557-1:2019	LVDC distribution systems	Describes equipment for testing and monitoring protective measures
IEC 61660	DC systems	Provides SC calculations for DC installations, however careful attention to the system configuration should be taken into account
IEEE 946:2020	DC power systems	Guidelines for safe battery operation SC calculations of different components Considerations to improve reliability and safety for DC power systems
IEEE 1547	ACMG	Extensive recommendations for AC power systems in islanding or grid-tied mode, can be extended to DC applications for most topics
IEEE 2030.10	DCMG in rural areas	Best practice for design and operation of islanding DCMG
NEN NPR9090:2018	DCMG	Safety classification and corresponding measures
NEC	DC technology	Some examples of codes within NEC that describe best practices: 625 (EV), 690 (PV), 692 (Fuel Cells)

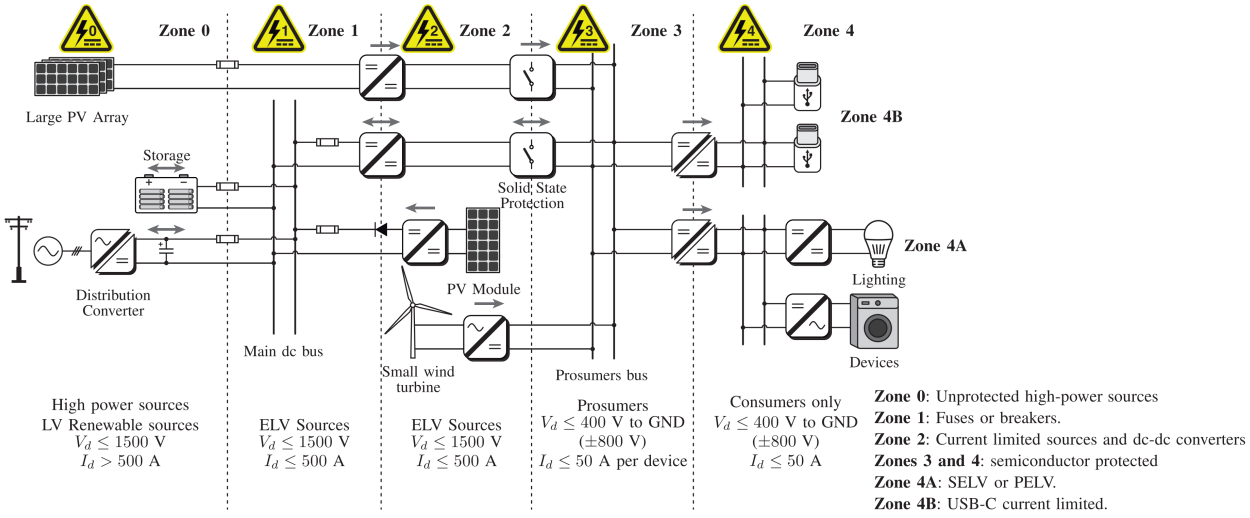

Fig. 6: Classification of risk zones in DC distribution according to NEN NPR 9090 [50, **?**]

arately.

In addition to the NEN, other esteemed institutions such as the IEC, IEEE, and NEC are actively engaged in the process of adapting standardization for DC systems. Following a thorough examination of these various codes, [45] concluded that the collective guidelines offer adequate direction, prompting the suggestion to consolidate them into a singular, specialised code for DCMG applications. A comprehensive summary of the relevant regulations documented in literature is provided in Table 4.

3.2 Continuous operations

In renewable energy-focused semi-off-grid DCMGs, a significant portion of safety hinges upon a the design of a protection system. Protection in this context encompasses various facets, including protection from

environmental hazards, fire prevention measures, and short-circuit safeguards, all aimed at facilitating continuous operation. Therefore, the ultimate goal of protection is to ensure continuous operations. This segment will delve into the underlying principles precipitating system disruptions, the associated detection methodologies, and the endeavours undertaken to mitigate adverse effects and ensure sustained operational continuity.

3.2.a System faults

Disruptions in DCMGs can be categorised into two main types: arc faults and short-circuit faults. The former category encompasses series arc faults, which occur within small connection gaps, and parallel faults, which arise between different conductors or ground [56]. In contrast, Short-Circuit (SC) faults occur due to physical contact between poles of the system, resulting in either a low-impedance pole-to-pole (PP) fault or a high-impedance pole-to-ground (PG) fault [46]. These fault types induce both transient and steady-state current responses from the system, with the transient component predominantly attributed to DC link capacitors and the steady-state response influenced by the connected assets [46]. Consequently, it is imperative to consider the various locations where faults can occur, as a fault at the bus itself poses greater danger than a fault in an easily isolated feeder [38].

Arc faults are triggered by a decrease in insulation and often associated with PV systems due to the increased wear by the environment [40]. Series arc faults, particularly in DC systems, present notable concerns for several reasons. Unlike AC systems, the absence of a zero voltage crossing in DC systems does not inherently extinguish the arc, which is highly detrimental [57]. Additionally, series arcs often fail to generate a sufficiently high fault current to trigger protective devices, often being mistaken for conventional load fluctuations [56]. Furthermore, the noise generated by series arc faults can easily propagate to neighbouring lines, impeding quick fault location and isolation [57]. In contrast, parallel arc faults draw significant current due to substantial potential differences, facilitating their detection and isolation. Consequently, parallel arc faults are managed by the short-circuit protection devices outlined in Section 3.2.b.

More detrimental to the DCMG and its connected assets is the occurrence of SC faults. Addressing these requires good understanding of the grounding, bus and system configurations [46]. For example, a single PG fault in a floating system does not trigger SC currents while in a grounded system it does. Compared to PP faults, PG faults are more likely to occur due to their susceptibility to insulation degradation, wear, tear and rodents, but are less severe [55]. PP faults trigger a sequence of events in converter interfaced DCMGs, first rapidly discharging of the DC side capacitors, diode freewheeling of the grid connecting converter resulting in possible feeding of the fault current by the AC grid [46]. Moreover, the current spike causes a voltage drop which in turn attracts more current of Constant Power Load (CPL) converters [40]. Blocking this high SC current with conventional Current Breakers (CB) is not possible due to the arcing behaviour of DC current, requiring more sophisticated devices [40]. Mathematical expressions for the actual produced SC currents are described in IEEE and IEC standards, however the inclusion of modern current limiting converters might overestimate the actual fault current, hence careful attention is required here [58].

3.2.b Protection devices

The aforementioned challenges posed by the fault characteristics of DCMGs present significant challenges on conventional protection devices, primarily attributable to the rapid current surges and arcing behaviour. Interrupting or limiting the transient fault current, that could potentially reach twenty times the nominal current [46], is of utmost importance for the protection of the interconnected assets. Reactivity to fault occurrences within DCMGs must be achieved within extremely short time frames, ideally within 5 ms [45] or even 0.5 ms [59] to ensure that such currents remain below twice the nominal value. Therefore, important properties for protection devices are speed, performance, selectivity, simplicity and economy [38]. Significant research is dedicated to retrofit conventional AC devices performance for the widespread introduction in DCMGs [60]. Extensive protection schemes consist of fault current limiting devices and current interrupting devices. This section will provide a brief overview of available protection devices, discuss potential future advancements, and conclude with a summarizing overview.

The most straightforward and traditional form of protection are fuses, which naturally melt upon experiencing an overcurrent. While their inherent simplicity is advantageous, they suffer from several drawbacks, notably the inability to differentiate between transient and permanent faults, as well as the requirement for manual replacement following activation [59]. Moreover, their slow response time renders them unsuitable for DCMG applications, although they may serve as a supplementary system behind more sophisticated devices [40].

A more suitable alternative for DCMG applications is the DC Circuit Breaker (DCCB), which is capable of interrupting higher currents with low steady-state loss and at a reduced cost [61]. Since its inception in the 1970s, a variety of DCCB designs have been proposed, among which Molded Case, Vacuum, and Mechanical Resonant types are particularly prominent [59]. In addressing the issue of arcing phenomena, researchers have put forth various designs for DCCBs, incorporating elements such as series inductors and uncharged capacitors to generate oscillating currents that facilitate the creation of zero-current crossings, thereby mitigating arcing [61]. More recently, mechanical switching variants have been complemented by Solid-State (SSCB) and Z-Source (ZSCB) devices, with the aim of improving response times [45].

SSCBs are based on semiconductor based switches and characterised by excellent arcing circumvention due to the absence of moving parts [62]. Candidates for semiconductor switches include IGBT, GTO, MOSFET, and JFET, each offering unique current, voltage, or loss characteristics. However, this technology suffers from higher steady-state losses, and a lack of galvanic isolation in the open state [59]. Necessitating external cooling systems, isolating switches as well as overvoltage protection circuits all contributing to elevated costs [62]. To address these limitations, hybrid circuit breakers have been proposed, aiming to combine the low losses of traditional MCBs with the rapid response of SSCBs. While this hybridization presents a promising solution, the exponential costs associated with such systems have impeded their widespread adoption [63].

The final interrupting device under discussion is the ZSCB, which offers autonomous fault response, simple control, effective isolation, and reduced steady-state power losses [64]. Additionally, bidirectional power flow is facilitated while concurrently inhibiting fault-limiting characteristics [59]. However, challenges persist, including the relative immaturity of the technology in terms of practical implementation, as well as the occurrence of unwanted negative currents at one end of the breaker and the short lifespans of the SCR switch [64]. Despite these hurdles, the positive trajectory suggests promising prospects for the future; however, both HCB and ZSCB designs are not currently deemed ready for widespread implementation. An overview of the discussed devices is presented in Table 5.

Furthermore, to enhance the DCMG protection, various fault limiting strategies can be implemented. These strategies encompass the integration of distinct fault limiting devices, the application of fault limiting control techniques to converters, or the mitigation of capacitor currents. Incorporating Fault Current Limiting (FCL) devices in series with DCCBs serves to reduce their nominal size. These devices possess inherent simplicity, operate swiftly and autonomously. Nonetheless, it is crucial not to overlook their potential impact on system-wide fault management [65]. Additionally, DCDC converters offer protective fault current limiting capabilities through adjustments in the primary control layer [66]. [45] presents a list of studies that propose schemes for FCL converters. For instance, [**?**] applied an adaptive droop algorithm to DCDC converters, reducing the breaking time requirements for DCCBs. Lastly, since DC-link capacitors supply the most substantial fault current peak, [67] proposed isolating them using fast-acting ETO SSCBs. In conjunction with FCL converters, this approach renders the system breaker-less, as the fault currents become manageable.

In summary, the rapid fault conditions lacking zero-current crossing present a formidable challenge for traditional AC protection methodologies. While the extensive discussion of this issue in literature has led to the emergence of numerous innovative protection devices and strategies, refer to Figure 7 for an overview, few are without limitations and boast substantial maturity. Achieving an effective protection scheme likely entails a resourceful combination of various devices.

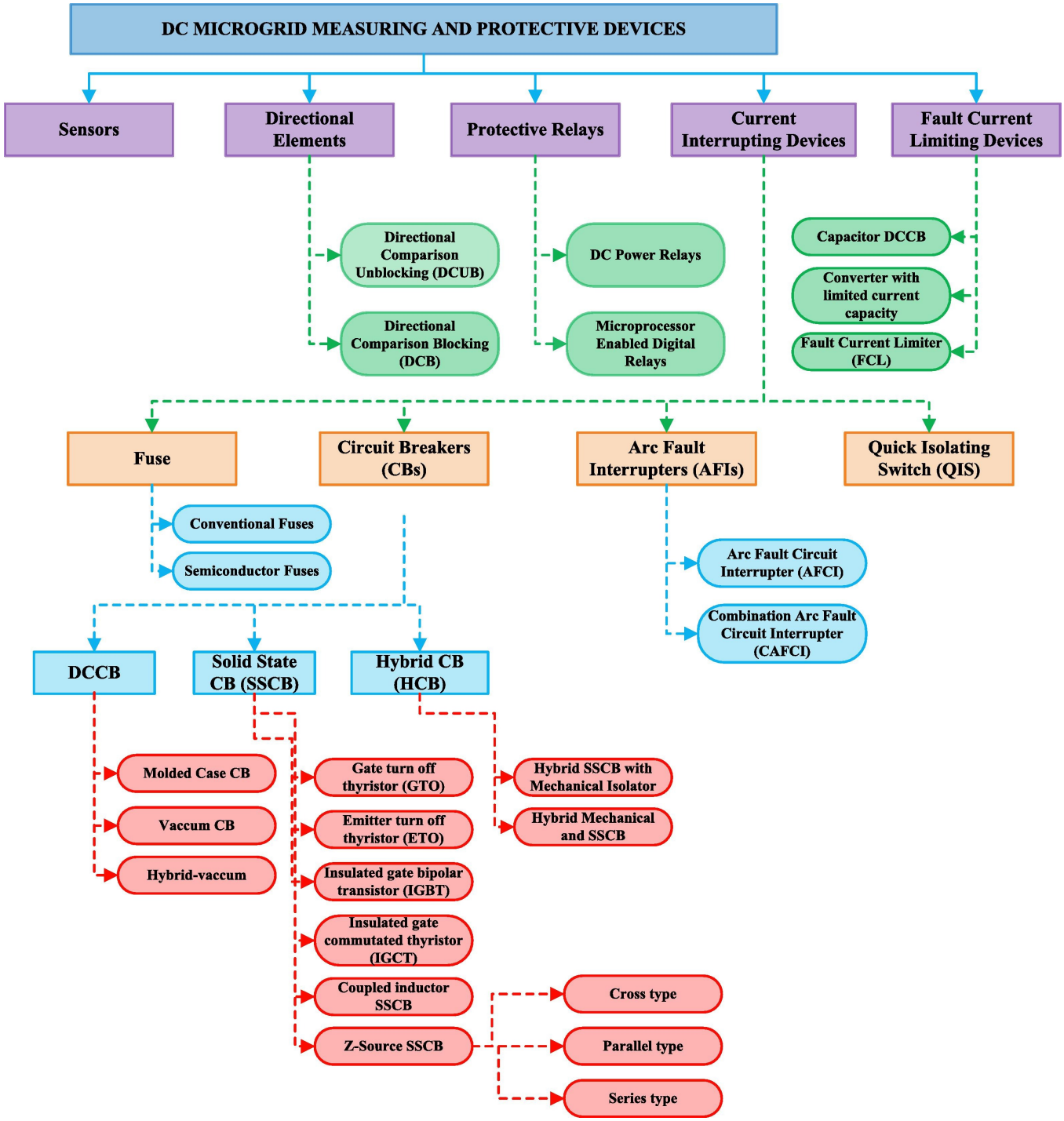

Fig. 7: Overview of protection candidates for DCMGs [40]

Table 5: Overview of protection devices and their main characteristics

	Speed (ms)	Steady power losses	Arc prevention	Operational life	Maturity	Cost
Fuses	<100	Very Low	No	Very Low	Very High	Very Low
MCB	<60	Very Low	No	Low	Very High	Low
SSCB	<0.1	Medium	Yes	High	Reasonable	High
HCB	<(5-30)	Low	Yes	Medium	Low	Very High
ZSCB	<0.1	Low	Yes	Medium	Low	Reasonable

3.2.c Protection schemes

Except for fuses and some of the FCLs the aforementioned devices primarily depend on trip signals to function. Detecting faults and subsequently sending trip signals incurs delays influenced by the communication infrastructure and the chosen detection method. Various sensing strategies have been proposed in the literature, evaluated based on their selectivity, reliability, speed, and system cost. Selectivity holds particular importance in DCMGs due to the presence of both temporary and permanent faults. Minimizing false tripping becomes crucial to ensure system reliability [40]. Moreover, the speed of the sensing method inherently affects the response time of DCCB tripping. A faster detection mechanism translates to quicker intervention, potentially reducing damage and downtime. Lastly, the cost is dictated by the amount of devices and communication infrastructure installed. The reported methods in literature are consequently ranked on these criteria where an overview is presented in Table 6.

The simplest methods mentioned are aimed at locally measuring the voltage or current and acting upon certain preset thresholds. The fundamental simplicity in logic and measuring equipment is enticing, however the associated lack of selectivity and measuring errors due to rapid transient current constitutes challenges in DCMGs [46]. To overcome the selectivity issues and achieve faster response derivative based tripping control has been proposed. The discrete derivatives based on Δi or Δv require sampling rates of a tenth of peak current reaching time thereby introducing noise and possibly faulty conclusions [46]. However, by combining the information of both current and voltage derivatives the reliability is increased while still presenting a fast protection scheme [40]. To acquire even better selectivity, robustness and response time differential methods, measuring voltage and current at both ends of each line, are a noteworthy and straightforward solution. The major drawback lies in the need for additional measuring units and fast communication infrastructure [47].

Besides passive local measurement based methods, active and communication dominated systems are mentioned as well. For instance, active impedance estimation methods involve the continuous insertion of a spectrum of voltage signals into the system to analyze the resulting current response, thus determining the impedance. Through the application of sophisticated algorithms, these methods can determine fault magnitude through the real part of impedance and fault location via the imaginary part [46]. Furthermore, emerging protection schemes applying time or frequency spectrum-based signal analysis are consistently under development, aiming to achieve rapid fault detection and precise fault location. However, the inherent complexity associated with these methodologies often places them beyond the practical scope of application within the FCPB system context. For a comprehensive understanding of these advanced techniques, interested readers are directed to [40, 46, 47].

3.3 Conclusion

The intrinsic technical advantages of DC over AC microgrids have excited a notable surge in research directed towards addressing the challenges inherent in DC systems. This section delved into the design aspects to gain insights into the current landscape of the literature. System topology and configuration, key determinants of flexibility, reliability, and cost-effectiveness, are reasonably well understood. However, given the infancy of the technology, inadequate system components, improper standards and lack of proven protection schemes, a pursuit of simplicity is strongly advised.

With regard to the safety of DCMGs, various issues have been identified, for which novel solutions have been proposed. Primarily within the realms of grounding configuration and fault handling, the inherent drawbacks of DC present significant challenges. Although a multitude of solutions has been proposed in the literature, they largely remain within the domain of research, resulting in the absence of a standardised, mature DCMG protection scheme.

4 FUEL CELL OPERATIONAL CHARACTERISTICS

Section 2.2 has previously mentioned the operational principles of a PEMFC as well as the associated risks inherent in its operation. It was deduced that despite the relative immaturity of complete systems, the operational risks of the PEMFC can be mitigated to acceptable levels. It is pertinent to note that unlike a LiB, the PEMFC functions solely as an energy conversion device, thus in the event of failure, it does

Table 6: Overview of sensing methods and their characteristics [40, 46, 47]

	Selectivity	**Reliability**	**Speed**	**Cost**
Overcurrent	Low	Moderate	Moderate	Moderate
Over/undervoltage	Low	Moderate	Moderate	Low
Derivative of current/voltage	Moderate	High	High	Moderate
Differential of current/voltage	High	High	Very High	High
Impedance	Moderate	Moderate	High	Moderate
Handshaking	Low	Moderate	Moderate	Low
Traveling wave	High	High	High	High
Frequency analysis	High	High	High	Moderate

not harbor substantial energy for release. Consequently, the primary concern lies in the storage of high-pressure hydrogen, which is susceptible to external hazards such as fire or accidents. This section aims to highlight the operational limits for the PEMFC to effectively mitigate the safety risks previously discussed. In addition, performance limits and lifetime are key aspects in the economical operation of the PEMFC asset, hence the attention to this topic. This section will commence with delineating the observed degradation, followed by the operational limits that reduce this degradation.

4.1 Degradation by component

Being a complex electro-chemical cell, the PEMFC is prone to a variety of different mechanical, chemical and thermal degrading effects, that have effects on the molecular to component scale. Studies that try to capture all the degradation phenomena commonly categorise the affects by the component of the FC [20, 21]. This section will provide insights in the degradation phenomena observed in the individual layers.

Recalling Figure 3, the principal components of a single cell are the Bipolar Plates (BP), Gas Diffusion Layer (GDL), Catalyst Layer (CL) and the Proton Exchange Membrane (PEM). Starting with the membrane, the key component in a PEMFC, which accommodates the protonic flow while insulating electrons. Due to the harsh environment the membrane should be mechanically and chemically strong, while keeping its protonic conductivity low [20]. Nafion membranes, based on PTFE with additional Fluor and Sulfur groups, are most common due to their excellent proton conductivity, albeit much dependent on the temperature and humidity [68]. The membrane integrity can be affected by thermal, chemical and mechanical factors. High temperatures impact the water content and therefore the protonic conductivity, while low temperatures might increase the risk of freeze/thaw cycles resulting in mechanical stresses the membrane [69]. Mechanical failures can be introduced before the start of operation by a too thin membrane or manufacturing defects, while during operation inadequate humidification or unequal pressure are the underlying causes [70]. Chemical degradation is mainly attributed to free radicals that attack the membrane. The radicals are formed as side reactions under open circuit voltage (OCV) or low humidity conditions [69], where the impact severely increases with temperatures above 90 °C, high gas pressures and the usage of pure hydrogen and pure oxygen [71].

The catalyst layer is responsible for initiating the chemical reaction at both interfaces, with particular emphasis on the reduction reaction of oxygen at the cathode, owing to its orders of magnitude slower dynamics [68]. Typically the CL is composed of Platinum (Pt) or Pt-alloyed metals supported on a conductive carbon substrate, submerged in an ionomer, where the carbon supports the electron flow and the ionomor the proton flow. The catalyst effective area is often referred to as the Electrochemical Surface Area (ECSA), directly impacting the reaction rate and therefore the power capabilities of the PEMFC. Over time, a reduction in ECSA is observed due to various mechanisms. For instance, the carbon substrate hosting the catalyst may undergo corrosion due to high cell potential, leading to Pt detachment. These detached Pt particles subsequently aggregate onto other Pt clusters, diminishing the available ECSA [20]. Another significant phenomenon is the

electrochemical Ostwald ripening process, driven by concentration gradients, which is accelerated under potential cycling conditions. During this process, Pt ions migrate from smaller to larger particles in accordance with Fick's law of diffusion. Potential cycling accelerates the dissolution rate of Pt ions into the ionomer, which subsequently redeposit on larger particles, further reducing the ECSA [72]. Besides the loss in ECSA, shrinking and swelling cycles caused by humidity cycling result in residual stresses and finally delamination of the CL, GDL and PEM due to their different strain characteristics [72]. Delamination of the subsequent layers hinders the electron flow, hence the ohmic resistance is increased. Additionally, it creates higher current density's in parts of the cell which are not affected by delamination, accelerating degradation even further in these regions.

The gas diffusion layer facilitates the distribution of gases, water, heat, and electrons, serving a multi-purpose role. Typically, the GDL is fabricated from carbon-based porous materials with hydrophobic coatings, commonly (PTFE) [69]. The degradation of its relatively straightforward functions poses challenges in its classification, often overshadowed by more severe mechanisms within the CL and PEM. Mechanisms outlined in literature include carbon cracking induced by corrosion, fatigue stemming from thermal cycling, and diminished hydrophobic behaviour due to radical attacks [73]. All of which contribute to a higher gas flow resistance resulting in lowered reaction rate and slower dynamic behaviour.

Lastly, the multi-functional BP, also denoted as the distribution layer, which serves to segregate the fuel, reactants and coolant streams from one another, collects the current and acts as the main structural component [69]. The characteristics of a robust BP should encompass corrosion and chemical resistance, as well as low weight and cost while retaining electrical and thermal conductivity. Research endeavors in this domain suggest noble metal-coated steel or composite graphite materials as prospective solutions to meet these exacting requirements [69]. The chief contributor to its degradation is corrosion, resulting in elevated electrical resistance and diminished power output, albeit to a lesser extent compared to other layers within the fuel cell [20].

Based on the aforementioned analysis, it is evident that all components of the PEMFC experience degradation to varying degrees. The performance of these fuel cells relies heavily on several key properties: the electrical conductivity of the components and their interfaces, the extent of remaining ECSA which dictates reaction rates, the integrity of the membrane to prevent permeability to oxygen and hydrogen, and the efficiency of mass transfer to supply reactants and prevent flooding. Consequently, any deterioration in these properties is likely to lead to a reduction in power output and should therefore be minimised during operation.

4.2 Operational impact on degradation

The preceding section highlighted the degradation phenomena occurring within the active layers of PEMFCs, with a notion of the internal contributing factors. However, practical application demands a focus on operational conditions rather than abstract internal behaviours, as operational parameters are controllable. Accordingly, this section will delineate literature findings pertaining to the correlation between operational conditions and internal degradation mechanisms.

In the context of mitigating degradation, it is preferable for the PEMFC to operate at a constant nominal current. Studies [72, 74] have identified various operational conditions, such as idling, high load, load fluctuation, and start-stop cycles, as primary contributors to degradation. These conditions lead to elevated potentials, water flooding, dynamic states, and even higher potentials respectively. According to their research in demanding automotive applications, dynamic loads account for 56%, followed by 33% for start/stop cycles, and 5% each for idling and high power operation.

4.2.a Idling state

The idling state of the PEMFC can be regarded as a stand-by mode, wherein the FC primarily provides power to its internal subsystems such as the water pump, re-circulation pump, and control systems, which typically necessitate only 1% of the rated power. Conversely, the air compressor may consume up to 15% of the power and is deactivated during stand-by mode [74]. During idling, the current demand is minimal, resulting in a high potential and increased gas permeation through the membrane. This elevated potential induces various chemical reactions,

including the migration of metal ions and Pt dissolution at the cathode, as elucidated in Equation 1 [72]. The cell potential during idling can reach up to 0.95 V, approaching the cathode potential since the anode overpotential is negligible [75]. Consequently, Pt dissolution typically occurs with the intermediate step of Pt oxide formation.

$$\begin{cases} Pt - 2e^- \rightarrow Pt^{2+} & E_0 = 1.188\text{V} \\ Pt + H_2O - 2e^- \rightarrow PtO + 2H^+ & E_0 = 0.980\text{V} \\ PtO + 2H^+ \rightarrow Pt^{2+} + H_2O & E_0 = 0.837\text{V} \end{cases} \quad (1)$$

The increased gas permeation is directly influenced by the lower reaction rate, pressure build-up, and subsequent diffusion according to Fick's law. The presence of oxygen at the anode and a favorable potential accelerates the formation of H_2O_2, which reacts with metal ions such as Fe^{2+} and Cu^{2+}. These ions, originating from the bipolar plates (BPs) or the production process, participate in Fenton reactions, producing several radicals [72], along with their associated consequences detailed in Section 4.1. At the same time crossover H_2 might react directly with O_2 on the cathode in a reaction that results in local hot spots. Where the increased temperature accelerates Pt dissolution and chemical degradation of the membrane [76]. In conclusion, prioritizing the avoidance of prolonged idling periods is imperative.

4.2.b High power

In contrast to idling conditions, high-power operation is associated with decreased cell potentials, thus mitigating many related issues. However, this heightened operational state also leads to increased reaction rates and current density, resulting in elevated temperatures and the occurrence of flooding. Notably, temperature has been empirically demonstrated to accelerate phenomena such as Pt particle growth, oxidation, deposition, and radical formation within the membrane [76]. Moreover, water flooding impedes mass transport resulting in reactant starvation and the accompanied cathode corrosion (see Section 4.2.c). Fortunately, the occurrence of water flooding can be detected by monitoring pressure drop within the cell, enabling timely intervention through temporary reduction of current demand [77]. Consequently, the extent of permanent degradation is diminished.

4.2.c Dynamic loads

During dynamic operation, the rise rate of current exhibits significantly faster dynamics compared to that of reactant supply to the FC, leading to hydrogen, oxygen, or both being subjected to starvation. The starvation behaviour results in a characteristic transient voltage response which over/undershoots and consequently recovers in time depending on the load step [78]. Although starvation is transient, it can inflict substantial irreversible damage to the cell. Oxygen deprivation at the cathode induces protons generating hydrogen instead of water, which is experimentally observed at the exhaust under air starvation conditions [72]. Consequently, adjacent to local areas experiencing air starvation, the generated hydrogen may directly react with oxygen, creating hot spots that must be avoided. On the other hand, hydrogen deprivation manifests as either local starvation or global starvation. The former stems from an uneven distribution of hydrogen, generating local low-pressure zones that drive air permeation through the membrane at these sites. Thereby, reversing the current within the cell locally, elevating cathode potential and promoting carbon corrosion at the cathode [75]. Under more severe circumstances, complete anode-side hydrogen deprivation can occur, elevating the anode potential from near 0 V to 2.5 V vs RHE [79]. This results in the anode potential exceeding that of the cathode, causing the entire fuel cell to reverse polarity, resembling an electrolyzer. This inherently disrupts flows and operations, with extreme potentials posing the greatest threat due to carbon corrosion on the anode side [75].

Secondly, dynamic operations induce fluctuations in temperature and water content. The degradation resulting from these processes is better understandable, as both temperature and water content cycles lead to shrinking and swelling, accompanied by associated mechanical degradation [80]. Potential cycling represents another detrimental effect associated with dynamic loads. Pt oxide formation and dissolution (as seen in Equation 1) are the primary contributors, with their consecutive occurrence leading to intensified dissolution, a phenomenon known as the place-exchange mechanism [81]. Since both reactions are influenced by different potentials, this phenomenon is not triggered under constant power conditions, but occurs during load changes, even at low powers. Overall, the dynamic states and fluid starvation induced by load changes pose a significant challenge to the in-

tegrity of the PEMFC.

4.2.d Start/Stop cycles

Lastly, phenomena related to start-stop operation are addressed. During both start-up and shut-down procedures, the transient presence of air at the anode is unavoidable, leading to carbon corrosion similar to the hydrogen starvation process. Electrochemical corrosion of the carbon supports is governed by the reactions presented in Equation 2. Although relatively low equilibrium potentials accompany this reaction, research indicates that corrosion begins at potentials exceeding 1 V [75]. Additionally, [82] found that the lack of current density uniformity in the cell during start-up results in areas more susceptible to degradation. Moreover, in subzero temperatures, the freezing of water induces increased mechanical stresses on the cell, which should be mitigated [72].

$$\begin{cases} C + 2H_2O - 4e^- \rightarrow CO_2 + 4H^+ & E_0 = 0.21\text{V} \\ C + H_2O - 2e^- \rightarrow CO + 2H^+ & E_0 = 0.52\text{V} \end{cases} \tag{2}$$

A comprehensive summary of all mechanisms discussed in this section is presented in Figure 8. The avoidance of all conditions outlined undeniably constrains the practical application of the PEMFC to a significant extent, a goal not pursued within this section. Nonetheless, these acceleration effects necessitating consideration in formulating a successful PEMFC implementation. Idling, high-power, and start-stop cycles present concrete conditions that can be avoided. In dynamic operational scenarios however, complexities arise, as the decision-making process incorporates the ramp rate, or speed of upscaling. Slowing the ramp rate mitigates issues related to starvation and dynamic water management, while temperature fluctuations are minimised through effective cooling strategies. Alternatively, preemptively increasing reactant supply to anticipate load changes can enhance ramp rate capability without inducing gas starvation from 2% per 0.1 s to 50% per 0.1 s [83]. Nevertheless, potential cycling (and the place-exchange mechanism) remains an inherent challenge irrespective of ramp rate and cycling frequency [72].

4.3 Costs components

The preceding section highlights that the majority of degradation mechanisms can be classified according to specific operational conditions. While complete circumvention of degradation is unattainable, it can be managed to an acceptable degree. This section aims to shed light on endeavors aimed at quantifying PEMFC degradation within operational contexts. It starts with an examination of methodologies quantifying the observed effects of particular mechanisms, succeeded by an overview of modeling endeavors pertaining to DCMGs including PEMFCs.

Determining the operational costs of the PEMFC entails the consideration of multiple factors. Primarily, the assessment involves accounting for both Capital Expenditures (CAPEX) and Operational Expenditures (OPEX). While CAPEX is contingent upon the manufacturer and falls beyond the scope of this literature review, OPEX encompasses maintenance costs, hydrogen expenses, and degradation. The latter two elements are notably influenced by operational conditions, given the fluctuating efficiency levels and degradation rates. Consequently, the question arises regarding the extent to which each discrete factor contributes to observable degradation and how best to model such dynamics effectively.

4.3.a Quantification of degradation

Numerous studies have experimentally demonstrated that degradation within PEMFC can be quantified in terms of voltage loss, per unit time or per specific event. For example, [84] compiled a comprehensive list of the degradation mechanisms outlined in Section 4.1, along with their corresponding voltage loss rates per hour. Notably, flooding, excess heat, and ice formation were identified as particularly detrimental factors. In a more practical approach, [85] assigned empirical voltage decay rates to each condition mentioned in Section 4.2. By establishing this direct correlation, the study linked operational conditions to operational costs, thereby offering on average reasonably accurate lifetime predictions. Expanding upon this earlier model, [86] incorporated additional factors such as the acceleration effects of temperature and relative humidity, along with a form of natural degradation, in an effort to capture a more physical behaviour. Especially, the inclusion of load change degradation dependent on the ramp rate appears advantageous, considering the starvation phenomena discussed in Section 4.2. An alternative approach was proposed by [87], wherein a model was

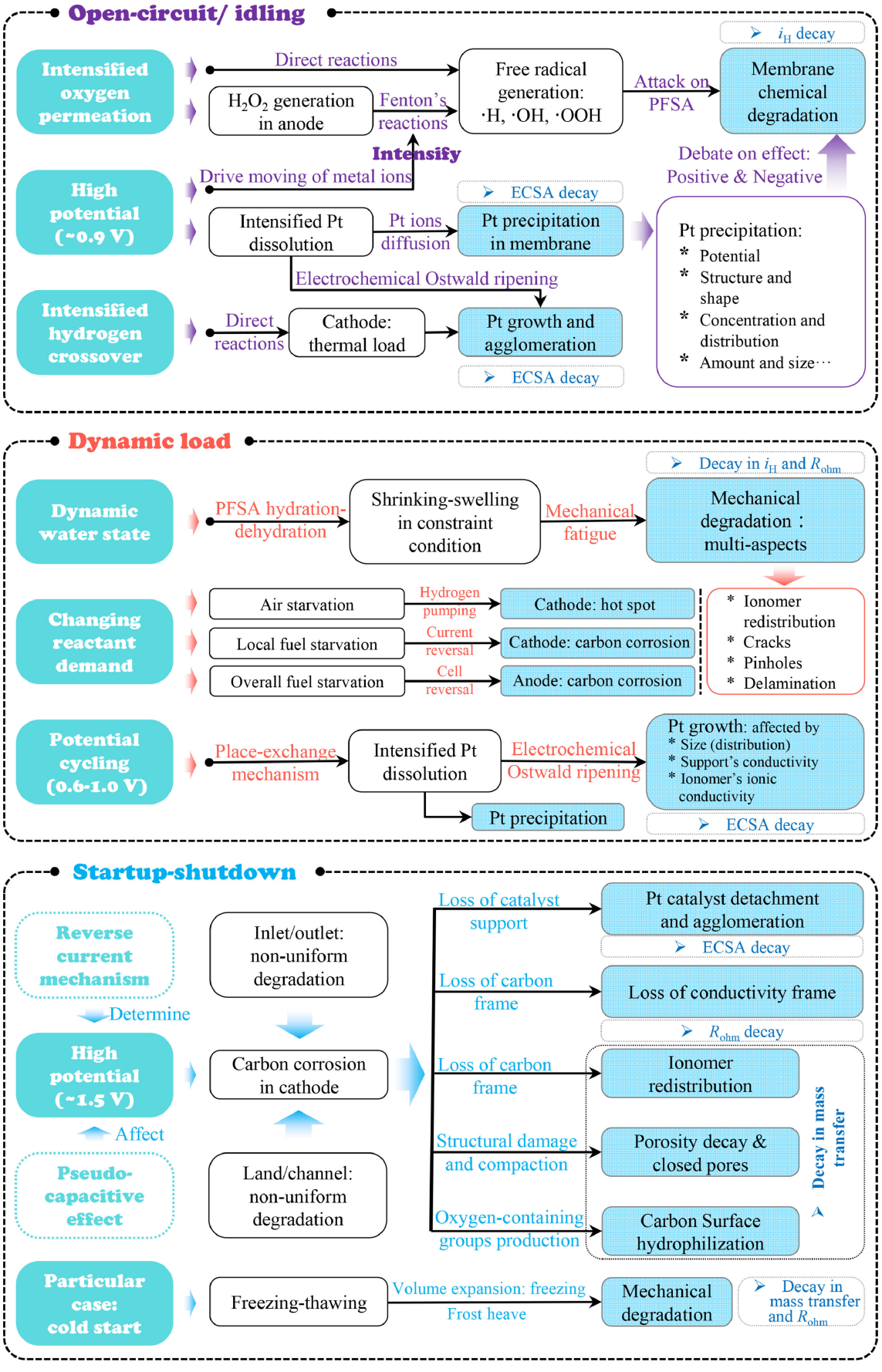

Fig. 8: Summary of degradation mechanisms grouped by the underlying operational conditions [72]

constructed to account for steady ECSA loss based on electrochemical dissolution, as well as transient ECSA loss based on empirical data. Both steady-state and transient contributions from the operational profile influence ECSA loss, with findings indicating that a 75% reduction in ECSA correlates with a 35% decline in power output at end of life.

These studies present similar numbers for degradation rates; a single start/stop cycle causes about 15 $\mu V/cycle$ or 0.0015% of degradation equalling approximately 35 load change cycles. Idling and high power operation contributions are in a similar order of magnitude between 8 and 12 $\mu V/hr$ [85, 86, 88]. The costs of degradation can be extrapolated out of the voltage loss when a certain end of life criterion has been set and the CAPEX is known.

4.3.b Health aware operation strategies

The models in the previous Section describe the loss as a function of the input conditions. However, for the purpose of health-aware operations more sophisticated models are required with the possibility to find the most optimal deployment strategy. This section aims to shed light on the modeling approaches taken in literature to optimally schedule FC operation including lifetime consideration. The discussion on different scheduling techniques for DCMGs is elaborated in Section **??**. On the contrary, this Section focuses on scheduling methods that include hydrogen technologies and its associated behaviour. The fundamental characteristics of PEM fuel cells and electrolyzers described by their minimum and maximum powers, and maximum allowed ramp rate are covered by all efforts. However, when looking more specifically into efficiency or the inclusion of degradation many differences arise.

A proper example describing the different scheduling techniques is given in [89] comparing the potential of Economic Dispatch (ED) and Economic Model Predictive Control (EMPC) strategies. Both methods pose an optimisation problem where the latter is more sophisticated by solving the problem at any time step given a predetermined prediction horizon. The problem is consequently solved by either Dynamic Programming (DP) or Mixed-Integer Linear Programming (MILP). The study concludes that solving the ED problem by DP is too computationally expansive while DP is preferred over MILP in terms of accuracy when solving the MPC problem. Since both solving routines require linear equations and constraints the non-linear effects of efficiency are hardly taken into account. [90] addresses the problem of non-linear plant dynamics, especially FC efficiency, by executing the non-linear equations outside the MPC loop, hence taking them constant in the optimisation.

In an effort to further develop the performance of the scheduling effort [91, 92] propose multi faceted MPC algorithms. The purpose is to separate the slow acting assets as the FC from the rapid acting assets as an ESS, for the sake of computational efficiency. Both models also include binary variables that determine the on/off state as to reduce the amount of start/stop cycles. Extending this binary variable principle, [93] introduces Mixed Logic Dynamic (MLD) for start/stop states and degradation state. The MLD framework allows for the introduction of the state variables which in turn is better suited for including certain degradation costs. The study suggests a MIQP solving routine since it was found that it is better able to reduce degradation compared to a MILP solver. Expanding on the MLD framework, [94] adds cold and warm intermediate states between on/off/standby for a more accurate representation of the timeline in the start-up process. Consequently costs are added to the state changes, however without taking into account how fast it changes. In a later study [95], the same authors go back to a 3 state system to alleviate the complexity and focus on a double MPC to better describe the fast acting assets.

Although, many effective efforts regarding the scheduling of hydrogen assets in microgrids have been presented above, none of them includes sufficient degradation dynamics as discussed in the models from Section 4.3.a. Finally, [96] does includes an empirical voltage degradation model aiming to prevent start/stop cycles, high power and fast ramping into an ED framework however the scheduling accuracy lacks far behind the studies mentioned before. A summary of this section is presented in Table 7, which clearly depicts the shortcomings of the proposed works and the possibilities of this work.

4.4 Conclusion

This section delved into the degradation mechanisms experienced by different components of PEMFCs, including the membrane, catalyst layer, gas diffusion layer, and bipolar plates. These components are susceptible to mechanical, chemical, and thermal degra-

Table 7: Overview of studies addressing hydrogen technologies in scheduling efforts focusing on degradation

	Model Approach			Degradation Characteristics				
	Method	**Solver**	**Efficiency**	**Start/ Stop**	**Load change**	**Standby**	**High power**	**General Lifetime**
[89]	ED vs EMPC	DP vs MILP	Linear					x
[90]	Adaptive EMPC	MILP	Non-Linear					x
[91]	Multi-stage MPC	MILP	Constant	x				x
[92]	Multi-time MPC	MILP	Constant	x				x
[93]	Multi-time MLD-MPC	MIQP	Constant	x	x			x
[94]	MLD-MPC	MILP	Constant	x	x	x		x
[95]	MLD Cascaded MPC	MILP	Constant	x		x		x
[96]	Economic dispatch	MILP	Linear	x	x		x	x

dation, which can lead to a reduction in power output and efficiency over time. Operational impacts on degradation, such as idling, high-power operation, dynamic loads, and start/stop cycles, are thoroughly examined, highlighting the correlation between operational conditions and internal degradation mechanisms. Moreover, the chapter discusses the costs associated with PEMFC degradation and explores various methodologies for quantifying and managing degradation within operational contexts. Start/stop cycles were found to be a factor 35 more severe than load cycles, while an hour of idling or high power contributes in the same order of magnitude as a single load change, raising the question as to what conditions are relevant to take into account. Furthermore, the chapter explores health-aware operation strategies, focusing on modeling approaches aimed at optimising PEMFC deployment while considering degradation dynamics. It was found that there exists a gap in the combination of optimal scheduling techniques and adequate degradation mitigation. In summary, valuable insights into the operational characteristics of PEMFCs are provided, highlighting the importance of managing degradation to ensure the safe, efficient, and cost-effective operation of PEMFC systems.

5 CONTROL STRATEGIES

Now that the impact of DCMG design and the characteristics of PEMFC systems are understood, attention has shifted towards the control of the integrated FCPB system. The core functionality of the FCPB hinges on effective control mechanisms serving multiple objectives. The assets in the FCPB are interconnected to a common DC bus via DC-DC converters, which facilitate the regulation of voltage and current levels. Additionally, appropriately controlled converters play a crucial role in limiting fault currents and providing (virtual) impedance for stability enhancement. Beyond the individual asset level, collaborative interaction with other assets is paramount for the efficient operation of the FCPB, influencing load distribution and resource optimisation. Moreover, at a higher level, the control strategy encompasses an Energy Management System (EMS), overseeing parameters such as minimal power losses and operational expenses. In summary, the control strategy encompasses the following objectives [39, 48, 97]:

- Inverter voltage and current regulation according to given set-points
- Asset collaboration and consequent load distribution
- Ensure stability of the system and robustness against fault events
- Ensure minimal transmission losses
- Operate the FCPB at optimal cost effectiveness

This chapter starts with a review of local control strategies and continues with several proposed EMS strategies. The aim is to get insights into how to combine both into a single algorithm addressing all the objectives stated above for the FCPB application.

5.1 Local DCMG control

As previously mentioned, the interfacing converters play a pivotal role in controlling the power flow within the grid. Each converter is equipped with a

local controller responsible for determining the duty cycle of the switching device, thereby regulating the output power. The primary objective of this controller is to adjust the asset power by tracking specific predetermined reference values, typically referred to as the inner control loop operating on a millisecond time scale. In addition to their primary function, the converters also engage in collaborative efforts to ensure load distribution and maintain bus voltage within acceptable limits, also referred to as the local control loop. Various methodologies addressing this collaborative functionality are presented in the literature, as will be discussed in Section 5.1.a.

5.1.a Centralised, Decentralised and Distributed

The collaborative control of a DCMG is commonly classified into centralised, decentralised, and distributed methods, determined by the extent of communication infrastructure among the assets. Centralised control schemes, as the name suggests, consolidate information from all assets at a single location, where it is processed to formulate the control strategy. An example of centralised control is the master-slave control, wherein one converter, typically the Energy Storage System (ESS), regulates the bus voltage and provides current references to the other converters. However, such systems necessitate a robust and rapid information-sharing infrastructure to minimise time delays, making them suitable primarily for smaller installations. While centralised control offers advantages such as comprehensive knowledge and improved power distribution, it is associated with significant drawbacks, including high communication costs, vulnerability to single points of failure, reduced flexibility, and the need for more complex algorithms [39, 97]. Considering the specific requirements of the FCPB system, which necessitates both high flexibility in load management and high operational reliability, a centralised control scheme appears unfavorable.

On the contrary, decentralised control strategies operate independently of communication infrastructure, relying instead on local voltage measurements to execute actions. In a DCMG, voltage levels serve as power surplus or deficit indicator, which is used to locally adjust power settings. Droop control and DC Bus Signaling (DBS) are common methodologies associated with this category [48]. Droop control establishes a feedback loop that encourages current sharing among assets, with the droop slope determining the trade-off between current sharing and voltage deviation [39]. DBS techniques partition the voltage range into intervals and assign specific control logic to each interval, with the effectiveness and stability of the system heavily reliant on the width of these intervals [98]. These approaches are characterised by their high reliability, autonomy, and independence from system layout. Their decentralised nature allows for straightforward integration or modification of assets within the system, without the need for extensive communication infrastructure or integrated control design. However, the sole reliance on decentralised methods has limitations, including a constrained control scope, the potential for steady voltage deviations, and operation that may not be economically optimal [39].

Finally, distributed control techniques aim to take advantage of the aforementioned strategies by integrating data from directly neighboring assets. Particularly in large systems, this approach has demonstrated an increase in current sharing capabilities and the mitigation of single-point failures [39]. Consensus-based algorithms and multi-agent-based algorithms exemplify these control schemes. Both methodologies hinge on communication protocols with neighboring assets to distribute the current, essentially simplifying the concept of an EMS. Given that the primary objective of the FCPB control is to implement a sophisticated EMS strategy alongside a reliable local controller, the addition of supplementary local EMS layers do not add much value.

5.1.b Droop control

As a conclusion from the above analysis it is clear that decentralised methods are outstanding candidates for the off-grid FCPB given the aforementioned mentioned advantages. Droop control is preferred over DBS methods because of its continuous feedback profile contrary to the fragmented feedback signals leading to heavily fluctuating operation profiles. In an effort to get rid of this chattering behaviour one retrieves a strategy very close to droop control, hence this section adopts droop philosophy as the basis of local control. The intrinsic droop equation is given in Equation 3, where V_i^* is the voltage reference to converter i, V_{dc}^* is the reference voltage of the DC bus, r_i

the droop coefficient and i_i the output current of converter i. In this equation the droop coefficient acts as a virtual resistor often calculated by dividing the allowed voltage deviation by the maximum current of the converter.

$$V_i^* = V_{dc}^* - r_d i_{dc} + \delta V_i \tag{3}$$

To enhance droop performance, numerous studies have proposed further refinements to the droop equation. These enhancements include the incorporation of a voltage correction term δV_i, adjustments to the droop coefficient r_d, or the introduction of nonlinear combinations of both. To achieve this objective, the decentralised primary control layer is frequently supplemented by a distributed secondary control layer, which delivers the required information for these additional terms. [99] discuss various strategies for incorporating a voltage shifting term to compensate for the voltage deviation induced by the droop term. This voltage shift can be achieved without communication by directly measuring the bus voltage, or in a distributed manner through static or dynamic averaging methods. Furthermore, the study proposes a distributed slope adjustment strategy, which involves the inclusion of average current and droop coefficient controllers to equalise the impedance across all converters. This approach leads to significantly enhanced current sharing and dynamic stability. Another approach, as outlined by [100], adopts a more computationally intensive method by introducing a distributed iterative droop coefficient optimisation scheme. This scheme resulted in a maximum voltage deviation of 0.7% during dynamic operations, a notable improvement compared to the typical deviation of 5%. In addressing stability concerns, [101] augments the droop scheme with a robust gain, thereby enhancing load sharing accuracy and concurrently suppressing voltage fluctuations. As a result, the drawbacks associated with inaccuracies in load sharing, voltage deviations, and stability issues are effectively mitigated.

Furthermore, various studies propose strategies for integrating EMS objectives into the local control framework. For instance, [102] employs a multi-objective optimisation approach that considers tracking error and power losses for all control variables of droop. Although optimisation algorithms may appear impractical within local control, this research underlines the potential of incorporating control parameters into EMS optimisation. Alternatively, [103] introduces an adaptive droop control scheme where the droop coefficient varies as a function of the battery SOC, thereby promoting battery charging at low SOC levels and vice versa. Concurrently, the interlinking converter within the system employs a subzone droop slope, mimicking the behaviour of a DBS methodology. This approach illustrates the interconnection possibilities between rapid local control and more extensive timescale optimisation techniques.

5.2 Energy management methodologies

The introductory section delineates the primary objectives of control, with the local controller previously examined effectively tackling the initial three objectives. However, achieving the latter two objectives of loss minimization and economical optimisation necessitates employing more intricate methodologies, which are impractical to implement within rapid time frames. Moreover, the decision-making process relies on system-level data inaccessible through decentralised means. Consequently, this section will highlight methodologies designed to address economical system optimisation, alongside the requisite solving routines.

5.2.a optimisation formulation

Traditionally, Economic Dispatch (ED) has served as the method for determining power set points within grids consisting of multiple generators and loads regardless of the transmission network, with a focus on minimizing overall system costs. Conversely, the fundamental Power Flow (PF) problem addresses the division of power flows within a meshed transmission network at a given moment, independent of power generation specifics and lacking optimisation considerations. Optimal Power Flow (OPF) emerged as a means to combine both approaches, aiming to achieve comprehensive optimisation for power system management. This undertaking involves tackling a highly nonlinear problem, offering flexibility for single or multiple objectives such as minimizing losses, maximizing profits, reducing interruptions, or extending equipment lifespan [**?**].

The comprehensive formulation of OPF, known as AC-OPF, encompasses the entire set of electrical system equations without approximations or assumptions. Constraints imposed on the optimisation re-

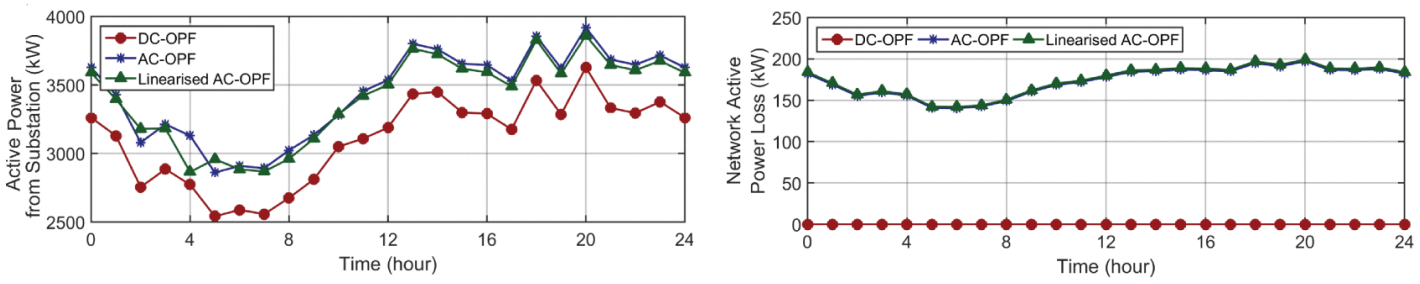

Fig. 9: Comparison of the performance of OPF formulations [104]

flect the unique characteristics of the system at hand, encompassing inequality constraints, binary constraints, and stochastic variables, significantly impacting solving methodologies. Given the intricacies involved, numerous studies have proposed simplifications through assumptions or by disregarding certain effects to tailor the problem to specific scenarios [105]. One notable simplification is the DC-OPF, which, despite its name, doesn't exclusively handle DC flows but rather eliminates reactive power flow. This simplification arises from the following assumptions: power cable resistance is neglected, constant voltage at all nodes, and the voltage angle is very small [106]. Although the DC-OPF offers computational advantages due to its linear nature, it comes at the expense of power loss information. Alternatively, a linearization method for AC-OPF, proposed in [104], preserves power loss considerations and voltage information, as can be seen in Figure 9. The study observed that the computational times for DC-OPF, linear AC-OPF, and full AC-OPF were 0.4, 4.1, and 30.3 seconds respectively, for calculating optimal flows over a day in a given system.

5.2.b Real-time energy management

As discussed in the preceding section, the computational demands associated with intricate optimisation techniques present an obstacle to their real-time application in the control of microgrids. Additionally, the inherent uncertainties within forecasts of renewable energy sources and load demand necessitate real-time adjustments to the anticipated optimal conditions. These factors underline the significance of collaborative efforts between the local controller (as discussed in Section 5.1.b) and the EMS algorithm. As previously noted, the EMS optimisation computes economically optimal set-points for a designated time frame, subsequently implemented by the autonomous local controller on a ms timescale.

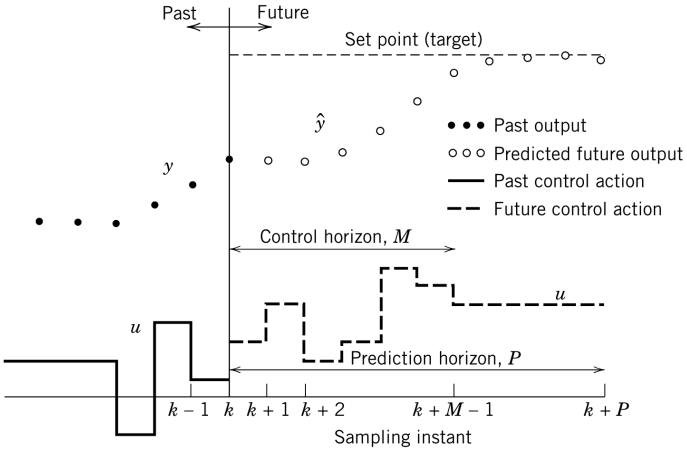

Fig. 10: Concept of a real-time MPC control structure [107]

An alternative approach to reconciling daily optimal control with local control is through Model Predictive Control (MPC), as which also appeared in in Section 4.3.b (Table 7). The MPC methodology involves a multi-time optimisation function characterised by a specified prediction horizon and control horizon. The fundamental concept entails incorporating system information spanning the prediction horizon into the optimisation process to derive optimal set-points. Consequently, how to arrive at the set-points, given the current system state, is optimally calculated within the control horizon. Notably, the controller applies solely the initial control action while disregarding future actions. Subsequently, in the second time step, the horizon regresses by one step, and the algorithm iterates, as illustrated schematically in Figure 10. This approach offers several advantages, including the multi-time integration of information, which proves highly advantageous in microgrid scheduling, while concurrently accommodating constant corrections for uncertain conditions. Moreover, within the optimisation step, there exists flexibility in defining a suitable objective function, as explored by [108], who included

the OPF formulation within a MPC framework. However, a notable drawback lies in the predictive aspect, necessitating intricate insight into the system's dynamic behaviour. Furthermore, the methodology is computationally intensive, requiring a multi-time optimisation calculation at each time-step.

5.2.c Solving methods

The missing part in the optimisation timeline is how to reach the solution of the optimisation problem. The objective function, along with its associated constraints, may encompass nonlinear combinations of decision variables, binary variables, and random variables, thereby rendering the problem non-convex with potential existence of several local minima. The complexity inherent to this problem has resulted in a variety of diverse solution algorithms. Accordingly, this section aims to present an overview to mitigate potential confusion stemming from the abundance of terminology.

An attempt to categorise all methodologies is outlined in [109], which distinguishes between conventional deterministic methods, AI-based methods, and stochastic heuristic methods. AI methods encompass fuzzy logic, game theory, multi-agent systems, neural networks, and deep learning techniques, offering a robust framework capable of addressing highly non-linear systems. Typically, this approach necessitates a substantial volume of data for training purposes, thus surpassing the scope of this research.

In parallel with AI-based approaches, heuristic methods are designed to seek a near-optimal solution when obtaining a deterministic solution proves to be difficult. These algorithms primarily leverage swarm intelligence or evolutionary principles, which consequently entail a substantial computational burden and iterative solving processes. Consequently, while heuristic methods necessitate less training compared to AI methods, their application in real-time systems often results in significantly prolonged computational times. Furthermore, the stochastic nature of many heuristic methods involves the utilization of randomly generated variables to explore the solution space, potentially yielding varying solutions to the same problem or converging towards a local minimum rather than the global optimum.

The final category encompasses deterministic methods that compute a singular solution to the problem at hand. This category includes linear, quadratic, non-linear, mixed-integer, dynamic, robust programming, and combinations thereof, each distinguished by various characteristics. Linear programming stands out as the simplest and fastest method but is limited to linear objective functions and constraints. Incorporating variables with binary values necessitates transitioning to mixed-integer linear programming (MILP), a step likely essential for adequately modeling the behaviour of the PEMFC, as discussed in Section 4. Extensions to mixed-integer non-linear programming (MINLP) become necessary to account for the non-linear relationships inherent in the full AC-OPF. However, the computational demands of this approach have incentivised efforts to linearise the AC-OPF, resulting in linear AC-OPF or even DC-OPF formulations, as previously mentioned in Section 5.2.a. Additionally, a class of robust programming methods has been developed to address uncertainties in the solution methodology [109].

From the perspective of real-time application, the derivation of fast solutions holds paramount importance. Therefore, the simplicity of the optimisation problem and its associated solver constitute the primary design objectives. To summarise this section, Figure 11 provides a schematic representation of deterministic conventional methods alongside stochastic heuristic methods.

5.3 Conclusion

In conclusion, this chapter underscores the critical role of control strategies in the safe and optimal operation of the FCPB system. By examining local control approaches and energy management methodologies, the complex interplay between hierarchical control layers is highlighted. Special attention has been given to droop control due to its robustness, autonomy, simplicity and flexibility, especially when coupled with a higher level EMS methodology into an adaptive form. MPC or similar multi-time formulations were found to provide a proper framework for energy management optimisation under off-grid scenarios with complex FC behaviour.

Furthermore, the exploration of optimisation formulations and solving methods underscores the need for balancing computational complexity and thus real-time applicability with accuracy. The fundamental

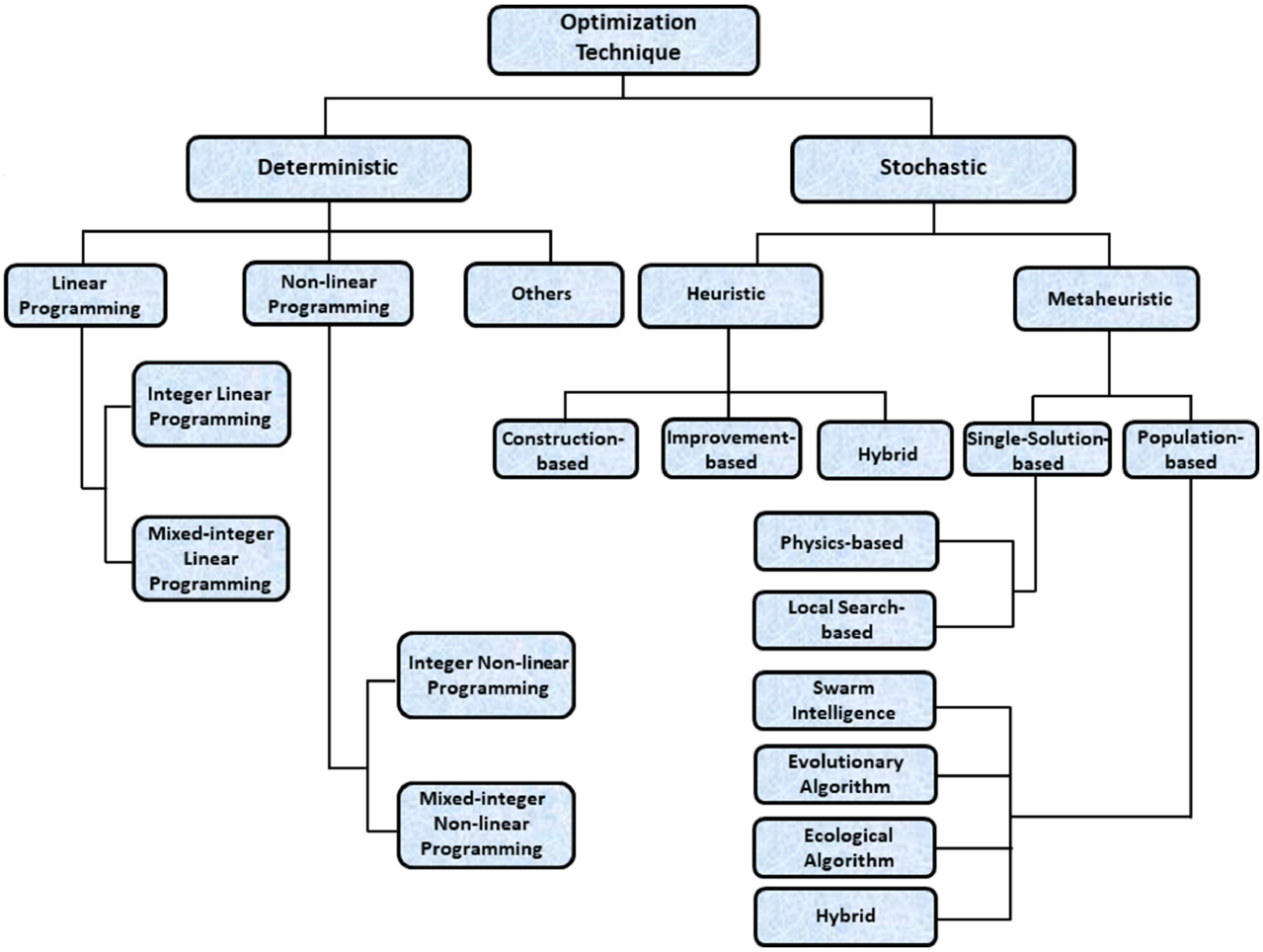

Fig. 11: Overview of solving methodologies applied in EMS applications [**?**]

OPF formulation can be linearised or simplified to achieve this desired balance. Deterministic methods offer fast singular solutions however struggle to find this solution in complex problems. To the contrary, stochastic heuristic approaches provide near-optimal solutions through iterative processes, capable of handling highly non-linear systems.

In conclusion, effective control strategies are essential for achieving multiple objectives such as voltage and current regulation, stability enhancement, and cost optimisation in FCPB systems. By synthesizing insights from local control techniques, energy management methodologies, and efficient solving methods, FCPB systems can operate optimally in diverse conditions while maintaining reliability and cost-effectiveness.

REFERENCES

1. I Belharouak, G M Koenig, and K Amine, Electrochemistry and safety of Li4Ti5O12 and graphite anodes paired with LiMn2O4 for hybrid electric vehicle Li-ion battery applications, *Journal of Power Sources*, (2011), 196(23):10344–10350.
2. Y Zhao, O Pohl, A I Bhatt, G E Collis, P J Mahon, T Rüther, and A F Hollenkamp, A Review on Battery Market Trends, Second-Life Reuse, and Recycling, (2021).
3. R Salgado, F Danzi, J E Oliveira, A El-Azab, P P Camanho, and M H Braga, The Latest Trends in Electric Vehicles Batteries, (2021).
4. J S Edge, S O'Kane, R Prosser, D Kirkaldy, A N Patel, A Hales, A Ghosh, W Ai, J Chen, J Yang, S Li, M Pang, L Bravo Diaz, A Tomaszewska, M W Marzook, K N Radhakrishnan, H Wang, Y Patel, B Wu, and G J Offer, Lithium ion battery degradation: what you need to know, *Physical Chemistry Chemical Physics*, (2021), 23(14):8200–8221.
5. N Collath, B Tepe, S Englberger, A Jossen, and H Hesse, Aging aware operation of lithium-ion battery energy storage systems: A review, *Journal of Energy Storage*, (2022), 55:105634.
6. X Han, L Lu, Y Zheng, X Feng, Z Li, J Li, and M Ouyang, A review on the key issues of the lithium ion battery degradation among the whole life cycle, *eTransportation*, (2019), 1:100005.
7. S El Moutchou, H Aziam, M Mansori, and I Saadoune, Thermal stability of Lithium-ion batteries: Case study of NMC811 and LFP cathode materials, *Materials Today: Proceedings*, (2022), 51:A1–A7.

8. X Feng, S Zheng, D Ren, X He, L Wang, H Cui, X Liu, C Jin, F Zhang, C Xu, H Hsu, S Gao, T Chen, Y Li, T Wang, H Wang, M Li, and M Ouyang, Investigating the thermal runaway mechanisms of lithium-ion batteries based on thermal analysis database, *Applied Energy*, (2019), 246:53–64.
9. M Kaliaperumal, M S Dharanendrakumar, S Prasanna, K V Abhishek, R K Chidambaram, S Adams, K Zaghib, and M V Reddy, Cause and Mitigation of Lithium-Ion Battery Failure—A Review, *Materials*, (2021), 14.
10. T Bank, J Feldmann, S Klamor, S Bihn, and D U Sauer, Extensive aging analysis of high-power lithium titanate oxide batteries: Impact of the passive electrode effect, *Journal of Power Sources*, (2020), 473:228566.
11. B L Choo and Y I Go, Energy storage for large scale/utility renewable energy system - An enhanced safety model and risk assessment, *Renewable Energy Focus*, (2022), 42:79–96.
12. E HY Moa and Y I Go, Large-scale energy storage system: safety and risk assessment, *Sustainable Energy Research*, (2023), 10(1):13.
13. C Hendricks, N Williard, S Mathew, and M Pecht, A failure modes, mechanisms, and effects analysis (FMMEA) of lithium-ion batteries, *Journal of Power Sources*, (2015), 297:113–120.
14. S Rohr, M Kerler, S Varta, M Müller, M Lienkamp, and A Jossen, *Risk Analysis of Lithium-Ion Energy Storage Systems in Grid Applications – a Norm-Based Approach*, (2014).
15. R Kirana, N Purwanto, N Azis, E Joelianto, S Santosa, B Budiman, L Nguyen, and A Turnip, Failure assessment in lithium-ion battery packs in electric vehicles using the failure modes and effects analysis (FMEA) approach, *Journal of Mechatronics, Electrical Power, and Vehicular Technology*, (2023), 14:94–104.
16. J Conzen, S Lakshmipathy, A Kapahi, S Kraft, and M DiDomizio, Lithium ion battery energy storage systems (BESS) hazards, *Journal of Loss Prevention in the Process Industries*, (2023), 81:104932.
17. T Alsuwian, S Ansari, M Ammirrul A, A Ayob, A Hussain, M S Hossain, A R H Alhawari, A H M Almawgani, S Almasabi, and A Taher Hindi, A review of expert hybrid and co-estimation techniques for SOH and RUL estimation in battery management system with electric vehicle application, *Expert Systems with Applications*, (2024), 246:123123.
18. S Colleen, History of Fuel Cells, (2017).
19. Y Wang, K S Chen, and S C Cho, *PEM Fuel Cells: Thermal and Water Management Fundamentals*, Momentum Press, (2013).
20. J Zhao and X Li, A review of polymer electrolyte membrane fuel cell durability for vehicular applications: Degradation modes and experimental techniques, *Energy Conversion and Management*, (2019), 199:112022.
21. M Yue, S Jemei, R Gouriveau, and N Zerhouni, Review on health-conscious energy management strategies for fuel cell hybrid electric vehicles: Degradation models and strategies, *International Journal of Hydrogen Energy*, (2019), 44(13):6844–6861.
22. J Hare, X Shi, S Gupta, and A Bazzi, Fault diagnostics in smart micro-grids: A survey, *Renewable and Sustainable Energy Reviews*, (2016), 60:1114–1124.
23. D Stephens, S Rose, S Flamberg, M R Stephen, and E G I Paul, Failure Modes and Effects Analysis for Hydrogen Fuel Cell Vehicles, Technical report, (2009).
24. U Mukherjee, A Maroufmashat, J Ranisau, M Barbouti, A Trainor, N Juthani, H El-Shayeb, and M Fowler, Techno-economic, environmental, and safety assessment of hydrogen powered community microgrids; case study in Canada, *International Journal of Hydrogen Energy*, (2017), 42.
25. Y Bultel, M Aurousseau, P Ozil, and L Perrin, Risk analysis on a fuel cell in electric vehicle using the MADS/MOSAR methodology, *Process Safety and Environmental Protection - PROCESS SAF ENVIRON PROT*, (2007), 85:241–250.
26. M Gerbec, V Jovan, and J Petrovčič, Operational and safety analyses of a commercial PEMFC system, *International Journal of Hydrogen Energy*, (2008), 33(15):4147–4160.
27. Y Shen, H Lv, Y Hu, J Li, H Lan, and C Zhang, Preliminary hazard identification for qualitative risk assessment on onboard hydrogen storage and supply systems of hydrogen fuel cell vehicles, *Renewable Energy*, (2023), 212:834–854.
28. G K Singh, Solar power generation by PV (photovoltaic) technology: A review, *Energy*, (2013), 53:1–13.
29. NREL, Best Research-Cell Efficiency Chart, (2023).
30. Alessandra Colli, Failure mode and effect analysis for photovoltaic systems, *Renewable and Sustainable Energy Reviews*, (2015), 50:804–809.
31. S Jadidi, H Badihi, and Y Zhang, Fault Diagnosis in Microgrids with Integration of Solar Photovoltaic Systems:A Review, *IFAC-PapersOnLine*, (2020), 53(2):12091–12096.
32. G R Venkatakrishnan, R Rengaraj, S Tamilselvi, J Harshini, Ansheela Sahoo, C Ahamed Saleel, Mohamed Abbas, Erdem Cuce, C Jazlyn, Saboor Shaik, Pinar Mert Cuce, and Saffa Riffat, Detection, location, and diagnosis of different faults in large solar PV system—a review, *International Journal of Low-Carbon Technologies*, (2023), 18:659–674.
33. T Kuo, T Pham, P Huang, H Nguyen, D M Bui, and P D Le, Reliability analysis of PV generating systems in the islanded DC microgrid under dynamic and transient operation, *IET Renewable Power Generation*, (2022), 16(5):988–1026.
34. R Pimpalkar, A Sahu, R B Patil, and A Roy, A comprehensive review on failure modes and effect analysis of solar photovoltaic system, *Materials Today: Proceedings*, (2023), 77:687–691.
35. S Gallardo-Saavedra, L Hernández-Callejo, and O Duque-Pérez, Quantitative failure rates and modes analysis in photovoltaic plants, *Energy*, (2019), 183:825–836.
36. J Li, Y Zhang, H Fang, and S Fang, Risk evaluation of photovoltaic power systems: An improved failure mode and effect analysis under uncertainty, *Journal of Cleaner Production*, (2023), 414:137620.
37. S Sarkar, M S Bhaskar, K Uma Rao, P V, D Almakhles, and U Subramaniam, Solar PV network installation standards and cost estimation guidelines for smart cities, *Alexandria Engineering Journal*, (2022), 61(2):1277–1287.
38. T Dragičević, X Lu, J C Vasquez, and J M Guerrero, DC Microgrids—Part II: A Review of Power Architectures, Applications, and Standardization Issues, *IEEE Transactions on Power Electronics*, (2016), 31(5):3528–3549.
39. J Kumar, A Agarwal, and V Agarwal, A review on overall control of DC microgrids, *Journal of Energy Storage*, (2019), 21:113–138.

40. M Mishra, B Patnaik, M Biswal, S Hasan, and R C Bansal, A systematic review on DC-microgrid protection and grounding techniques: Issues, challenges and future perspective, *Applied Energy*, (2022), 313:118810.
41. V Pires, A Pires, and A Cordeiro, DC Microgrids: Benefits, Architectures, Perspectives and Challenges, (2023).
42. J J Justo, F Mwasilu, J Lee, and JW Jung, AC-microgrids versus DC-microgrids with distributed energy resources: A review, *Renewable and Sustainable Energy Reviews*, (2013), 24:387–405.
43. W de Jager and P Bos, design of a public dc grid of a business park, Technical report, KIVI, (2017).
44. A M I Mohamad and Y A R I Mohamed, Investigation and Enhancement of Stability in Grid-Connected Active DC Distribution Systems With High Penetration Level of Dynamic Loads, *IEEE Transactions on Power Electronics*, (2019), 34(9):9170–9190.
45. F Mohan and N Sasidharan, Protection of low voltage DC microgrids: A review, *Electric Power Systems Research*, (2023), 225:109822.
46. A Chandra, G K Singh, and V Pant, Protection techniques for DC microgrid- A review, *Electric Power Systems Research*, (2020), 187:106439.
47. S Sarangi, B K Sahu, and P K Rout, A comprehensive review of distribution generation integrated DC microgrid protection: issues, strategies, and future direction, *International Journal of Energy Research*, (2021), 45(4):5006–5031.
48. B Modu, M P Abdullah, M A Sanusi, and M F Hamza, DC-based microgrid: Topologies, control schemes, and implementations, *Alexandria Engineering Journal*, (2023), 70:61–92.
49. V F Pires, A Cordeiro, C Roncero-Clemente, S Rivera, and T Dragičević, DC–DC Converters for Bipolar Microgrid Voltage Balancing: A Comprehensive Review of Architectures and Topologies, *IEEE Journal of Emerging and Selected Topics in Power Electronics*, (2023), 11(1):981–998.
50. S Rivera, R Fuentes, S Kouro, T Dragicevic, and B Wu, Bipolar DC Power Conversion: State-of-the-Art and Emerging Technologies, *IEEE Journal of Emerging and Selected Topics in Power Electronics*, 3 2020, PP:1.
51. D K J S Jayamaha, N W A Lidula, and A D Rajapakse, Protection and grounding methods in DC microgrids: Comprehensive review and analysis, *Renewable and Sustainable Energy Reviews*, (2020), 120:109631.
52. D Paul, DC traction power system grounding, *Industry Applications, IEEE Transactions on*, 6 2002, 38:818–824.
53. K Hirose, T Tanaka, T Babasaki, S Person, O Foucault, B Sonnenberg, and M Szpek, Grounding concept considerations and recommendations for 400VDC distribution system, In: *Proc. , 2011 IEEE 33rd International Telecommunications Energy Conference (INTELEC)*, (2011), 1–8.
54. D Kumar, F Zare, and A Ghosh, DC Microgrid Technology: System Architectures, AC Grid Interfaces, Grounding Schemes, Power Quality, Communication Networks, Applications, and Standardizations Aspects, *IEEE Access*, (2017), 5:12230–12256.
55. M Mobarrez, D Fregosi, S Bhattacharya, and M A Bahmani, Grounding architectures for enabling ground fault ride-through capability in DC microgrids, In: *Proc. , 2017 IEEE Second International Conference on DC Microgrids (ICDCM)*, (2017), 81–87.
56. S Lu, T Phung, and D Zhang, *Study on DC series arc fault in photovoltaic systems for condition monitoring purpose*, (2017).
57. L Herrera and X Yao, Parameter Identification Approach to Series DC Arc Fault Detection and Localization, In: *Proc. , 2018 IEEE Energy Conversion Congress and Exposition (ECCE)*, (2018), 497–501.
58. S Favuzza, M Mitolo, S Moradi, R Musca, and G Zizzo, A General Methodology for Short-circuit Calculations in Hybrid AC/DC Microgrids, *IEEE Transactions on Industry Applications*, (2023), 59(3):2742–2749.
59. B Perea-Mena, J A. Valencia-Velasquez, J M. López-Lezama, J B. Cano-Quintero, and N Muñoz-Galeano, Circuit Breakers in Low- and Medium-Voltage DC Microgrids for Protection against Short-Circuit Electrical Faults: Evolution and Future Challenges, *Applied Sciences*, 12 2021, 12(1):15.
60. T Wu, Z Wang, C Fang, and S Liu, Research on current limiting solid state circuit breaker for DC microgrid, *Electric Power Systems Research*, 8 2022, 209:107950.
61. S Beheshtaein, R M Cuzner, M Forouzesh, M Savaghebi, and JM Guerrero, DC Microgrid Protection: A Comprehensive Review, *IEEE Journal of Emerging and Selected Topics in Power Electronics*, (2019), 1.
62. IS Anselmo and M H Rashid, Solid-State Circuit Breakers for D.C. Microgrid Applications, In: *Proc. , 2020 International Conference on Electrical, Communication, and Computer Engineering (ICECCE)*, (2020), 1–4.
63. A Shukla and G D Demetriades, A Survey on Hybrid Circuit-Breaker Topologies, *IEEE Transactions on Power Delivery*, (2015), 30(2):627–641.
64. I Venkata Raghavendra, S N Banavath, and S Thamballa, Modified Z-Source DC Circuit Breaker With Enhanced Performance During Commissioning and Reclosing, *IEEE Transactions on Power Electronics*, (2022), 37(1):910–919.
65. N Bayati, H R Baghaee, M Savaghebi, A Hajizadeh, M N. Soltani, and Z Lin, DC Fault Current Analyzing, Limiting, and Clearing in DC Microgrid Clusters, *Energies*, (2021), 14(19).
66. H Noroozi and I Sadeghkhani, Smooth reference modulation based protection of fault current limiting DC/DC converters, *Measurement and Control*, (2020), 53(9-10):1662–1668.
67. M E Baran and N R Mahajan, Overcurrent Protection on Voltage-Source-Converter-Based Multiterminal DC Distribution Systems, *IEEE Transactions on Power Delivery*, (2007), 22(1):406–412.
68. L Fan, Z Tu, and S H Chan, Recent development in design a state-of-art proton exchange membrane fuel cell from stack to system: Theory, integration and prospective, *International Journal of Hydrogen Energy*, (2023), 48(21):7828–7865.
69. J Wu, X Yuan, J J Martin, H Wang, J Zhang, J Shen, S Wu, and W Merida, A review of PEM fuel cell durability: Degradation mechanisms and mitigation strategies, *Journal of Power Sources*, (2008), 184(1):104–119.
70. A Collier, H Wang, X Zi Yuan, J Zhang, and D P Wilkinson, Degradation of polymer electrolyte membranes, *International Journal of Hydrogen Energy*, (2006), 31(13):1838–1854.
71. F A de Bruijn, V A T Dam, and G J M Janssen, Review: Durability and Degradation Issues of PEM Fuel Cell Components, *Fuel Cells*, (2008), 8(1):3–22.

72. P Ren, P Pei, Y Li, Z Wu, D Chen, and S Huang, Degradation mechanisms of proton exchange membrane fuel cell under typical automotive operating conditions, *Progress in Energy and Combustion Science*, (2020), 80:100859.

73. M Jouin, Gouriveau, D Hissel, M Péra, and N Zerhouni, Degradations analysis and aging modeling for health assessment and prognostics of PEMFC, *Reliability Engineering & System Safety*, (2016), 148:78–95.

74. M Chandran, P Karthikeyan, K Babu NB, and O Das, A study of the influence of current ramp rate on the performance of polymer electrolyte membrane fuel cell, *Scientific Reports*, 3 2022, 12:21888.

75. J Kim, J Lee, and Y Tak, Relationship between carbon corrosion and positive electrode potential in a proton-exchange membrane fuel cell during start/stop operation, *Journal of Power Sources*, (2009), 192(2):674–678.

76. F Nandjou, J.-P. Poirot-Crouvezier, M Chandesris, J.-F. Blachot, C Bonnaud, and Y Bultel, Impact of heat and water management on proton exchange membrane fuel cells degradation in automotive application, *Journal of Power Sources*, (2016), 326:182–192.

77. Y Li, P Pei, Z Ma, P Ren, Z Wu, D Chen, and H Huang, Characteristic analysis in lowering current density based on pressure drop for avoiding flooding in proton exchange membrane fuel cell, *Applied Energy*, (2019), 248:321–329.

78. A Loskutov, A Kurkin, A Shalukho, I Lipuzhin, and R Bedretdinov, Investigation of PEM Fuel Cell Characteristics in Steady and Dynamic Operation Modes, *Energies*, (2022), 15(19).

79. C Qin, J Wang, D Yang, B Li, and C Zhang, Proton Exchange Membrane Fuel Cell Reversal: A Review, *Catalysts*, (2016), 6(12).

80. E Wallnöfer-Ogris, F Poimer, R Köll, M Macherhammer, and A Trattner, Main degradation mechanisms of polymer electrolyte membrane fuel cell stacks – Mechanisms, influencing factors, consequences, and mitigation strategies, *International Journal of Hydrogen Energy*, (2024), 50:1159–1182.

81. A Topalov, S Cherevko, A Zeradjanin, J Meier, I Katsounaros, and K Mayrhofer, Towards a comprehensive understanding of platinum dissolution in acidic media, *Chemical science (Royal Society of Chemistry)*, 3 2014, 5:631–638.

82. X Yang, J Sun, X Meng, S Sun, and Z Shao, Cold start degradation of proton exchange membrane fuel cell: Dynamic and mechanism, *Chemical Engineering Journal*, (2023), 455:140823.

83. K Nikiforow, J Pennanen, J Ihonen, S Uski, and P Koski, Power ramp rate capabilities of a 5kW proton exchange membrane fuel cell system with discrete ejector control, *Journal of Power Sources*, (2018), 381:30–37.

84. M Whiteley, S Dunnett, and Jackson, Failure Mode and Effect Analysis, and Fault Tree Analysis of Polymer Electrolyte Membrane Fuel Cells, *International Journal of Hydrogen Energy*, (2016), 41(2):1187–1202.

85. H Chen, P Pei, and M Song, Lifetime prediction and the economic lifetime of Proton Exchange Membrane fuel cells, *Applied Energy*, (2015), 142:154–163.

86. J M Desantes, R Novella, B Pla, and M Lopez-Juarez, A modeling framework for predicting the effect of the operating conditions and component sizing on fuel cell degradation and performance for automotive applications, *Applied Energy*, (2022), 317:119137.

87. Y Ao, S Laghrouche, D Depernet, and K Chen, Lifetime prediction for proton exchange membrane fuel cell under real driving cycles based on platinum particle dissolve model, *International Journal of Hydrogen Energy*, (2020), 45(56):32388–32401.

88. P Pei, Q Chang, and T Tang, A quick evaluating method for automotive fuel cell lifetime, *International Journal of Hydrogen Energy*, (2008), 33(14):3829–3836.

89. Q Li, X Zou, Y Pu, and W Chen, Real-time Energy Management Method for Electric-hydrogen Hybrid Energy Storage Microgrids Based on DP-MPC, *CSEE Journal of Power and Energy Systems*, (2024), 10(1):324–336.

90. C Huang, Y Zong, S You, and C Træholt, Economic model predictive control for multi-energy system considering hydrogen-thermal-electric dynamics and waste heat recovery of MW-level alkaline electrolyzer, *Energy Conversion and Management*, (2022), 265:115697.

91. X Fang, W Dong, Y Wang, and Q Yang, Multi-stage and multi-timescale optimal energy management for hydrogen-based integrated energy systems, *Energy*, (2024), 286:129576.

92. W Shen, B Zeng, and M Zeng, Multi-timescale rolling optimization dispatch method for integrated energy system with hybrid energy storage system, *Energy*, (2023), 283:129006.

93. F Garcia-Torres and C Bordons, Optimal Economical Schedule of Hydrogen-Based Microgrids With Hybrid Storage Using Model Predictive Control, *IEEE Transactions on Industrial Electronics*, (2015), 62(8):5195–5207.

94. M B Abdelghany, M F Shehzad, D Liuzza, V Mariani, and L Glielmo, Optimal operations for hydrogen-based energy storage systems in wind farms via model predictive control, *International Journal of Hydrogen Energy*, (2021), 46(57):29297–29313.

95. M B Abdelghany, V Mariani, D Liuzza, and L Glielmo, Hierarchical model predictive control for islanded and grid-connected microgrids with wind generation and hydrogen energy storage systems, *International Journal of Hydrogen Energy*, (2024), 51:595–610.

96. C Dall'Armi, D Pivetta, and R Taccani, Health-Conscious Optimization of Long-Term Operation for Hybrid PEMFC Ship Propulsion Systems, *Energies*, (2021), 14(13).

97. S Sen and V Kumar, Microgrid control: A comprehensive survey, *Annual Reviews in Control*, (2018), 45:118–151.

98. Z Shuai, J Fang, F Ning, and Z J Shen, Hierarchical structure and bus voltage control of DC microgrid, *Renewable and Sustainable Energy Reviews*, (2018), 82:3670–3682.

99. P Wang, X Lu, X Yang, W Wang, and D Xu, An Improved Distributed Secondary Control Method for DC Microgrids With Enhanced Dynamic Current Sharing Performance, *IEEE Transactions on Power Electronics*, (2016), 31(9):6658–6673.

100. B A Taye and N B Choudhury, A dynamic droop control for a DC microgrid to enhance voltage profile and proportional current sharing, *Electric Power Systems Research*, (2023), 221:109438.

101. Z Shuai, D He, J Fang, Z J Shen, C Tu, and J Wang, Robust droop control of DC distribution networks, *IET Renewable Power Generation*, (2016), 10(6):807–814.

102. Y Zhou, Q Hua, P Liu, and L Sun, Multi-objective optimal droop control of solid oxide fuel cell based integrated energy system, *International Journal of Hydrogen Energy*, (2023), 48(30):11382–11389.

103. X Yang, F Tang, X Wu, and X Jin, Hierarchical control strategy of grid-connected DC microgrids, In: *Proc. , 2016 IEEE 8th International Power Electronics and Motion Control Conference (IPEMC-ECCE Asia)*, (2016), 3723–3727.

104. A Soleimani, V Vahidinasab, and J Aghaei, A Linear Stochastic Formulation for Distribution Energy Management Systems Considering Lifetime Extension of Battery Storage Devices, *IEEE Access*, (2022), 10:44564–44576.

105. E Mohagheghi, M Alramlawi, A Gabash, and P Li, A Survey of Real-Time Optimal Power Flow, *Energies*, (2018), 11(11).

106. L Mones, A Gentle Introduction to Optimal Power Flow, (2021).

107. D Seborg, T Edgar, D Mellichamp, and F Doyle, Model Predictive Control, In: , *Process Dynamics and Control*. Wiley, 4th edition edition, (2016), chapter 20, 368–389.

108. D Erazo-Caicedo, E Mojica-Nava, and J Revelo-Fuelagán, Model predictive control for optimal power flow in grid-connected unbalanced microgrids, *Electric Power Systems Research*, (2022), 209:108000.

109. G S Thirunavukkarasu, M Seyedmahmoudian, E Jamei, B Horan, S Mekhilef, and A Stojcevski, Role of optimization techniques in microgrid energy management systems—A review, *Energy Strategy Reviews*, (2022), 43:100899.